To the Graduate Council:

I am submitting herewith a thesis written by James Patrick McClanahan entitled "Monitoring Electric Motor Aging Using Vibration and Current Signatures." I have examined the final copy of this thesis for form and content and recommend that it be accepted in partial fulfillment of the requirements for the degree of Master of Science with a major in Nuclear Engineering.

Belle R Upadhyaya

Dr. B. R. Upadhyaya, Major Professor

We have read this thesis and recommend its acceptance:

Laurence F Miller

J Wesley Hines

Accepted for the Council:

C W Minkel

Associate Vice Chancellor and
Dean of the Graduate School

Monitoring Electric Motor Aging Using Vibration and Current Signatures

A Thesis
Presented for the
Master of Science Degree
The University of Tennessee, Knoxville

James Patrick McClanahan
December 1998

ACKNOWLEGDEMENTS

I would like to thank the major professor and my advisor, Dr. B. R. Upadhyaya for his special guidance and assistance in my research.

I would also like to thank the committee members, Dr. L. F. Miller and Dr. J. W. Hines for their guidance and assistance. Also a special thanks to Dr. T. E. Shannon, Dr. H. L. Dodds and Dr. T. W. Kerlin for their support. Special thanks to Richard Bailey and Gary Graves for their technical support and expertise. I would also like to thank Kathy Phillips for her helpful computer operational hints and overall office skills.

The support for my graduate studies and for this research was made possible by the Institute for Nuclear Power Operations, Maintenance and Reliability Center, The University of Tennessee and the Duke Energy Corporation fellowship program.

Finally, I would like to thank all my family, and specifically James K. and Deana McClanahan, my parents and Christopher McClanahan, my brother, for their moral and sometimes financial support.

ABSTRACT

The purpose of this research project is to analyze and characterize vibration and motor current signatures in order to monitor certain motor degradations caused by aging mechanisms. As part of a project sponsored by the Maintenance and Reliability Center, the changes in these signatures were studied for the stator thermal aging and bearing fluting cases. The research included the following tasks: spectral peak identification, determination of specific frequency ranges of interest, establishing correlations among various signals and quantifying and trending signal RMS values at different frequency bands.

The changes in spectral peaks were used for the detection and identification of motor faults. The interesting frequency ranges were defined as regions within the spectrum that have significant shifts in magnitudes. The interesting frequency ranges were isolated and quantified. The trends in these parameters showed degradation of the motor's condition. Finally, correlations between the signals (motor current and/or vibration) were examined. Highly correlated signals can be substituted for one another if needed. A change in correlation from one cycle to the next would indicate a change in the relationship between the signals.

From the literature review it was found that bearing and insulation failures account for about 60% of induction motor failures. Bearing fluting and insulation aging test data, corresponding to 100% load, were processed in this study. The determination of specific signals for data analysis was crucial. Since motors were tested to failure, there were certain signals that showed dramatic changes from the initial cycle to the final. Preliminary processing of the fluted motor parameters showed that all the vibration signals displayed considerable changes in all frequency bands, and more prominently in the high-frequency ranges. For the stator-aged motors, the 60-Hz current peak showed the largest changes. The frequency bands of interest were isolated using the wavelet transform and multi-resolution analysis and used for degradation trending.

With the signals identified, it was a straightforward process to establish almost all the major peaks of the current spectrum. The vibration spectra were much more complicated. The interesting frequency ranges were separated using 1-D wavelet decomposition into eight levels. In general, the quantified interesting frequency range trended better than the full RMS values of the signals. The coherence among motor currents was high, among the vibration signals it was extremely high, and the coherence between vibration and motor current was low except for specific frequencies. The relationship between the signals changed as the aging process progressed. The power spectra of the stator current signals indicated bearing related characteristics at frequencies greater than 30 Hz.

In summary, this study established five major points.

- From the literature review it was found that bearing and insulation failures amount to about 60% of induction motor failures
- Few unidentifiable peaks and one interesting frequency range were seen in the motor current signature for the stator-aged motors. Many bearing induced frequency peaks were seen in the motor current spectra.
- Many high frequency peaks and interesting frequency ranges were seen in the vibration signature for the bearing-fluted motors. Bearing pitting, frosting and other anomalies were seen at greater than normal frequency ranges often described in the literature.
- Either the motor current or vibration signatures at certain frequency bands can be trended with high accuracy in order to monitor the degradation of induction motors due to insulation thermal aging or bearing fluting.
- The relationship between the signals changed as the aging process progressed.

TABLE OF CONTENTS

List of Tables

List of Figures

List of Acronyms

AC	Alternating Current
DC	Direct Current
PIP	Polarization Index Profile
g	Acceleration due to Gravity
dB	deciBel
PSD	Power Spectral Density
RMS	Root Mean Square
RPM	Revolutions per Minute
SPCC	Signal Pair Correlation Coefficient
SSPCC	Summed Signal Pair Correlation Coefficient
1-D	One Dimension
USEM	United States Electrical Motors
MRC	Maintenance and Reliability Center
MCrA	Motor Circuit Analysis
RTG	Resistance to Ground
MRA	Multi-Resolution Analysis
DWT	Discrete Wavelet Transform
CWT	Continuous Wavelet Transform

Chapter 1

INTRODUCTION

1.0. Purpose and Scope

Induction motors are widely used in various industry sectors. The motors range in size from fractional horsepower to thousands of horsepowers. Two of the major causes of induction motor breakdown are found either within the stator or the bearings and it is natural to look for prevailing problems using electric and vibration signals of the motor. Thus, by analyzing these two signals, the majority of problems that arise in an induction motor should be detected, identified and possibly trended. By trending the condition of the motor, a determination of time to failure can be made. This knowledge is valuable for increased production, economic operation and for planning maintenance tasks.

The purpose of this thesis is to analyze and characterize vibration and motor current signatures in order to monitor certain motor degradation caused by aging mechanisms. By using the information and data generated from the motor aging project, major spectral characteristics in both the vibration and current signals were identified. These features are widely used to determine the condition of an induction motor. The trending and comparison of full-signal and interesting frequency ranges were investigated. The trending allows the overall condition of a motor to be tracked with time.

1.1. Definition of Tasks

The objectives of the thesis were accomplished by the completion of the following tasks.

- A critical literature review of methods used to determine the condition of electric motors.
- Specification of the motors and signals to be analyzed.

- Preliminary analysis of the specified motor signals.
- Identification of spectral peaks for the specified motor signals.
- Establishing the interesting frequency ranges and their physical interpretation.
- Determination of relationships among the analyzed signals.
- Quantification of the RMS values of characteristic frequency ranges for the specified signals using wavelet transform and multi-resolution analysis.
- Trending the frequency ranges by cycle for comparison to full-range signals.

1.2. Contributions of the Thesis

The significant contributions of this research are summarized as follows.

- A thorough review of induction motor faults and their detection methods.
- A better understanding of the motor current and vibration spectra by peak identification and comparison with theoretical values.
- Better trending methods, using characteristic frequency ranges, when using vibration or current signals for motors that are aged in similar processes. Wavelet transform and multi-resolution analysis are used to establish the various frequency bands.
- Establishment of the relationship between motor current and vibration signatures at high frequency bands.

1.3. Organization of the Thesis

Chapter 2 contains the literature review. Chapter 3 contains a description of the project's electric motor and the aging experiments. Chapter 4 describes the analysis theory for both motor current and vibration. The contents of Chapter 5 include time- and frequency-domain theory and processing, wavelet theory and processing, and first-order least-squares regression using fractional RMS errors. Chapter 6 contains preliminary analysis of the data using both Fourier and wavelet analysis. Chapter 7 contains results and discussion. Conclusions and recommendations for future work are given in chapter 8.

Chapter 2

REVIEW OF INDUCTION MOTOR FAILURES AND THEIR DETECTION METHODS

2.0. Introduction

A complete literature review, pertaining to the induction motor modes of failure and the methods to detect failures was performed. This chapter contains a detailed description of the methods and illustrations to clarify these methods.

The testing and monitoring methods include the following. Motor current analysis, vibration analysis, motor power analysis (instantaneous and torque derived), impact resonance analysis, thermal analysis, magnetic flux analysis, motor circuit analysis and the various static tests used in industry.

2.1. Brief Description of an Induction Motor

The induction motor is composed of three main parts: the stator, the rotor and the shaft. The stator employs wound, electrically charged coils to generate a rotating magnetic field. With the rotor located inside the stator, this rotating magnetic field induces an opposing magnetic field within the rotor. This opposing magnetic field causes the rotor to turn. The rotor is mounted on the shaft, thus the induced magnetic field causes the shaft to rotate.

The stator and rotor are usually protected by a casing. The stator is solidly mounted to the casing. This casing also serves as a mount for the bearings which allow the shaft (and rotor) to rotate within the stator.

2.2. Failure Modes of Induction Motors

Failure modes of induction motors can be divided into four groups: stator, rotor, bearings, and other. The three groups given by stator, rotor, and bearing are the major components of an induction motor and account for 88 % of the total failures for motors [1]. Given the large percentage for these three modes, their failure modes are discussed first. For the group given by others in Table 2.1, only the major problems in this group are discussed. A detailed failure mode percentage breakdown is given in Table 2.1.

2.2.1. Stator

2.2.1.1. Frame: The stator frame encloses the stator and protects it from the environment. It should be robust enough to withstand the mechanical vibrations in the machine and the high torsional forces transmitted to it from the air gap during startup or due to excessive loading [2].

2.2.1.2. Core: Insulation shrinkage of stator core laminations is a problem in large motors. For smaller motors, this does not pose any significant problem [2].

2.2.1.3. Windings: Stator windings consist of an insulated conductors. The conductor is usually copper in larger motors and aluminum in small motors. The insulation is the most common site of failure in electrical machines. Every strand, turn and coil is insulated from its neighbor. Insulation failure leads to turn-to-turn, phase-to-phase or three-phase short circuit [2].

2.2.2. Rotor

2.2.2.1. Problems Common to the Rotor: The rotor is subjected to the same forces as the stator, such as forces due to load, machine vibration, misalignment and environmental factors [2]. Since the windings are not composed of wound copper wire, but instead metal bars, there are different problems associated with the rotor assembly. These problems are discussed below.

Table 2.1. Percentages of failure modes as given by major components

Failure Modes	Percentage
Bearing Related	**Total - 41%**
Sleeve Bearings	16 %
Anti-Friction Bearings	8%
Seals	6%
Thrust Bearings	3%
Oil Leakage	3%
Other	3%
Stator Related	**Total - 37%**
Ground Insulation	23%
Turn Insulation	4%
Bracing	3%
Wedges	1%
Frame	1%
Core	1%
Other	1%
Rotor Related	**Total - 10%**
Cage	5%
Shaft	2%
Core	1%
Other	2%
All Other	**Total - 12%**

This was adapted from information was based on an 872 failed motor survey conducted by EPRI [1].

2.2.2.2. Rotor Bars: The hypothesis on which broken-rotor-bar detection is based is that the apparent rotor resistance of an induction motor will increase when a rotor bar breaks or develops cracks. Typical detectors examine axial flux, stator current, rotor velocity, and rotor vibration in search of variation resulting from the unbalanced currents caused by broken rotor bars [3].

2.2.2.3. Rotational Problems (vibration and centrifugal forces): If the rotor is not balanced properly, or if the shaft is not straight, the rotation of the rotor will cause vibration. With this rotation, the components of the rotor are also subjected to centrifugal forces that pull the rotor components away from the shaft and away from each other in a direction perpendicular to the axis of rotation.

2.2.2.4. Thermal Expansion and Contraction of Windings: Rotor cages undergo thermal excursion due to load. The energy losses produced during acceleration are directly related to the energy stored in the rotating inertia of the drive system at rated speed and may produce more pronounced thermal excursions [2].

2.2.3. Bearings

2.2.3.1. Seals: Bearing seals perform two important tasks: (1) the seal does not allow outside contamination to infiltrate the interior of the bearing, and (2) the seal keeps internal lubrication from leaking into the motor or the environment.

2.2.3.2. Ball: This element of the bearing transmits the forces between the inner and outer races. If for any reason this element has a defect, the result will be seen in a specific frequency of vibration of the bearing itself. The vibration frequency is often referred to as the Ball Spin Frequency (BPS).

2.2.3.3. Inner and Outer Races: These bearing elements are the surfaces that the rolling elements (for example, balls) are in contact with. The inner race is in contact with the rotor shaft and the outer race is in contact with the motor frame that houses the internal components of the motor. Both the inner and outer races are usually securely mounted. If for any reason these elements have a defect, the result will be seen in a specific frequency of vibration of the bearing itself. These vibration frequencies are sometimes referred to as the Ball Pass Frequency of the Inner or the Outer Race.

2.2.3.4. Cage Race: The function of the cage or the cage race is to keep proper spacing between the rolling elements within the bearing. Any problem with this component will also cause a vibration that is related to the frequency that the retainer turns with the rolling elements. These vibration frequencies are sometimes referred to as Fundamental Train Frequencies.

2.2.3.5. Seating: The seating refers to the alignment of the bearings with each other, to the rotor and to the stator. Any misalignment will cause vibration of the bearings and also the motor system.

2.2.4. Other

2.2.4.1. Electrical Faults: The most prominent electrical fault is the current imbalance. Current imbalance is mainly caused by imbalance in phase impedances. Resistive imbalance may be caused by a number of defects mainly found in circuit connections, contacts and external terminals ... circuit reactance changes when windings short with one another (turn-to-turn) or with the ground (phase-to-phase) [4]. But, circuit reactance is included with stator or winding faults above. These faults cause the insulation of the windings to overheat and degrade at an accelerated rate.

2.2.4.2. Loading: Another important reason for the failure of motors is overloading them mechanically. "By reducing the shaft stress by 10%, the fatigue life of the shafts increases by 1.8

times and the bearing life increases by 37%; a 20% load reduction gives 3.4 times longer shaft life and 95% more bearing life; and a 50% reduction yields 47 times the original shaft life and 800% increase in bearing life [5]."

2.2.4.3. Bad Coupling: A bad coupling refers to the actual linkage between the motor and an external system and/or the fact that the external system is not a perfect system. The linkage may be a number of different types and also the problems that the external system introduces to the motor are complex as well.

2.2.4.4. Soft Feet: The term "soft feet" implies that the motor is not properly anchored to a base. There are two main reason this happens: (1) the motor is not properly secured, and (2) the motor base and the anchoring base do not seat together properly.

2.3. Induction Motor Fault Detection and Isolation

The various detection methods to determine the failure modes of typical induction motors are described. Examples are provided to further assist in understanding the available techniques.

2.3.1. Motor Current Analysis

Motor current analysis can be used to determine the condition of various components within the motor system. These components include: rotor cage defects, broken rotor bars, shorted stator turns, shorted laminations, high resistance connections, and motor bearing damage [6].

An example of an ideal three phase current supply is shown in Figure 2.1. We notice that each phase of the current is 60 or 120 degrees out of phase with the other phases. The power spectra of the currents should reveal a large peak at 60 Hz as seen in Figure 2.2. Often seen in the spectrum are many other peaks associated with the harmonics of the line current and harmonics

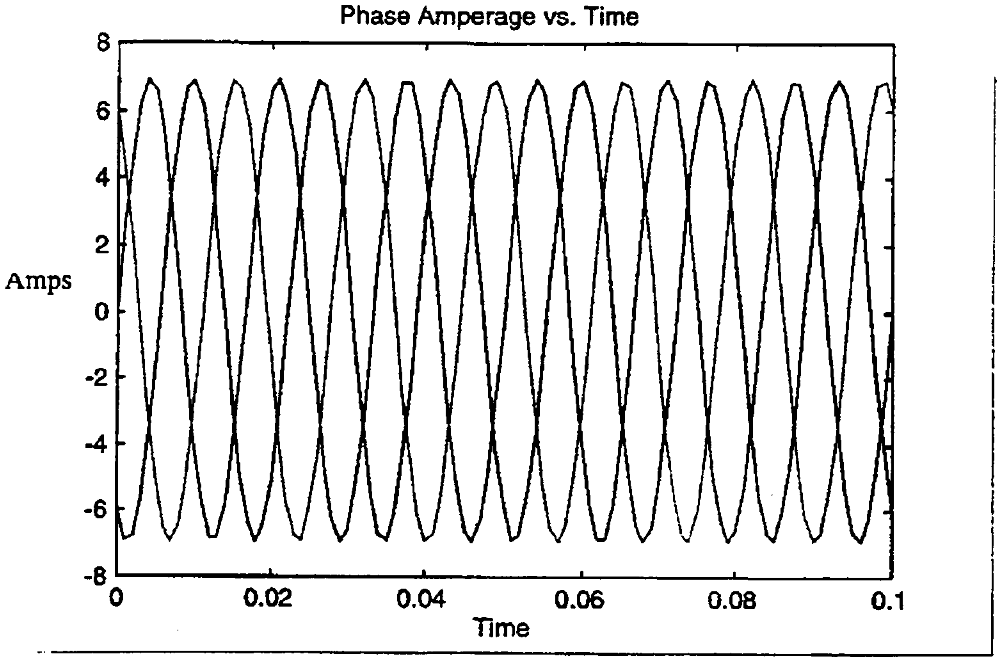

Figure 2.1. Three phase current.

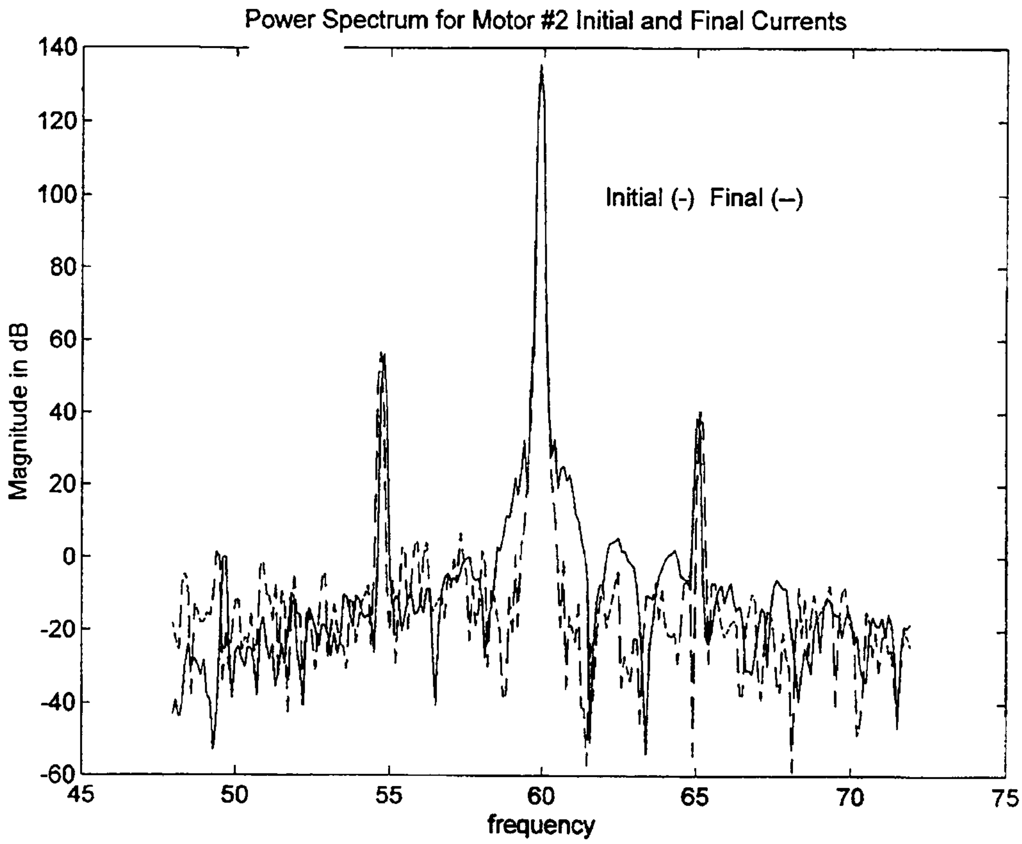

Figure 2.2. A motor current spectrum emphasizing 60 Hz peak with side-bands.

of the actual operating (synchronous) frequency of the motor and movement of the rotor shaft. Most types of problems will show up in the current spectrum as abnormalities added to the ideal three-phase spectrum around 60 Hz.

2.3.2. Vibration Analysis

Vibration is caused by movement within and/or outside of the motor. The purpose of a motor is to supply mechanical energy to an outside system. The observable moving part of the motor is the motor shaft. The motor shaft has the rotor mounted on it. The rotor/shaft assembly rotates, with a fundamental frequency, with supports provided by bearings. A simple representation is given in Figure 2.3 [7].

There are two main areas of the motor system that cause vibration, one is within the motor and related to the motion of the shaft, and the other due to the manner in which the motor is coupled to the outside system.

The motion within the motor can be caused by imbalance, misalignment, bearings, and/or looseness. Imbalance is caused when the center of mass of the rotor/shaft system is not centered along the axis of rotation. An example of an imbalance vibration signal is given in Figure 2.4 [7].

Bearing problems can be divided into six categories: fundamental train, ball spin, ball pass of the outer race, ball pass of the inner race, misalignment, and oil whirl (journal bearings). An example of a vibration spectrum showing bearing frequencies is presented in Figure 2.5 [7].

Looseness can occur anywhere in the motor or attached system because of parts that are not securely mounted. An example of mechanical system with looseness is given in Figure 2.6 [7].

The two major problems with rotating machines are due to the coupling with other components. These are imbalance and misalignment. Imbalance of this nature occurs when the shaft is coupled to a system whose center of mass does not rotate along the axis of rotation.

Putting all the component vibration factors together, one may encounter a vibration spectrum similar to the one shown in figure 2.7 [7].

Note, however, that there are problems that are seen in the current analysis that do not

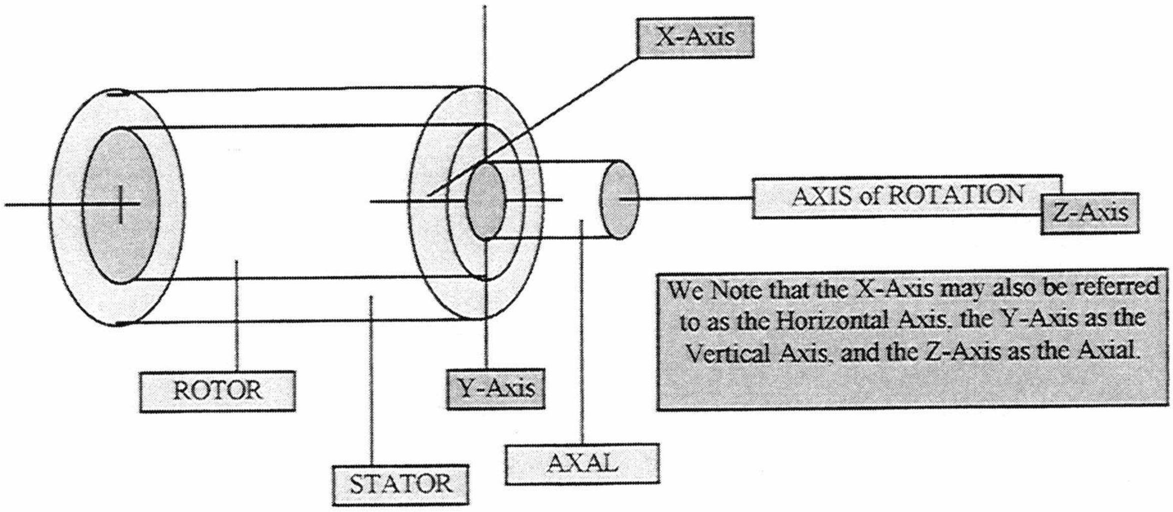

Figure 2.3. Basic induction motor components.

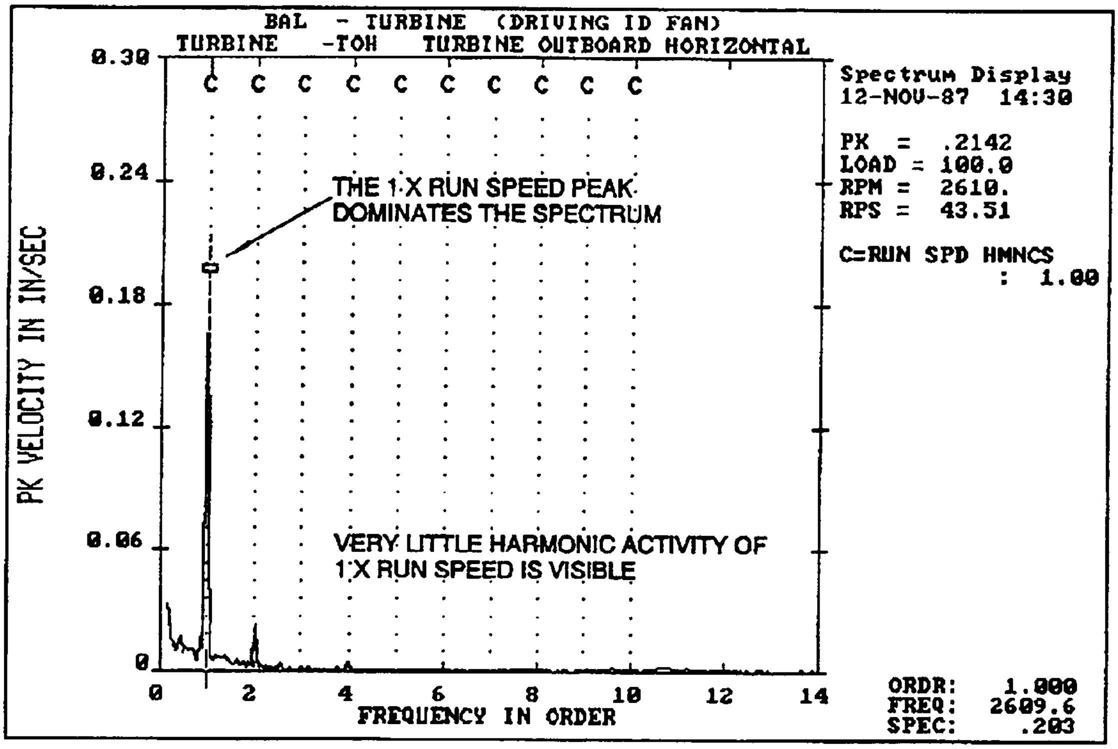

Figure 2.4. Imbalance example [10].

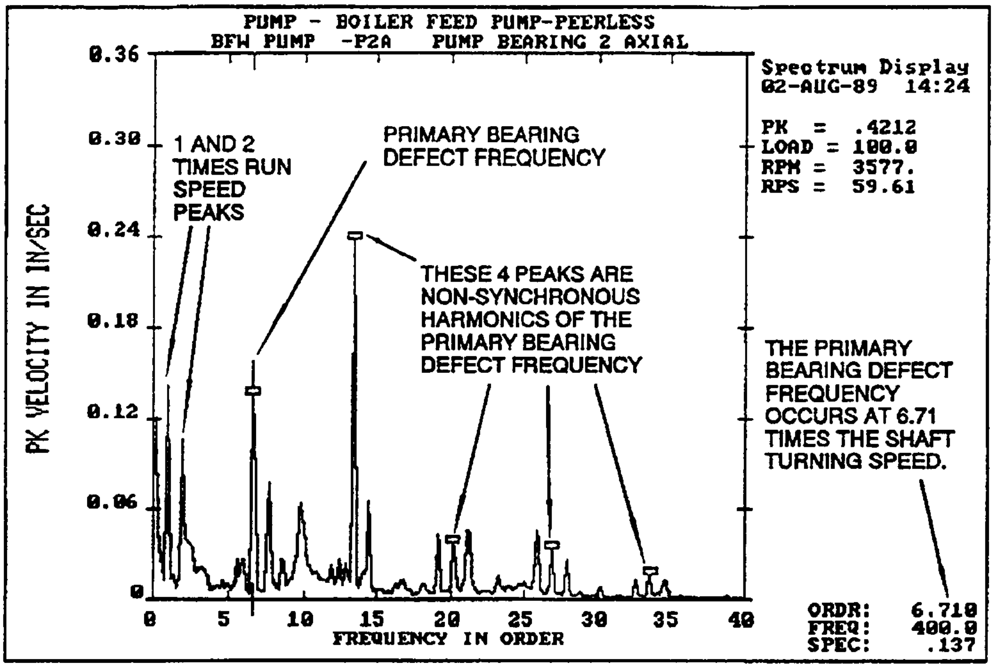

Figure 2.5. Example of bearing vibration spectrum [10].

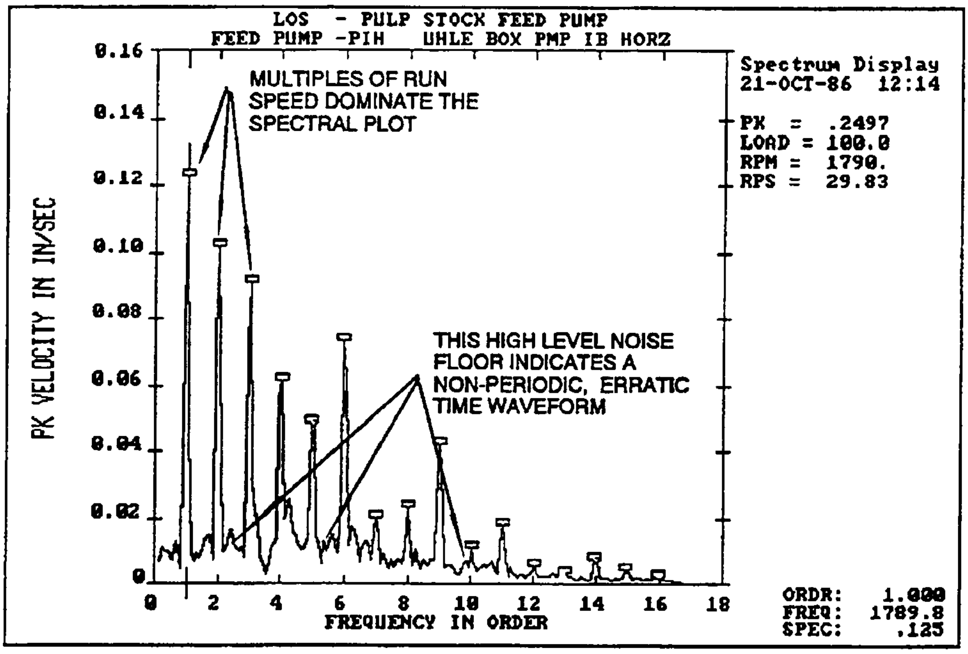

Figure 2.6. Example of a Looseness spectrum [10].

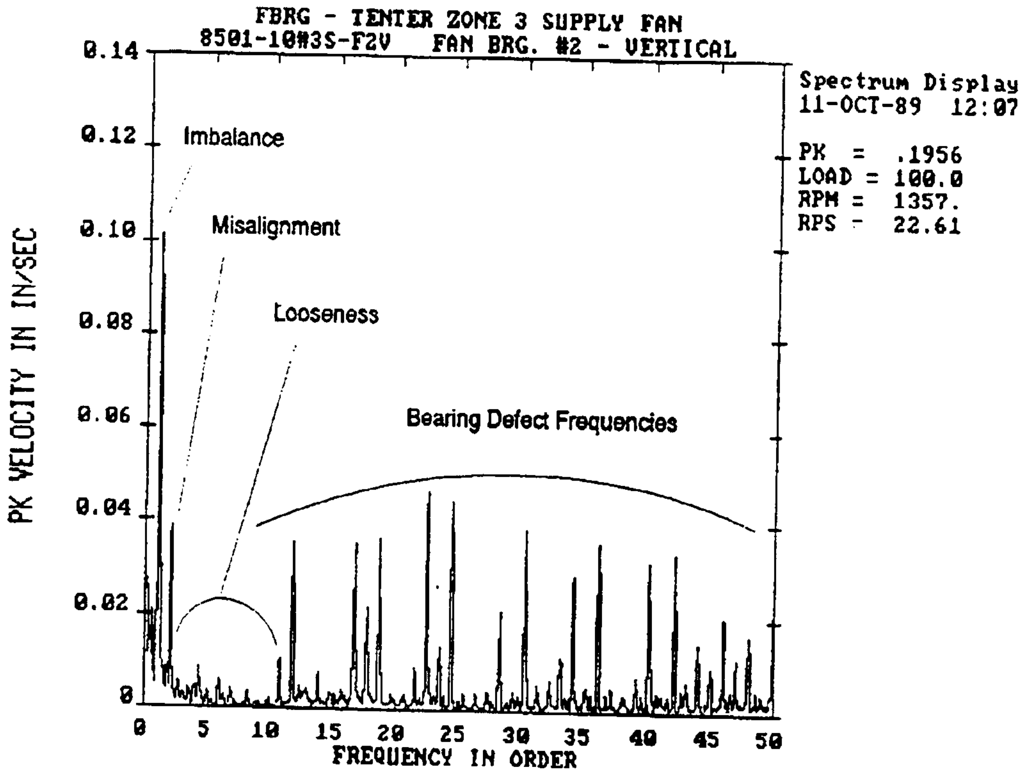

Figure 2.7. Vibration spectrum [10].

appear in the vibration analysis. These problems are broken rotor bars, cracked end rings, high resistance squirrel cage joints, casting porosity in the die cast joints, static and dynamic air gap irregularities, and unbalanced magnetic pull [8]. Therefore, since there is extra information contained in the current signature, there should not be an exact match or coherence between current and vibration signals at all frequencies.

2.3.3 Motor Power Analysis

"If mechanical abnormality develops in a drive system, harmonic torques are generated in the motor, accompanied by speed oscillation and modulation of the stator current. Frequency components characteristic of the type of abnormality appear in the power spectrum of the stator current. Location of these components allows identifying the abnormality [9]."

Power analysis, as discussed in this section, refers to either the instantaneous power input to the stator windings (power input to the motor, Instantaneous Power) or the power input into the dynamometer (power output of the motor, Torque Derived Power).

2.3.3.1 Instantaneous Power

Instantaneous power is defined as the instantaneous voltage between any to phases multiplied by the instantaneous current drawn by either phase. For a three-phase induction motor, the motor may be wired either in delta or Y-configuration. The currents and voltages are defined for the delta configuration as

$$I_p = \frac{1}{\sqrt{3}} I_l \tag{2.1}$$

and

$$V_p = V_l \tag{2.2}$$

Where: I_p = RMS Phase current

I_l = RMS Line current

V_p = RMS Phase voltage

V_l = RMS Line voltage.

For a balanced three-phase induction motor wired in the delta configuration, the active power is given by

$$P_{act} = \sqrt{3}\ I_l\, V_l \cos(\theta) \tag{2.3}$$

where theta equals the angular displacement of the sinusoidal voltage to the sinusoidal current waveform, expressed in degrees, and also referred to as the phase angle. However if the system is not balanced or if the waveform is not exactly sinusoidal, instantaneous power can be calculated as

$$P_{instant} = \frac{1}{\sqrt{3}}(I_x V_{xy} + I_y V_{yz} + I_z V_{zx}). \tag{2.4}$$

The time average of the instantaneous power over one period of the waveform is referred to as the active power. Similarly, apparent power is defined using the RMS values of the line current and voltages as

$$P_{apparent} = \frac{1}{\sqrt{3}}\ [\mathrm{rms}(I_x)\ \mathrm{rms}(V_x) + \mathrm{rms}(I_y)\ \mathrm{rms}(V_y) + \mathrm{rms}(I_z)\ \mathrm{rms}(V_z)]. \tag{2.5}$$

The ratio of the active power to the apparent power now defines the power factor and is equal to the cos(θ) for a balanced system [10].

$$\cos(\theta) = P_{active} / P_{apparent}. \tag{2.6}$$

If a mechanical abnormality develops in the drive system, harmonic torques are generated in the motor, accompanied by speed oscillations and modulation of the stator current. Frequency components characteristic of the type of abnormality appear in the power spectrum of the stator current. Location of these components allows identifying the abnormality.

Power analysis provides much of he same information that current analysis provides but may also provide additional information because of the addition of the voltage signal. When the power factor is low, the motor power is a better representation of the load than the motor current. The characteristic spectral component of the power appears directly at the frequency of the disturbance, independently of the synchronous speed of the motor. The irrelevant frequency components, i.e. those at multiples of the supply frequency, are screened out.

The side-band components provide an important additional piece of information about motor defects. Torsional vibration, broken rotor bars, mechanical imperfections in the drive train, such as imbalance and eccentricities of the rotating parts and misalignment of the motor and load shafts are among the problems that can be detected [9]. It is worth mentioning that application of the instantaneous input power for detection of electrical faults in the stator has already been proposed in another paper [11].

An example of a stator current spectrum with a variable load is shown in Figure 2.8. As shown earlier in Figure 2.2, the motor current has a large 60 Hz peak which corresponds to the electrical line input, side-bands and also two line harmonics at 120 and 180 Hz.

The next example, Figure 2.9, shows the power spectrum of instantaneous power of the motor. The same type of peaks are seen, those being the power peak at 120 Hz and the power harmonics at 60, 180 and 240 Hz. But also notice that there is a peak at 10 Hz (marked by the arrow) that is the frequency of load oscillation. The peak is not found in the line current spectrum. Thus, motor power analysis is very similar to the motor current analysis except for the added information mentioned above.

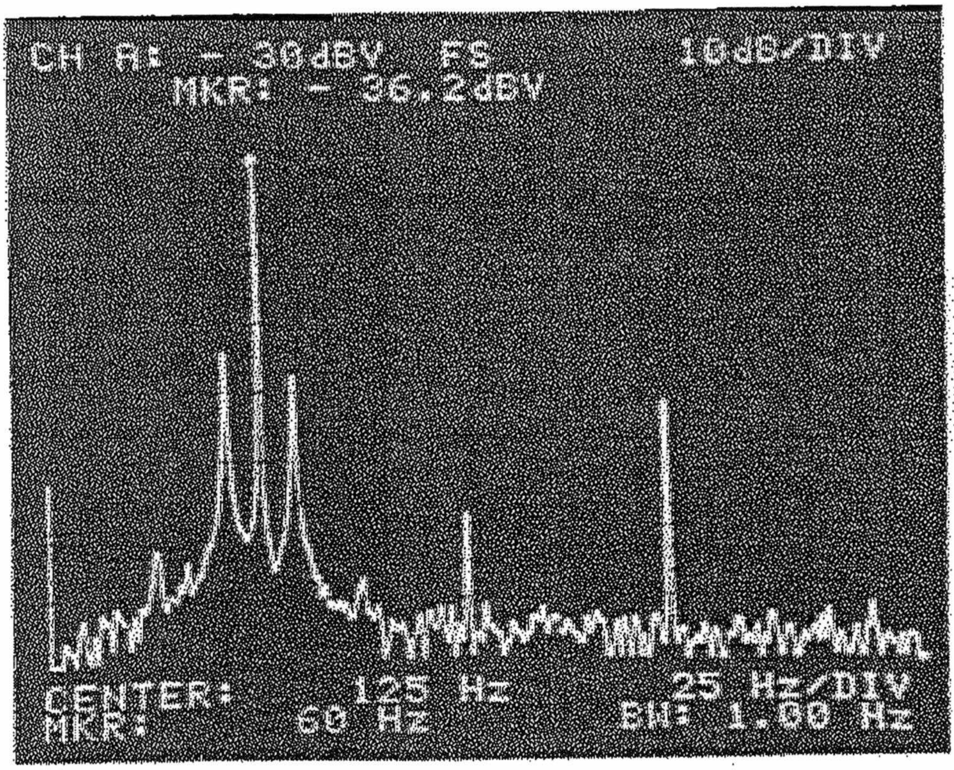

Figure 2.8. Motor current spectrum [12].

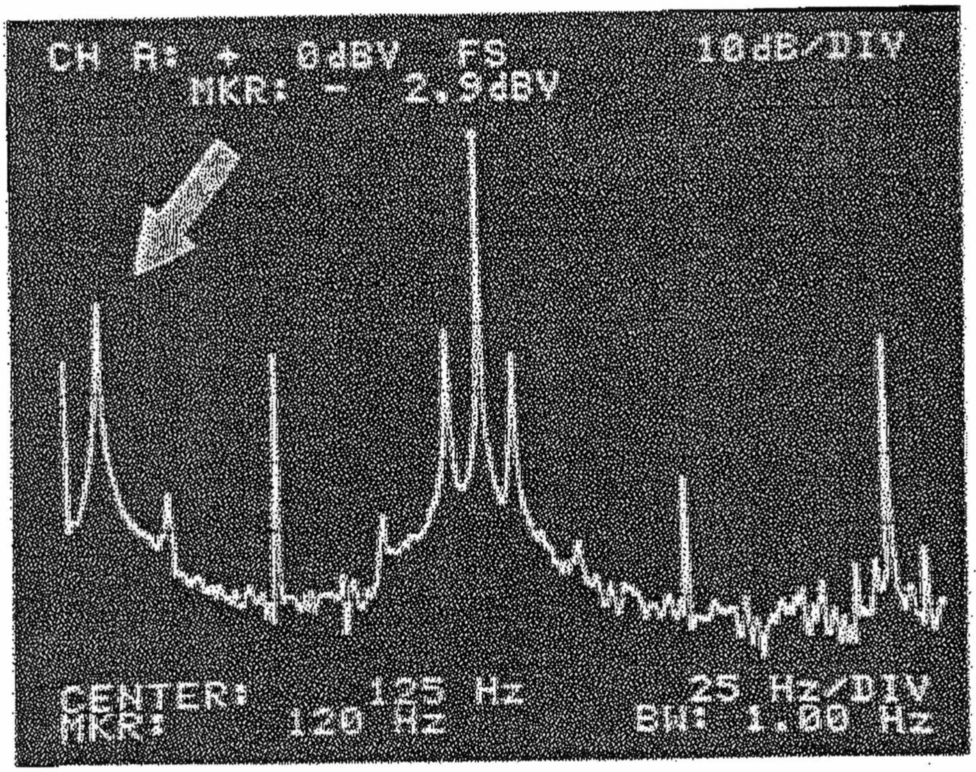

Figure 2.9. Instantaneous motor power spectrum with variable load [12].

2.3.3.2. Torque Derived

The power input into the dynamometer can be determined by using the RPM, and the torque. The equation relating the power to RPM and torque is given by:

$$\text{Power} = \text{constant} * \text{RPM} * \text{torque} \tag{2.7}$$

The torque and RPM are usually instantaneous readings that are multiplied together. This is another method in which motor load power can be monitored. The difference is that the instantaneous power is derived from current and voltage input into the motor, and the torque-derived power is measured as the motor mechanical output.

2.3.4. Impact Resonance

Impact resonance involves an analysis of vibration spectra generated when the motor is struck sharply in order to generate an impulse shock wave. This is used to determine the resonance frequency of the structure.

2.3.5. Thermal Analysis

Thermal analysis is usually performed by two methods: measurement by direct contact or by thermal imaging. Direct contact gives a more precise reading as far as the location is concerned. The detection device may be positioned almost anywhere inside or outside of the motor. Thermal imaging gives an overview of the temperatures on the surface of the motor. But both can provide valuable information.

Excessive and prolonged heat is the main factor responsible for shortening the life expectancy of motors. The two components most affected by excessive heat are the winding insulation and the bearings. Trending temperature measurements is a simple and fast method of estimating motor overheating. Common methods of overheating are overloading, bearing seizure, misalignment, ventilation, single phasing, high ambient temperatures, excessive duty cycles, and power supply variations. Motor temperature rise is a function of bearing friction, windage, core loss, copper losses (referred to as I^2R losses) and stray losses [12]. Other problems that may exist in the rotor are thermal unbalance and hot spots [13]. These specific problems are discussed later in this section.

2.3.6. Magnetic Flux

Any small imbalance in the magnetic or electric circuit of motors is reflected in the axially transmitted fluxes. A simple sensor for detecting these signals is a flux coil. Many of the frequencies are related to the speed of the motor. It also appears that flux measurement can supply a preliminary indication of rotor bar defects, electrical faults, increase side-band frequencies, unbalanced voltage, stator faults, and shaft currents [12]. The coil should be placed on the axial outboard end of the motor. The magnetic flux would detect many of the same problems that current analysis yields. An example of the magnetic flux spectrum is shown in Figure 2.10.

The majority of the peaks in the flux coil spectrum occur at frequencies which have some relationship to running speed. Therefore, the speed of the motor can also be determined. By knowing the running speed, an estimate of the load can be made.

The magnetic flux spectrum has been shown to provide information about rotor bar condition. Flux spectrum frequencies associated with the rotor bar condition occur at (number of poles X slip frequency) side-bands of the line frequency (just as seen in the motor current measurements). An example of the rotor bar anomaly detection is shown in Figure 2.11. While the amplitude differences may not be the same as found from the current measurements, the relative difference between the line frequency and the appropriate side-band decreases as the rotor degrades.

Any phenomenon producing electric or magnetic changes, such as turn-to-turn winding shorts and unbalances in supply voltages, create greater asymmetries [12]. Figure 2.12 shows an example of a magnetic flux spectrum with a 2.9% unbalance in the supply voltage. We can

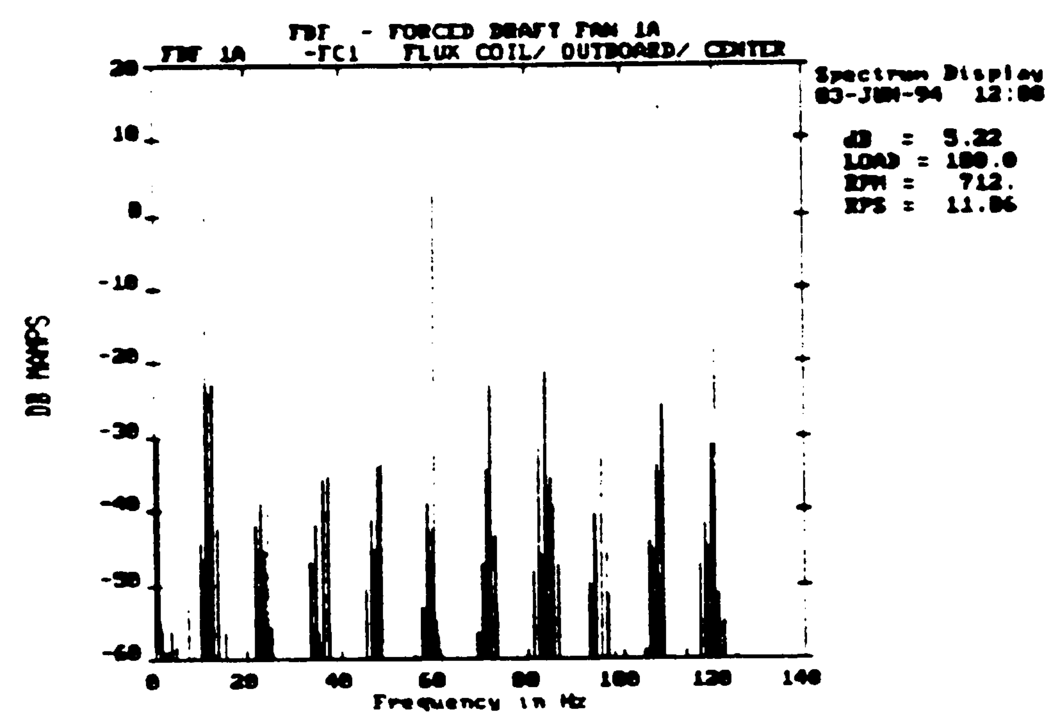

Figure 2.10. Magnetic flux spectrum [14].

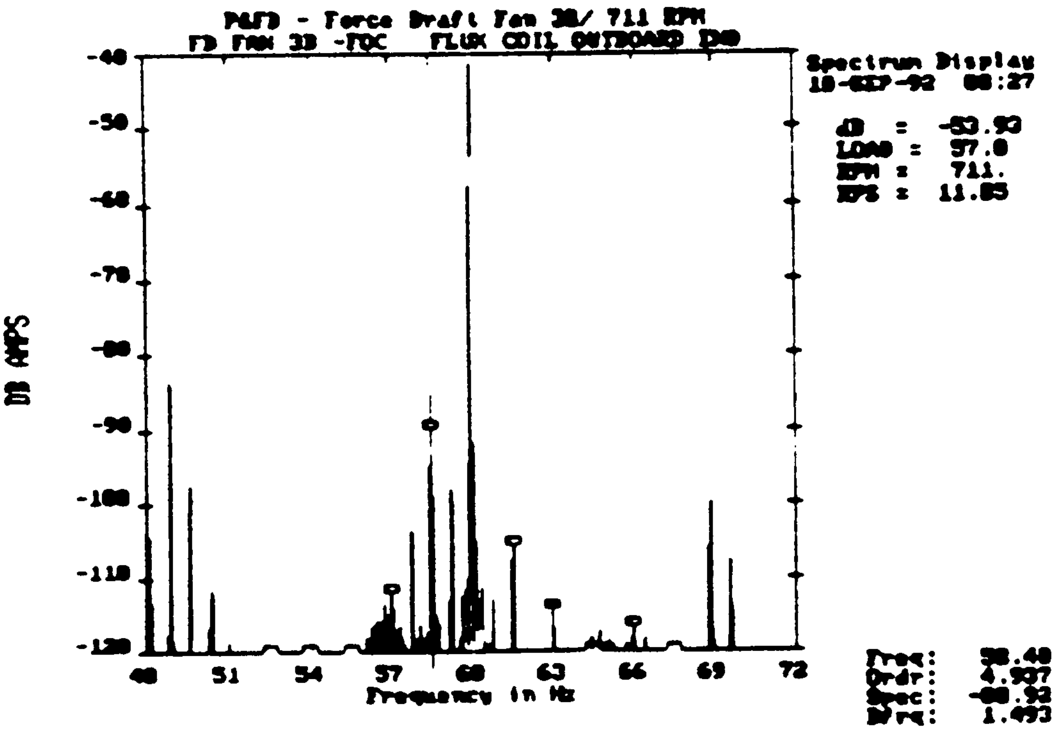

Figure 2.11. Magnetic flux spectrum with rotor bar problems [14].

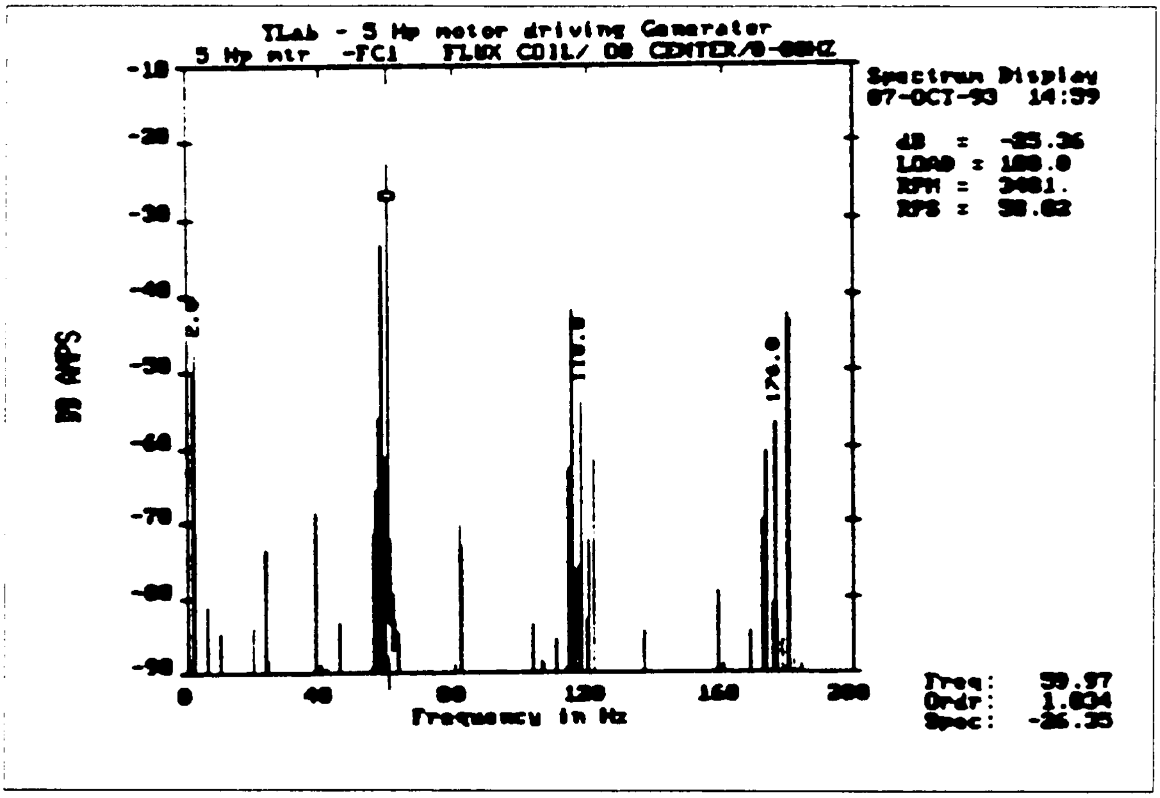

Figure 2.12. Magnetic flux spectrum with voltage imbalance [14].

identify the major magnetic flux frequency as 60 Hz, with many integer harmonics such as 120, 180, ... Hz. The magnitudes of the side-bands around these peaks indicate that there is a voltage imbalance.

Figure 2.13, shows the magnetic flux spectrum for a motor with shorted stator turns. For a motor with shorted stator turns (Figure 2.13), notice that the peaks for the 60 Hz harmonics (120, 180, etc.) are larger in magnitude than for a healthy motor.

2.3.7. Motor Circuit Analysis (MCrA)

Motor Circuit Analysis (MCrA) involves off-line measurements of four "natural" electrical parameters using closely controlled AC and DC input signals from a computer-based test unit. The measurement values are resistance in the conductor path, inductance, capacitance to ground and resistance to ground (RTG). The analysis involves development of trends, pattern recognition, correlation of combinations of patterns, statistical comparison where possible, calculation of unbalance and graphs for diagnosis of defects.

Results can be compared to well accepted standards or empirically derived guidelines. The guidelines are based on experience in analyzing tens of thousands of motors and reflect the experience of many utilities, government entities, and manufacturers who use this technology. Motor predictive maintenance personnel can then quantitatively characterize present motor circuit electrical conditions and predict future conditions such as resistive imbalance in AC three-phase motor circuits, excessive resistance in DC motor circuits, inductive imbalance, loss of inductance or resistance of armature winding circuits, presence of broken or cracked rotor bars or end rings or rotor eccentricities, DC armature shorts or opens or grounds, temperature-corrected and time-consistent RTG conditions, buildup or presence of dirt or moisture on the outside of the winding insulation systems, polarization index, dielectric absorption, or other ratios from the RTG readings and polarization index profile (PIPs) [14].

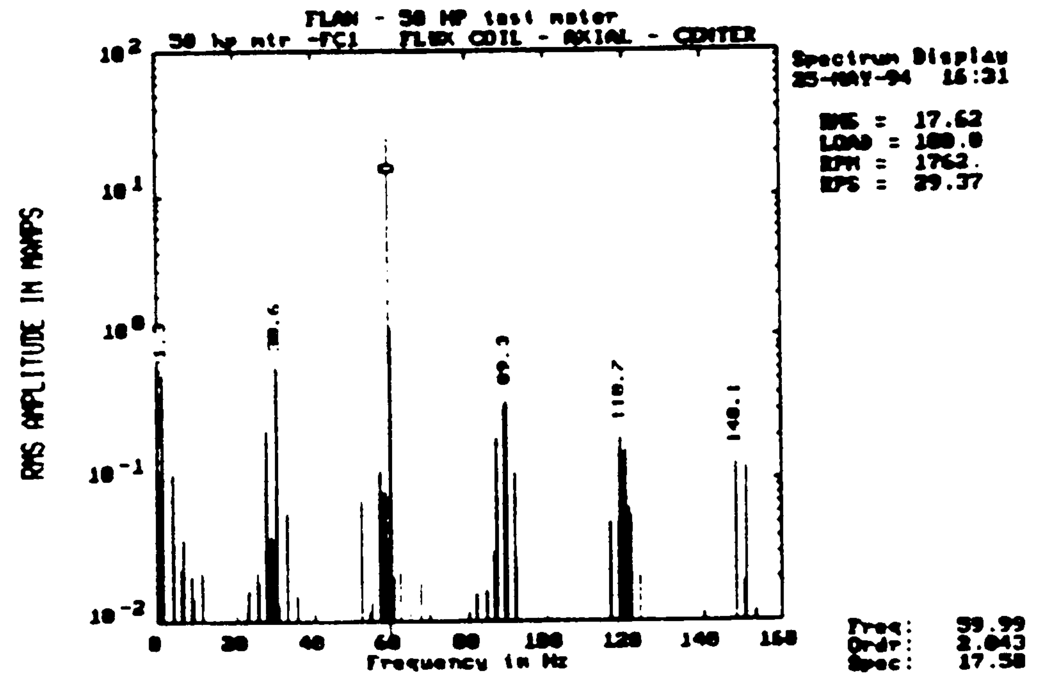

Figure 2.13. Magnetic flux spectrum with shorted stator turns [14].

2.3.8. Torque

Torque can be calculated using a dynamometer. The dynamometer applies a specific load to the shaft of the motor by coupling the shaft of the dynamometer to that of the motor. The dynamometer's stator produces and a magnetic field that reacts with the permanent magnet mounted on the dynamometer's rotor. The resistance produced is in opposite direction to that of the motor's rotation. The torque is measured by a force cell mounted at a specific distance away on the dynamometer from the axis of rotation. The torque is given by

$$\text{Torque} = \text{Force} * \text{Distance}. \tag{2.8}$$

Torque may also be measured by a variety of other methods, but this was the method used for the project. Torque may be used to calculate the power input into the dynamometer for the setup mentioned above. It is given by the relationship

$$\text{Power} = k*\text{Torque}*\text{RPM} \tag{2.9}$$

where: RPM = revolutions per minute

k = constant.

The power input into the dynamometer can be assumed to be the power output of the motor at the shaft. Power output at the shaft can be used in a variety of methods, one such method involves the calculation of motor efficiency.

2.3.9. Efficiency

The efficiency of a motor is given by the ratio of the power input to the power output. Thus, the efficiency is defined as

$$\text{Efficiency} = \text{Power output} / \text{Power input}. \tag{2.10}$$

This is a unitless number ranging from 0 to 1 or 0% to 100%. This measurement tells directly how well a motor is functioning. If the value is close to 100%, the motor is converting almost all the power input into it into output rotational energy. Conversely, if the efficiency becomes small, there is a serious problem within the motor that is causing the energy not being used in the output energy transfer.

2.3.10. Growler

One inexpensive way of locating a shorted coil is by the use of a growler and a thin piece of steel. The poles are shaped to fit the curvature of the teeth in use in a stator. Figure 2.14, shows a simplified schematic for the use of a growler.

The growler should be placed in the core (such that the windings are perpendicular to the growler) and the thin piece of steel should be placed the distance of one coil span away from the growler. Then, by moving the growler around the bore of the stator and always keeping the steel strip the same distance away from it, all of the coils can be tested. If any of the coils has one or more shorted turns, the piece of steel will vibrate very rapidly and will cause a loud humming noise [15].

2.3.11. Surge Comparison Test

"The surge comparison test evaluates the quality of turn-to-turn, coil-to-coil, and phase-to-phase insulation and detects open coils, reversed coils, and faulty insulation to ground. Sensitivity is such that even a one turn winding short circuit can be detected so that action may be taken before the problem propagates into a full scale winding failure. In the surge comparison test, two identical high voltage, high frequency pulses are simultaneously imposed on two phases of the motor windings, and the induced reflections of both pulses are displayed on the instrument oscilloscope [16]."

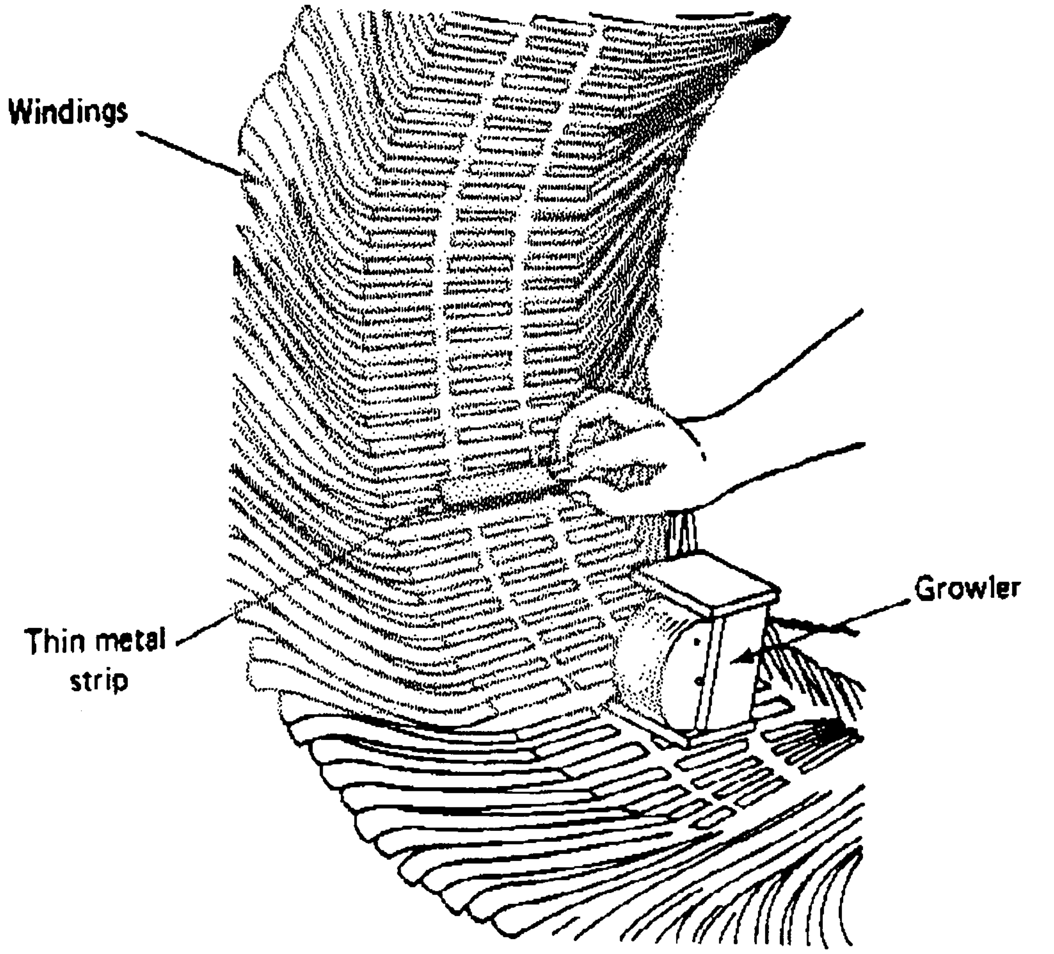

Figure 2.14. Visual example of growler use [16].

2.3.12. Partial Discharge

Partial discharges are small electrical sparks that occur in thermally aged insulation inside and outside the stator winding slots and in contaminated or damaged end turns. In medium voltage (3.3 to 4 kV) motors, a precursor to imminent winding insulation failure is an increase in partial discharge activity that occurs only a few weeks or months before complete insulation breakdown occurs [14].

2.3.13. Hi-pot Test

The DC high potential test investigates the integrity of insulation to ground. Test voltage is increased in uniform increments up to the maximum prescribed for the motor. Leakage current is read on a test instrument micro-ammeter, and the leakage current is plotted versus the test voltage on a graph paper. Healthy insulation results in a uniform increase in the current for every increase in test voltage early in the test, after which the increase in the current tapers off.

2.3.14. Tap Test

The tap test is used to detect broken or loose rotor bars. The method is to lightly tap the rotor assembly with a mallet. Broken or loose rotor bars have a distinct sound.

2.3.15. Shaft Current

Shaft current is introduced by transformer action; an alternating current flowing in the primary develops a fluctuating magnetic field that introduces a voltage in the secondary. Asymmetrical air gaps result in a net magnetic field that induces a voltage in the rotor, with the rotor acting as a single turn secondary. The resultant current flow has a path through the rotor, bearings, and frame [17].

Figure 2.15 shows the usual path that the shaft current takes within the motor. Note that the path of the current is through the bearings. Thus a large current may damage the bearings over time. The damage is often called bearing fluting.

2.3.16. Positive, Negative and Zero-Sequence Indexes and Ground Fault Current

The following transformations are used in order to calculate the zero-, positive- and negative-sequence components of each current and voltage measurement as indicated in Figure 2.1:

$$\begin{bmatrix} I^0 \\ I_x^+ \\ I_x^- \\ I_y^+ \\ I_y^- \\ I_z^+ \\ I_z^- \end{bmatrix} = \frac{1}{3} * \begin{bmatrix} 1 & 1 & 1 \\ 1 & \Psi & \Psi^2 \\ 1 & \Psi^2 & \Psi \\ \Psi & 1 & \Psi^2 \\ \Psi^2 & 1 & \Psi \\ \Psi & \Psi^2 & 1 \\ \Psi^2 & \Psi & 1 \end{bmatrix} \begin{bmatrix} I_x \\ I_y \\ I_z \end{bmatrix} \tag{2.11}$$

where

$$\Psi = e^{j\frac{2}{3}\pi} = -0.5 + j * 0.866 \text{ and } \Psi^2 = e^{j\frac{4}{3}\pi} = -0.5 - j * 0.866 \tag{2.12}$$

The superscript 0 denotes the zero-, + denote positive and - denotes negative-sequence-component of the corresponding x, y and z phase currents. The component analysis for the voltage has the same format as the following equation:

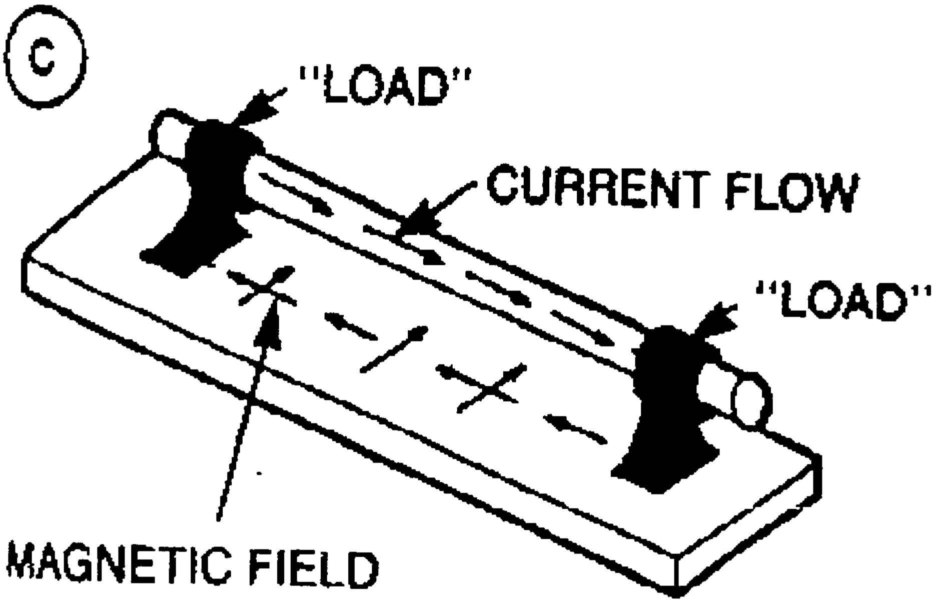

Figure 2.15. Shaft current [18].

$$\begin{bmatrix} V^0 \\ V_x^+ \\ V_x^- \\ V_y^+ \\ V_y^- \\ V_z^+ \\ V_z^- \end{bmatrix} = \frac{1}{3} * \begin{bmatrix} 1 & 1 & 1 \\ 1 & \Psi & \Psi^2 \\ 1 & \Psi^2 & \Psi \\ \Psi & 1 & \Psi^2 \\ \Psi^2 & 1 & \Psi \\ \Psi & \Psi^2 & 1 \\ \Psi^2 & \Psi & 1 \end{bmatrix} \begin{bmatrix} V_x \\ V_y \\ V_z \end{bmatrix} \tag{2.13}$$

where the equivalent phase-to neutral voltages are expressed in terms of phase-to-phase voltages as:

$$V_x = \frac{V_{xy}}{\sqrt{3}}, \ V_y = \frac{V_{yz}}{\sqrt{3}} \text{ and } V_z = \frac{V_{zx}}{\sqrt{3}} \tag{2.14}$$

The component analysis for impedance is given by

$$\begin{bmatrix} Z^0 \\ Z_x^+ \\ Z_x^- \\ Z_y^+ \\ Z_y^- \\ Z_z^+ \\ Z_z^- \end{bmatrix} = \begin{bmatrix} V^0 / I^0 \\ V_x^+ / I_x^+ \\ V_x^- / I_x^- \\ V_y^+ / I_y^+ \\ V_y^- / I_y^- \\ V_z^+ / I_z^+ \\ V_z^- / I_z^- \end{bmatrix} \tag{2.15}$$

It is seen that, except for the zero-sequence component all of the other components are complex. So, the RMS magnitude and angle of the component sequences are trended for current, voltage and impedance. Using this methodology, the amount of phase imbalance can accurately be determined independent of motor load and source imbalance by using the ratio of the negative sequence voltage to the negative sequence current. This sequence impedance index or impedance due to phase imbalance is a good indicator of turn-to-turn insulation condition since it is independent of slip.

The negative sequence indexes are given by

$$Z_x^- = \frac{|V_x^-|}{|I_x^-|}, \quad Z_y^- = \frac{|V_y^-|}{|I_y^-|} \text{ and } Z_z^- = \frac{|V_z^-|}{|I_z^-|} \tag{2.16}$$

Ground fault current is a symptom of turn-to-ground insulation failure. Very low level ground fault currents between 100 mA to 2 amps can be used only as a possible indication of a fault, since capacitance charge currents can indicate a false ground fault. However, the combination of low-level negative sequence impedance and low-level ground fault is a positive indication of insulation failure. On the other hand, a ground fault current that propagates to a threshold level of 5 amps or more is an imminent indication of motor failure [18,19].

2.3.17. Resistance to Ground (RTG) Testing

RTG instruments measure the current flowing to and through an insulated system to ground under the pressure of a known electromotive force. The test result, in ohms, is derived by dividing the known voltage by the measured current. The condition being monitored is the integrity of the insulation system isolating the power conductors from the ground [14].

2.3.18. Polarization Index (PI)

"Polarization Index tests require the application for a period of 10 minutes of a DC voltage from an RTG (resistance to ground) test unit. The value of the resistance at 10 minutes divided by the value at 1 minute gives the unitless ratio called the 'Polarization Index' [20]." This test is used to determine the condition of the stator insulation.

2.3.19. Polarization Index Profile (PIP)

The PIP (or Polarization Index Profile) is an extension of the PI test. The PI test only uses the value of resistance at 10 minutes and 1 minute to determine a ratio. The PIP graphs all the values during the 10 minutes it takes in the PI test to generate the PI. The graph generated has time for the x-axis and resistance for the y-axis. The units for resistance are usually in megaohms with time measured in seconds for the entire 10 minutes.

The example, shown in Figure 2.16, exhibits a good PIP of a DC motor with good resistance to ground and low RTG ratios measured over a 10 minute time interval. The example in Figure 2.17, is a PIP of a DC shunt field with intermittent grounds caused by moisture in a deteriorating insulation system. Notice the oscillating values of RTG [20].

2.3.20. Cepstral Analysis

"Cepstrum analysis is basically a spectrum of a spectrum. It is a technique which is able to detect and quantify periodicity in spectral data using the FFT. Harmonics appear in the spectrum at equally spaced peaks - equally spaced peaks equate to a periodicity. So if we take an FFT of the spectrum, we will have a new data set with peaks at the frequency of the source of the harmonics [20]." Other related cepstra sources are listed in references [22] and [23].

2.4. Other Tests

The tests reviewed in this section were mentioned in the literature used for this report, but the specifics of the tests are not described. These included such tests or test methods as **Rotor Core Loop Test, Single-Phase Rotational Test, No-Load Saturation Test, Ultrasonic, Visual, Current Pulse Under Load, and Phase Angle Displacement**.

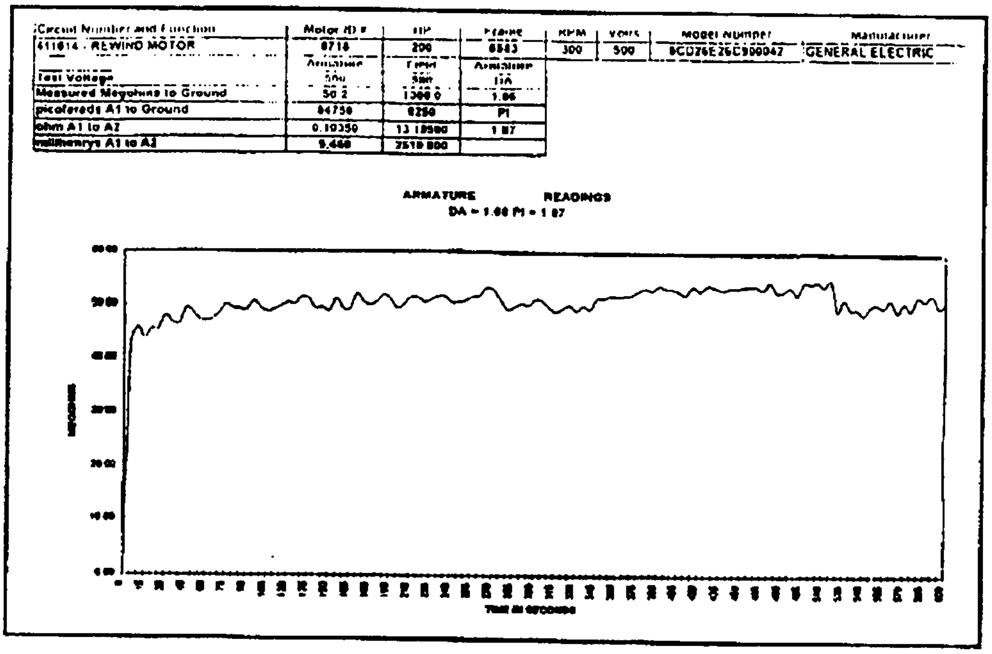

Figure 2.16. PIP of a good DC motor [20].

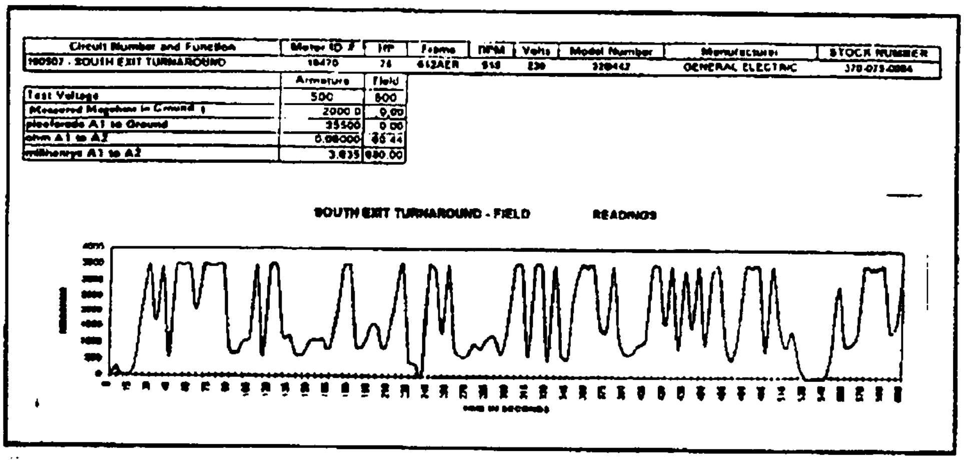

Figure 2.17. PIP of deteriorating DC motor [20].

Chapter 3

DESCRIPTION OF MOTOR AGING EXPERIMENTS AND LOAD TESTING

3.0. Electric Motor Description

The induction motors used for the motor aging project were 5-HP, three-phase, 220-Volt, 15-Ampere (maximum start-up), 12 Amperes continuous, squirrel cage motor. To start the description, discussion of the electrical aspects of the project electric motors are given.

The three-phase induction motor may be wired in two different fashion, star and delta connections. The motors used for the project were connected in the delta configuration. The delta configuration is given by the basic diagram in Figure 3.1.

As seen in Figure 3.1, there are three different voltages and currents corresponding to each motor. In this configuration, the phase current (I_p) and phase voltage (V_p) are related to the line current (I_l) and the line voltage (V_l), respectively as follows.

$$I_p = \frac{1}{\sqrt{3}} I_l \tag{3.1}$$

and

$$V_p = V_l \tag{3.2}$$

where: I_p = RMS Phase current

I_l = RMS Line current

V_p = RMS Phase voltage

V_l = RMS Line voltage.

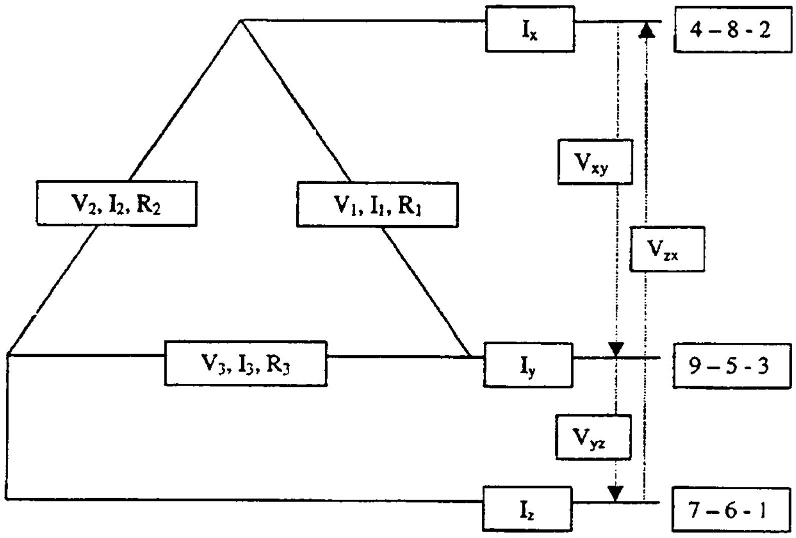

Figure 3.1. Delta configuration for a three-phase induction motor [10].

Since there are three different phases, there are three separate electrical waveforms being used by the motor. Each electrical waveform is separated from the other by a phase angle of 60 degrees. If the currents or voltages are plotted against time, each waveform is identical except for the phase difference. This is shown in Figure 2.1.

Measurement of the input currents to the motor yields a slightly different graph for the three currents than shown above. The time-domain plots of the currents show small variations in the input current. The variations are rather small in nature and at a higher or lower frequency than the example above. The variations in the measured input current to the motor are caused by the electrical design and abnormalities associated with the motor. These variations are the data to be analyzed.

3.1 Stator Aging Procedure

The objective of this aging mode is to subject the stator insulation to elevated temperatures. In order to accomplish this, the motors were subjected to repeated on-off cycling, using a motor relay which is controlled by a time delay. This unit is powered with a standard 110 Volt AC line source. Upon application of the power, which is the on and off button of the whole test setup, a preset delay begins. This is the off delay time and can be programmed from 0.6 seconds up to 24 hours. At the end of the preset delay, the relay contacts transfer and remain in that condition for a specified, independently adjustable preset time. This time is called the on time and is also adjustable from 0.6 seconds to 24 hours. At the end of this preset time, the relay contacts drop out and the sequence repeats until the power is cut off. The Winding Insulation Aging Test has only two of three phases, phases X (connections 7-6-1) and Z (connections 4-8-2) in order to heat the motor to a constant 205 C for the specified aging time of 48 hours [10].

3.2. Bearing Fluting Aging Procedure

Fluting is a fault in which the ball bearing surface, and/or the inner and outer races of the bearing get damaged caused by electrical sparking. As a result, rolling elements and the races get damaged. This surface degradation causes extreme vibration levels of the bearing and its eventual failure.

The fluting run has a duration of 30 minutes with the motor rotating at no load, and an externally applied shaft current of 27 Amperes at 30 Volts AC (see Figure 3.2). The motor is delta connected with Phase X (black) connected to 4-8-2. Phase Y (red) is connected to 9-5-3. Phase Z (white) is then connected to 7-6-1. This wire connection was used for all test motors.

The fluting aging is followed by thermal and chemical aging in order to increase and accelerate the aging process. One test cycle is defined as follows

1. The motor is fluted for 30 minutes.
2. Afterwards, the motor is put into the oven, which is at 140 C.
3. The motor is heated at this temperature for 72 hours. It is then removed from the oven and cooled for 6 hours.
4. The motor is then fully immersed in water for 15 minutes and then taken out and put into the oven immediately for another 72 hours of heating.
5. The motor is taken out of the oven after 72 hours and cooled for 6 hours.
6. At the end of each aging cycle the motor is tested on the dynamometer [10].

3.3. Motor Load Testing

Initially and after each aging cycle the motors were tested at varying loads. The testing started with the motor off and then turned on with the motor uncoupled from the dynamometer. This was done to capture the start-up current rush of the motor. The motor was then allowed to run until the temperature of the motor stabilizes. Stabilization of the temperature indicates that

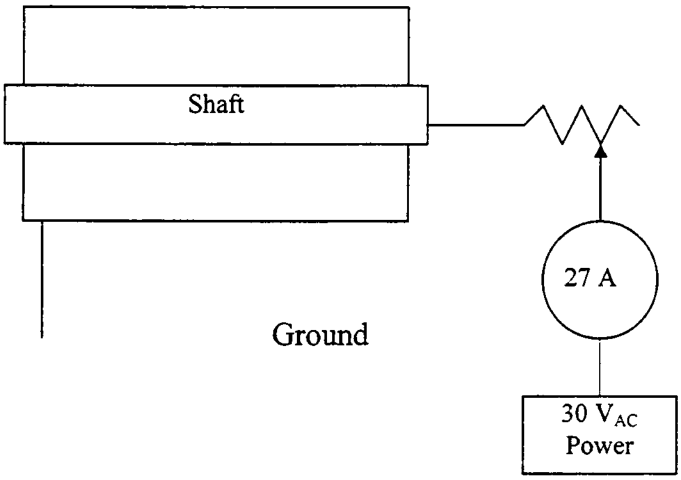

Figure 3.2. Schematic of the electrical motor bearing fluting setup.

the motor was at steady state. Once the temperature stabilizes, the motor signals were recorded. Once the recording was finished for steady state, shutdown was also recorded for the uncoupled situation. The motor was then coupled to the dynamometer with the dynamometer set to 0% load. Again, as before in the uncoupled testing, the same procedure was followed except that the motor was not turned off and the shutdown was not recorded. Once the signal acquisition was completed for 0% load, the motor load was set at 115% for a specified period of time. This procedure helped speed up the increase in motor temperature. After the specified period of time, the dynamometer was then set to 25% load. The motor was run till the temperature stabilized and then the data acquisition was accomplished. This was repeated for 50%, 75%, 100% and 115% loads. Once these loads were recorded, a shutdown at 115% load was recorded. The motor was then ready for another cycle of aging. Figure 3.3 is a schematic of the motor test facility and data acquisition system. Table 3.1 shows a list of signals recorded for each test.

The vibration data were measured at three perpendicular points on the motor, axial, vertical, and horizontal. The axial vibration data were measured at the end of the motor, opposite from the shaft. The vertical data were collected at the shaft end of the motor at a 10 o'clock position relative to the floor. The horizontal data were collected at the 2 o'clock position also relative to the floor. There was also a motor cover vibration sensor mounted in the middle of the motor at the 2:00 position. The current was sampled utilizing the three different phases for three separate measurements.

For high frequency data acquisition, the data were sampled for 10 seconds at a sampling rate of 12 kHz. For each individual vibration set, using 10-second data acquisition, there is a total of 120,000 data points. For the low frequency acquisition, the data were sampled at 200 Hz for 60 seconds, producing 12,000 data points.

The data were sampled at a high rate in order to avoid Nyquist folding of the signal. Nyquist folding (or alaising) occurs when the signal is sampled at a rate less than 2 time the maximum frequency of the sampled signal. Using the Nyquist criterion, a maximum frequency of 6 kHz was available.

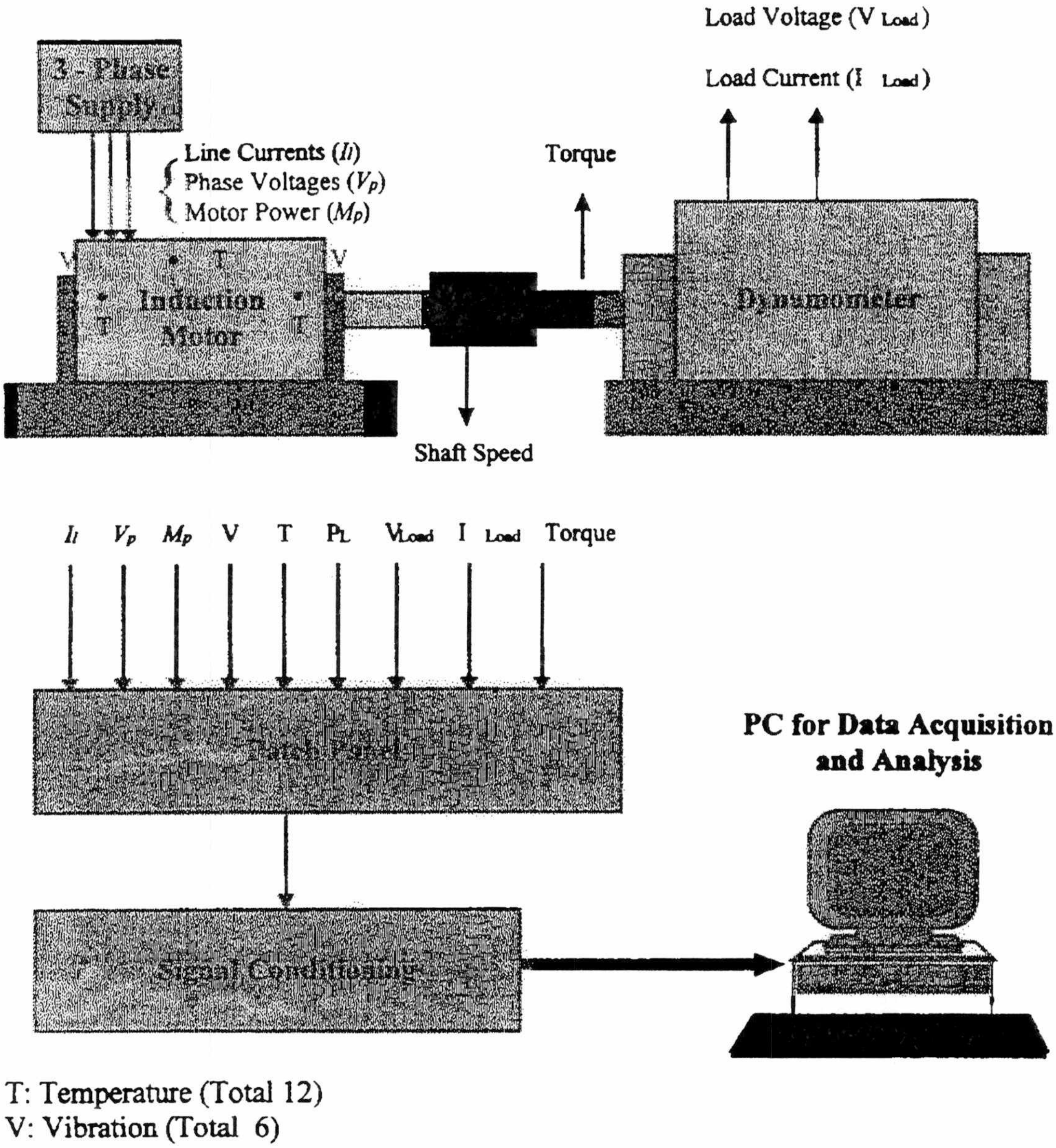

Figure 3.3. Schematic of the motor test facility and the data acquisition system.

Table 3.1. List of signals recorded for each test. Type of signal in bold.

Line Currents	**Line Voltages**
I_x	V_x
I_y	V_y
I_z	V_z
Load Current	**Load Voltage**
I_l	V_l
Fan Cover Vibrations	**Motor Cover Vibrations**
V_A	$V_{10:00}$
V_H	$V_{2:00}$
V_V	V_{cover}
Motor Power	
M_p	
Torque	
Temperatures (12)	

The sampled data were stored in binary form on the data acquisition computer. The data were then transformed into an ASCII file so that the data could be read directly into the MATLAB framework by using the 'load' function along with the file name.

Chapter 4

ANALYSIS THEORY FOR DEFECT CHARACTERIZATION

4.0. Introduction

This chapter describes the theory used for calculating specific frequencies seen in both the vibration and motor current signals as determined by physical characteristics of the motor and its components. It is divided into three sections, motor current, vibration and the relationship between motor current and vibration.

4.1. Motor Current Analysis

As stated before, Motor Current Analysis can be used to determine the condition of various parameters within the motor system. These parameters include: rotor cage defects, broken rotor bars, shorted stator turns, shorted laminations, high resistance connections, and motor bearing damage [24].

The power spectra of the currents should reveal a large peak at 60 Hz, as seen in Figure 2.2, and also many other peaks associated with the harmonics of the line current and harmonics of the actual operating frequency of the motor and movement of the rotor shaft. Most types of problems will show up in the current spectrum as abnormalities added to the ideal current spectrum around 60 Hz.

The motor shaft frequency is less than the synchronous field frequency. There are also motor current spectral frequencies generated by the difference in the frequency of rotation of the shaft and the motor's synchronous frequency. The equation below gives most of the harmonic frequencies seen in a current spectrum caused by this difference [25].

$$f_{ecs} = fe * [1 \pm (k * f_{slip} * P)] \tag{4.1}$$

where: fe = electrical supply frequency

P = number of poles = 4

$f_{synch} = 2*fe / P$

f_{shaft} = shaft turn frequency ~ 29 Hz.

f_{slip} = slip frequency = $f_{synch} - f_{shaft}$

k = 1, 2, 3, ...

Thus, by using Equation (4.1), we obtain frequency peaks that should be seen in the current spectrum. Some appear in side bands of the 60 Hz supply frequency.

The predicted stator current frequencies (fe_{bng}) caused by bearing vibrations, which induce rotor movement are [25]

$$fe_{bng} = | fe \pm m^*fv_{bng} | \tag{4.2}$$

where: m = 1, 2, 3, ...

fe = electrical supply frequency

fv_{bng} = characteristic vibration frequencies.

Note that the 60 Hz spectral peak, along with slip frequencies, are determined by using the appropriate input data into Equation (4.1). Therefore, by using the above two equations, identification of most of the major peaks within a motor current spectrum can be accomplished.

4.2. Vibration Analysis

The purpose of a motor is to supply mechanical energy to an outside system. The observable moving part of the motor is the motor shaft. The motor shaft has the rotor mounted on it. The rotor/shaft assembly rotates with supports provided by bearings. The bearings are solid mounted in the motor casing and to the rotor/shaft assembly, thereby allowing the rotor shaft to rotate within the bearings but also to be a solid fixture of the motor system.

There are two main areas of the motor system that cause vibration, one is within the motor and related to the motion of the shaft, and the other due to the manner in which the motor is coupled to the outside system. Before these problems are analyzed, the fundamental frequency of rotation must be defined.

The speed of the rotation is used to determine the fundamental frequency of the motor system. The unit of frequency is a Hertz (cycles / second) or Hz, with the fundamental frequency of the motor defined by

$$fundamental\,frequency = f_{fund} = \frac{RPM}{60} \tag{4.3}$$

where: RPM = shaft revolutions per minute.

The fundamental frequency is used throughout the vibration analysis to determine the frequency components in the vibration spectra caused by various problems. The focus now is on the vibration modes associated with a rotating system.

The motion within the motor could be caused by an imbalance, misalignment, bearing defects, and/or looseness. Imbalance is caused when the center of mass of the rotor/shaft system is not centered along the axis of rotation. The imbalance is characterized by vibration with a frequency equal to that of the rotational speed of the shaft.

$$f_{imbal} = 1 * f_{fund} \tag{4.4}$$

where: f_{fund} = fundamental frequency of rotation.

The highest magnitude vibrations are at 90 degrees perpendicular to the shaft.

Misalignment vibrations occur at 1 and 2 times the rotational speed. "Oil whirl happens at integer multiples of 38-49% of the fundamental rotational frequency. All other associated vibrations occur at characteristic sub-harmonic and integer multiples of the rotational frequencies and associated harmonics.

These characteristic numbers are given by physical characteristics of the bearings themselves. Thus, these generated bearing vibration frequencies are defined by the fundamental frequency of rotation by

$$f_{misalign} = N^* f_{fund} \tag{4.5}$$

$$f_{bearings} = M^*(characteristic\ sub\text{-}harmonic\ or\ integer\ frequency) \tag{4.6}$$

$$f_{oilwhirl} = 0.38\ to\ 0.49^* M^* f_{fund} \tag{4.7}$$

with N = 1 and 2

M = 1, 2, 3, ...

In practical applications, the bearing frequencies usually show up at higher frequencies in the vibration spectrum. Higher frequencies meaning between 5-50 times the fundamental frequency [7]."

Looseness can occur anywhere in the motor or attached system because of parts that are not securely mounted. Looseness vibration components occur at approximately 0.5 times rotational speed and the associated harmonics. Thus looseness is defined in terms of the fundamental frequency as

$$f_{loose} = 0.5^* N^* f_{fund} \tag{4.8}$$

where N = 1, 2, 3, ...

The two major problems with rotating machines are due to the coupling with other components. They are imbalance and misalignment. Imbalance occurs when the shaft is coupled to a system whose center of mass does not rotate along the axis of rotation. The vibration is also found in the same frequency range as the internal imbalance defined above.

Misalignment occurs when the motor shaft axis is not aligned along the axis of rotation for the coupled system. The two types of misalignment are called offset and angular. Angular misalignment has a strong vibration at the same frequency range as the rotation of the shaft and is in the axial direction. Offset misalignment causes vibration at 1 and 2 times the rotational frequency. This is also the same as the internal misalignment.

The characteristic frequencies for the ball bearings are based upon the bearing dimensions shown below in Figure 4.1. In radially loaded bearings, the contact areas of the balls and raceways carry the heaviest loads causing most fatigue failures involving these components [26]. Bearing problems can be divided into six categories: fundamental train, ball spin, ball pass of the outer race, ball pass of the inner race, misalignment, and oil whirl (journal bearings).

The pre-calculated frequency problems for the inner and outer race, cage train, and ball defect for each type of bearing (SKF 6205 and 6206 European) used in the motors occur at the following frequencies (Hz) shown in Table 4.1 for a motor operating at 1,000 RPM.

Since the SKF bearing defect frequencies were calculated at 1,000 RPM, we must correct for our usage speed, which was determined to be approximately 1,740 RPM. This speed corresponds to a 100% loaded motor. Thus, the corrected frequency is given by the equation

$$\textit{Actual bearing frequency (Hz)} = 0.001 * RPM * \textit{Pre-calculated frequency} \tag{4.9}$$

The bearing frequencies for the SKF 6205 and 6206 (European) at the operating rotor speed are given in Table 4.2. These characteristic bearing vibration frequencies also have integer harmonics associated with each component.

The ball spin frequency is caused by the rotation of each ball about its center. Since a defect on a ball will make contact with both the inner and outer races during every revolution, the ball defect frequency is twice the spin frequency and can be written as

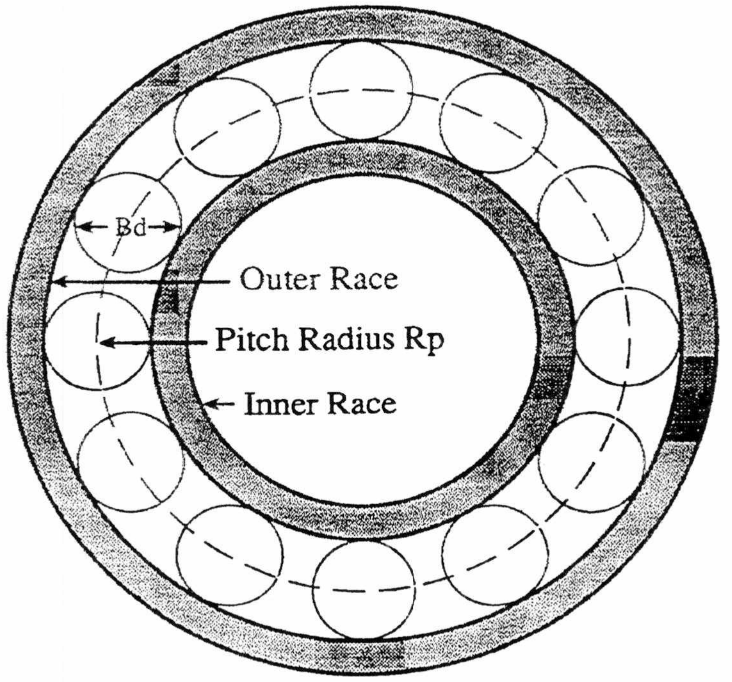

Figure 4.1. Cross-sectional view of a ball bearing [7].

Table 4.1. Fundamental bearing frequencies (Hz)

Type of Problem / Bearing	**SKF 6205**	**SKF 6206 European**
Inner Race frequency	90.25	90.530
Outer Race " "	59.75	59.470
Cage Train " "	6.639	6.608
Ball/Roller Defect " "	78.580	77.039

Table 4.2. Bearing fundamental frequencies at 1,740 RPM (Hz)

Type of Problem / Bearing	**6205**	**6206 (European)**
Inner Race frequency	156.13 Hz	157.52
Outer Race " "	103.36	103.47
Cage Train " "	11.48	11.49
Ball " "	135.94	134.04

$$fb = \frac{PD}{BD} f_{rm} [1 - (\frac{BD}{PD} cos(\beta))^2] \tag{4.10}$$

where: PD = the bearing pitch diameter

BD = ball diameter

β = contact angle of the balls on the races

f_{rm} = mechanical rotor speed in Hz (or f_{fund}).

Figure 4.2 shows the mechanical structure mentioned above.

The outer and inner raceway frequencies are produced when each ball passes over a defect. This occurs n-times during a complete circuit of the raceway where n is the number of balls. This causes the inner and outer race frequencies to be defined as

$$fo = \frac{n}{2} f_{rm} [1 - (\frac{BD}{PD} cos(\beta))]; \tag{4.11}$$

$$fi = \frac{n}{2} f_{rm} [1 + (\frac{BD}{PD} cos(\beta))]. \tag{4.12}$$

Bearing cage faults generally bind the balls producing skidding and slipping along the raceway. These effects generate high frequency vibrations to be generated [25].

The specifications for fundamental bearing frequencies given by SKF for bearing models 6205 and 6206 (European) found in Table 4.1 were determined using the above equations by utilizing bearing physical characteristics.

An example is given in Figure 4.3. In this example there is a large increase in the high frequency activity between the initial testing and the 6th cycle of an aging process. The aging was performed to cause bearing problems. Figure 4.3 illustrates how the vibration spectrum can be used to detect problems within a mechanical system. At the time the 6th cycle was monitored, the motor showed no other sign of any mechanical problems.

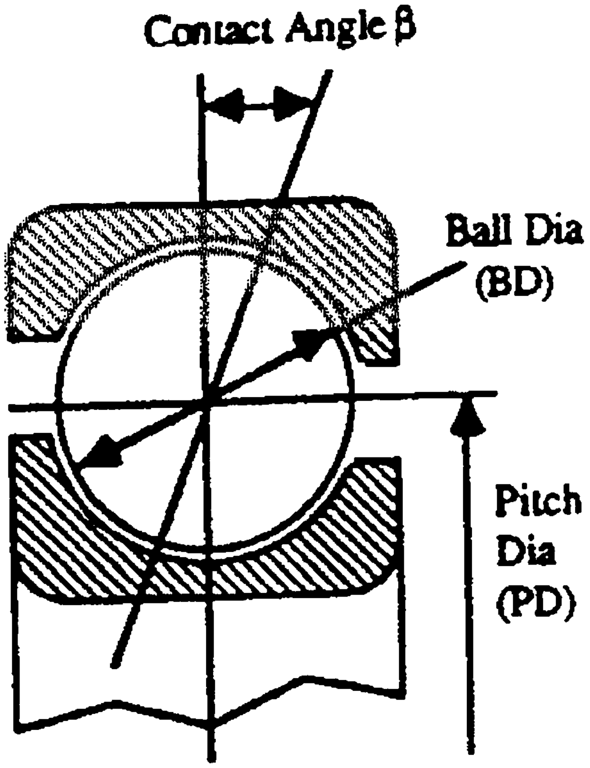

Figure 4.2. Explanation of bearing terms PD, BD, and contact angle β [24].

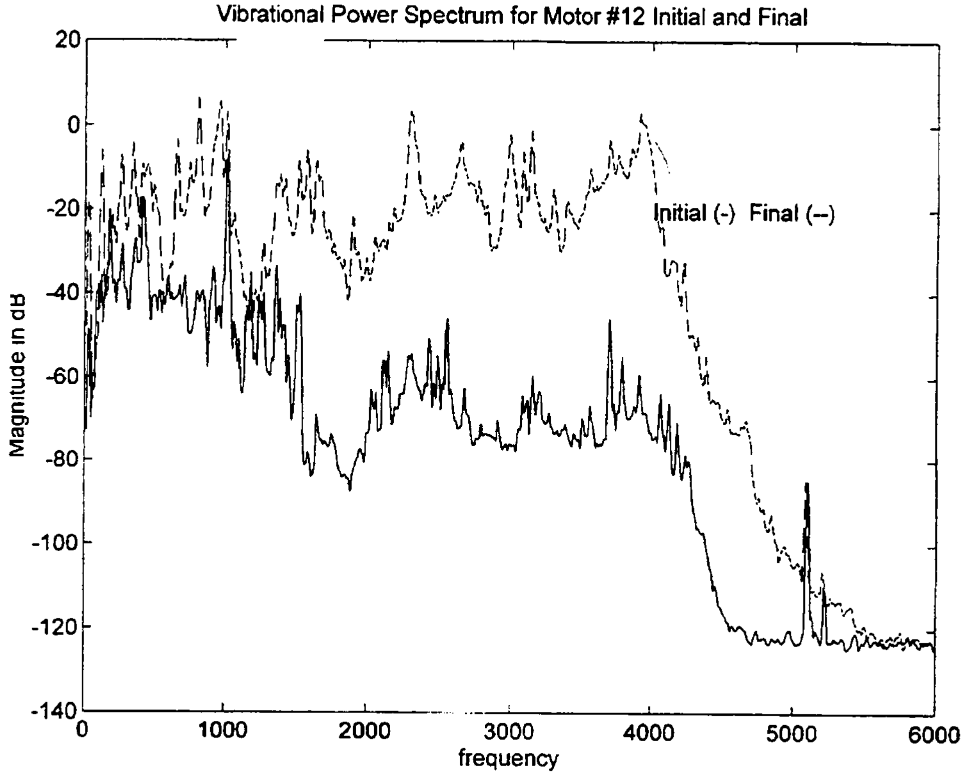

Figure 4.3. Motor vibration spectrum from an aging experiment.

The vibration spectrum consists of many peaks. Of these peaks, a large number may be contributed to harmonics of primary vibrations caused by any of the aforementioned motor vibration problems. To identify these harmonic peaks, a MATLAB program using Equations (4.5)-(4.8) and the bearing frequencies in Tables 4.1 and 4.2 are used to generate many of the harmonics seen in the spectrum.

Peak identification for the vibration spectra generated by fluting motors #11, 12 and 13 may be more difficult than identifying the peaks within the electrical spectra. In a paper recently published by CSI [27], fluted bearing frequencies were tried to identify bearing characteristics and fluting damage characteristics.

Bearing damage resulting from shaft voltages and currents (i.e. fluting) can be seen in high frequency resolution vibration spectrum. This type of fault consists of high frequency modulated energy and appears as a mound of energy in the high frequency range between 2,000-4,000 Hz. At this time no reason can be given to explain why it shows up in the vibration spectrum at the frequency band. The location of the mound of energy due to electrical discharge machining (EDM) does not appear to be related to running speed or any other speed variable [27].

Also note that the fluting damage shown in the CSI report, Figure 4.4 and Figure 4.5, does not appear to be the same type of damage as seen in the motor used in the aging project, shown in Figure 4.6. But, the resulting spectra seem to be very similar with respect to where the fluting frequencies appear. The damage is sometimes referred to as pitting.

One explanation between the different damages seen in the two cases may be that the damage inflicted upon the project motors resulted from a higher voltage and current than usual industrial fluting. Usual industrial fluting occurs at 3 volts DC or 10 volts peak with the current level about 1 mAmp. The fluting aging experiment used much larger voltages and currents (27 Amperes at 30 Volts) [28]. The bearing damage is a combination of pitting and frosting.

4.3. Relationship between Motor Current and Vibration

There are problems that are seen in the motor current analysis that do not appear in the vibration data, as mentioned in Section 2.2.2. Since there is extra information contained in the

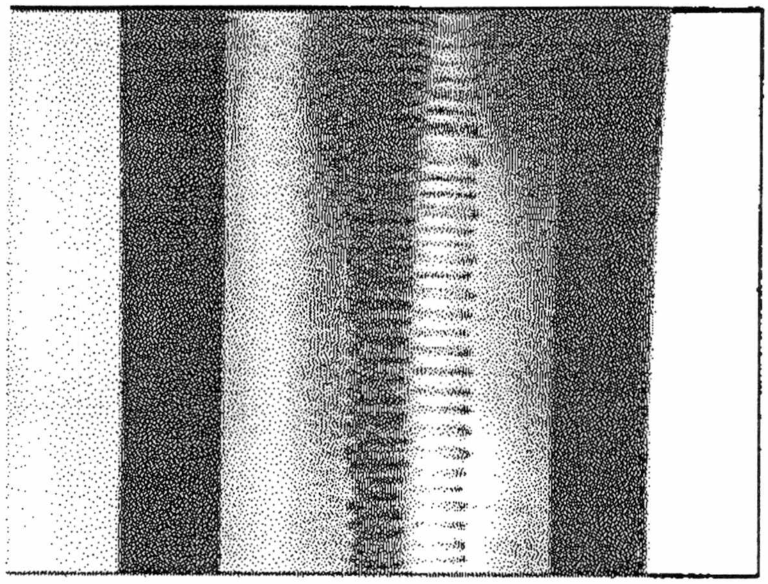

Figure 4.4. Outer race of a bearing with fluting damage [26].

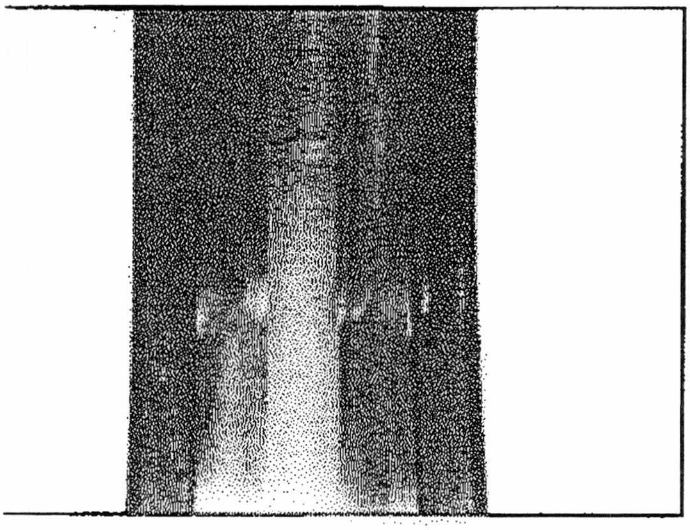

Figure 4.5. Outer race of a bearing with frosting [26].

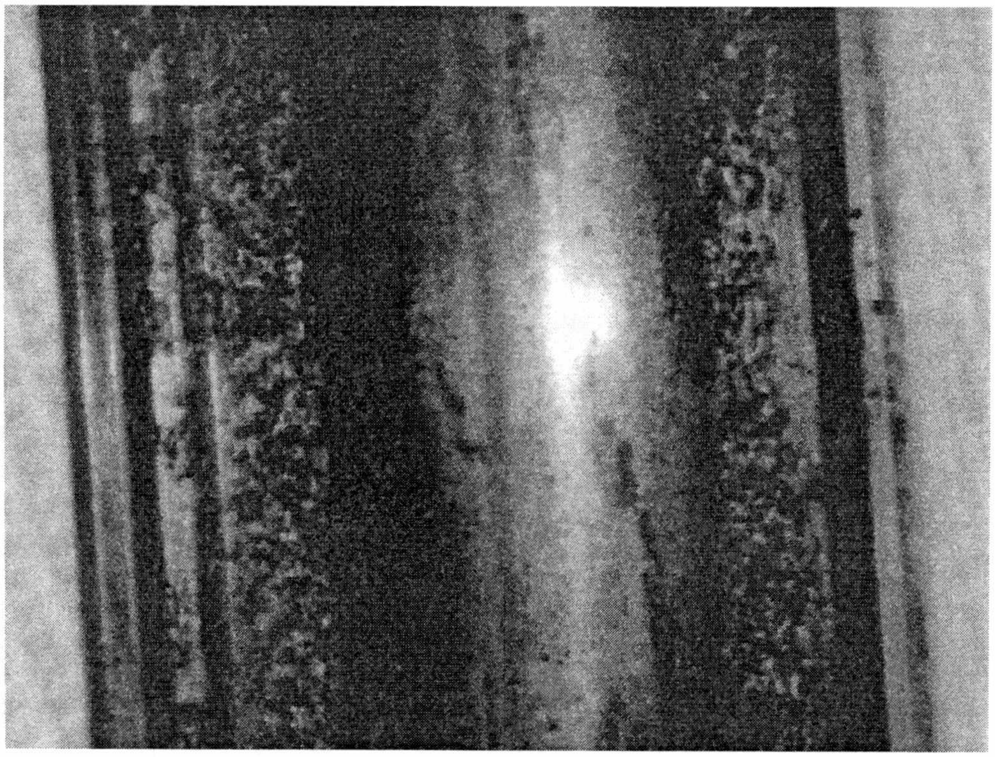

Figure 4.6. Bearing with pitting damage.

current signature, there should not be an exact match or correlation between current and vibration at all frequencies.

4.3.1. The Relationship between Currents

The three phase currents for each individual motor should initially be quite similar, except for the fact that they are 60 degrees out of phase. But, as the motor aged, this may not be true. As the motor insulation ages, it develops a current among the phases. This imbalance is caused by a change in resistance in each phase. A plot of the RMS values of motor current for each cycle may indicate dissimilar currents.

4.3.2. The Relationship between Vibrations

Examination of the relationship between vibration sensor positions for specific motor cycles or the relationship between specific sensors initially and its final cycle for a motor may yield valuable information. For example, if the sensors exhibit a large correlation, only one of the sensors need be recorded because of a large overlap of information.

By combining all the frequencies produced by the above mentioned problems, we should be able to identify most of the major peaks contained in the vibration spectrum.

Chapter 5

DATA ANALYSIS TECHNIQUES FOR MOTOR DEFECT MONITORING

5.0. Introduction

This chapter describes the various tome-domain and frequency-domain techniques implemented for processing both motor current and vibration measurements from testing of motors used in aging studies. Three vibration signals and three phase currents were used for analysis. At least six aging cycles were available for each motor and the measurements were made at 100% load tests. The following data processing techniques are discussed.

- Time-domain analysis of signals.
- Frequency-domain analysis of signals.
- Wavelet transforms and multi-resolution analysis for sub-band RMS trending.
- Linear regression for signature characterization.
- Correlation and coherence analysis.

5.1. Time Series Evaluation

The time series evaluation section is divided into two sub-sections, theory and data processing procedures. The theory sub-section contains brief explanation of the analysis theory. The data processing procedure sub-section contains an explanation of how the data were analyzed.

5.1.1. Time Series Analysis Theory

The data files are a series of measurements at fixed time intervals. Thus, X1(n) and X1(n+1) were separated by a time interval that is dictated by the speed (or frequency) of sampling. For the sampling rate of 12 kHz, the time interval between samples (deltat) is 1/12000 or 0.000083 second and for the lower frequency of 0.2 kHz with deltat = 0.005 seconds.

Then approximate each measurement group for each motor for each test (Ix, Iy, Iz, Vc, V10:00 and V2:00) as X1(n), X2(n), ... , and X6(n). For the X's, n ranges from 1 to 120,000 corresponding to the total number of samples. For simplicity, use X1(n) and/or X2(n) for the discussion of statistical quantities and properties.

To start the discussion, use the data to determine the mean or average value of the data set. It is also called the first moment of Xl or X1. The mean or average of the data set is given by the equation:

$$\underline{\boldsymbol{X1}} = \frac{1}{n}\sum_{i=1}^{N} X1_i \tag{5.1}$$

for i = 1 to N, with N = Number of data points.

The next step in the data analysis, was to subtract the mean value from each data point. This was done so that there is no DC gain within the data set. The data set fluctuated around the x-axis with a mean value equal to 0. The equation is given by

$$\boldsymbol{X1_i'} = \boldsymbol{X_i} - \underline{\boldsymbol{X1}} \tag{5.2}$$

The $\mathbf{X1_i}'$ sequence were used to determine the rest of the statistical values. The RMS (root mean square) value of the signal is defined as

$$RMS_{X1'} = [\ \frac{1}{N}\sum_{i=1}^{N} X1'^{\,2}_{i}\ ]^{1/2} \tag{5.3}$$

for i = 1 to N, with N = Number of data points.

The RMS values were determined for each individual signal and cycle to help determine the choice of signals to process in the frequency domain.

The auto-correlation function was found by using one specific signal, but the cross correlation was found by using two different signals from the same test. "The auto-correlation provides insight into existence of periodic signal components in the random data and the nature of wide-band and narrow-band noise properties [29]." If the auto-correlation function changes rapidly as a function of the time lag, then the signal has predominantly high frequency components; and conversely [30]. The auto-correlation also provides insight into "system memory." If the system has a large time-dependent signal or signals, $R_{X1'X1'}(k)$ decays to zero very slowly compared to a small time-dependent signal.

The auto-correlation is defined as:

$$R_{X1'X1'}(k) = \frac{1}{N}\sum_{i=1}^{N} X1_i' X1_{i+k}' \tag{5.4}$$

for k = 1, 2, 3, ...

Note that for discrete data N>>k, or at least, k = 1/10 * N.

The cross correlation function is computed as follows.

$$R_{X1'X2'}(k) = \frac{1}{N}\sum_{i=1}^{N} X1_i' X2_{i+k}' \tag{5.5}$$

for k = 1, 2, 3, ...

The cross correlation describes the general dependence of the values of one set of data on another set. "The cross correlation has three main applications: 1) measurement of a time delay; 2) determination of transmission paths by observing multiple peaks in the output of the function; 3) detection of signals in noise and their recovery [29]."

The correlation coefficient or normalized cross correlation is defined as:

$$\rho(k) = R_{X1'X2'}(k) \,/\, \{ [R_{X1'X1'}(0)\, R_{X2'X2'}(0)]^{(1/2)} \} \tag{5.6}$$

The correlation coefficient function is in the range [+1, -1].

5.1.2. Time Series Data Processing Procedures

Time series analysis of the motor data, using MATLAB program motpro.m, contained the following time series calculations.

1. Mean
2. RMS value

3. RMS value with the mean subtracted from the signal.

4. Correlation Coefficients

The RMS value of the raw motor signal was checked for DC gain that may occur in the signal. The mean value was subtracted from the raw motor signal regardless of the mean value and processed and stored in this form. This was done as a precautionary measure to establish a signal with no DC gain.

The MATLAB program rmsplot.m was used to plot the RMS values for each motor for each signal versus cycle. Then, rmsplot.m calculated the first order least-squares fit with fractional RMS error. The signal was the raw data signal using all 120,000 data points.

The correlation coefficients were calculated for each signal and cycle for each motor. This processing was accomplished using a MATLAB program called ccm.m. After the correlation coefficients were calculated, they were saved to a MATLAB .mat file.

The correlation coefficient .mat files were then loaded and graphed using ccplot1.m. The routine Ccplot1.m graphs the absolute value of the correlation coefficients by signal type and by cycle for each motor. The highest overall series of correlation coefficient total for a signal group was used for each motor. This was accomplished by taking the absolute value of each signal pair correlation coefficient (SPCC) for a specific motor then averaging for all cycles. The resultant number is called the summed signal pair correlation coefficient or SSPCC. The equation is given as:

$$SSPCC = \frac{1}{N}\sum_{i=1}^{N} | SPCC_i | \tag{5.7}$$

where N = total number of cycles

This was how the correlation coefficients were used to determine the choice of motor signals to process to compute coherence functions. Three coherence functions for each motor aging group were analyzed: current vs. current, current vs. vibration and vibration vs. vibration.

5.2. Frequency Domain Analysis

The frequency domain evaluation section is divided into theory and data processing procedures. The theory section contains brief explanation of the analysis theory.

5.2.1. Frequency Domain Analysis Theory

To discuss characteristics in the frequency domain, the time domain data must be transformed into the frequency domain. To accomplish this the fast Fourier transform algorithm was used. The discrete Fourier transform, for a discrete data set that is stationary within a time interval = [0 to T], is defined as

$$x(m * deltaf) = \frac{1}{N}\sum_{n=1}^{N} \mathrm{x(n * deltat)\,exp\{-2\pi j * [m * deltaf]\,[n * deltat]\}} \qquad (5.8)$$

with: n = 0 to N-1

m = 1, 2, ... , N/2

$$\mathrm{deltaf} = \frac{1}{N * deltat}$$

N = Number of samples per block.

The above parameters were determined from the data acquisition set-up used to collect the individual signals. Also note that the resulting x(m*deltaf) is a periodic function, with m = 0, 1, ... , N/2. The actual computation uses the fast Fourier transform (FFT) algorithm with appropriate windowing to minimize side-band leakage.

The fast Fourier transforms use a block size whose length is an integer power of two. Thus $N = 2^n$. For example, the motor signal data size is 120,000 points. The nearest power of two is 2^{17} which equals 131,072. Therefore, to use the algorithm, the motor signal data must be padded with zeros to obtain the required number of data points. With Fourier transform, it would take N^2 computation, but with the fast Fourier transform it only takes $N*\log_2(N)$. The computational savings are equal to $N^2 / N*\log_2(N)$. Thus, for the motor signal data, the computation was reduced by a factor of

$$\textit{Computational Reduction Factor} = \frac{131{,}072^2}{132{,}072 * \log 2\,(132{,}072)}$$

$$= 16{,}509 \qquad (5.9)$$

This is a large reduction in the computation time.

In order to avoid aliasing of the sampled data, the sampling frequency must be at least twice the maximum frequency content of the signal. This condition is assumed by properly removing the high frequency component using a low-pass (or anti-aliasing) filter.

The spectral and time-domain signatures are related to each other as follows.

$$S_{X_1'X_1'}(f) = \int_{-\infty}^{\infty} R_{X_1'X_1'}(\tau)\ \exp\{-2\,\pi j f \tau\}\, d\tau \qquad (5.10)$$

where: $j = \sqrt{-1}$.

The auto-power spectrum is used extensively in this study.

Similarly the cross-power spectra is related to the cross-correlation as

$$S_{X1'X2'}(f) = \int_{-\infty}^{\infty} R_{X1'X2'}(\tau)\ \exp\{-2\ \pi j\ f\ \tau\}\ d\tau \qquad (5.11)$$

where: $j = \sqrt{-1}$.

"We note that for a real random process, the auto power spectrum is real and non-negative, whereas the cross-power spectrum is a complex number [29]." The cross power spectral density function is used to determine the phase between the two variables.

The phase (radians) between X1' and X2' is determined by the following:

$$Phase = invtan\ [\ S_{X1'X2'}\ imaginary\ /\ S_{X1'X2'}\ real\ ] \qquad (5.12)$$

If the signals of X1' and X2', are respectively treated as input and output from a linear, constant parameter system, then the transfer function may be determined by

$$H(f) = S_{X1'X2'}\ /\ S_{X1'X1'} \qquad (5.13)$$

"Thus for the system described above, the magnitude of H(f) and the phase relationships can be given. In general, however, the system may be corrupted by noise, or non-linear trends, etc. In this case the confidence in the phase estimate will not be 100%. A measure of this confidence is given by the coherence function [29]."

The coherence function is defined as

$$coh^2 = | S_{X1'X2'} |^2 / (S_{X1'X1'} \, S_{X2'X2'}). \tag{5.14}$$

With the coherence function ranging from 0 to 1. The function is plotted against frequency, therefore determining which frequency components contribute the most to the relationship between the signals is simple. If the relationship between X1' and X2' was perfect, then the coherence will be equal to unity for all frequencies. If there was no relationship between the two variables, X1' and X2', then the coherence function is equal to 0 for all frequencies. In general there are three reasons that the coherence function is less than 1.

1. There is noise in the measurement of one or both of the signals.
2. The system is nonlinear.
3. The output (if the signals being processed are of an input/output nature) is due to more than one input.

Cepstrum analysis is basically a spectrum of a spectrum. It is a technique which is able to detect and quantify periodicity in spectral data using the FFT. Harmonics appear in the spectrum as equally spaced peaks; equally spaced peaks equate to a periodicity. So if an FFT of the spectrum is taken, a new data set with peaks at the frequency of the source of the harmonics is generated.

5.2.2. Frequency Domain Data Processing Procedures

Power spectral densities (PSD) for each signal, cycle and motor were calculated and plotted using motpros.m. The PSDs were calculated using two sets of variables dictated by MATLAB's PSD function.

MATLAB's PSD function uses the following constant for processing: nfft, Fs, Noverlap and window. Fs is the sampling frequency used when acquiring the raw motor data. This was 12 kHz. Nfft is the number of raw data points to be used in a block of processing. MATLAB allows for the data to be processed in blocks. Block procesing is faster and allows for averaging of the processed block outputs. Noverlap assigns the number of points that may overlap between each block of data. Window refers to a weighting window function in order to minimize spectral distortion.

The vibration data were processed using two different nfft values, with all the other parameters fixed. The current was processed using only one set of PSD parameter values. The values are as follows:

nfft (for vibration spectrum #1)	= 16,384
nfft (for vibration spectrum #2)	= 1,024
nfft (for current spectrum)	= 8,196
Fs	= 12,000
Noverlap	= 0
Window	= "Hanning".

Using the specified variables above, the frequency resolution in the spectrally analyzed data may be determined. The frequency resolution is given by the following equation

$$\textit{frequency resolution} = \textit{sampling frequency} / \textit{nfft} \tag{5.15}$$

Therefore, if the nfft is 16,384, a frequency resolution of 0.73 Hz is obtained. The other frequency resolutions are 1.46 and 11.7 for nfft's equal to 8,196 and 1,024, respectively. Note that the vibration PSDs generated using nfft = 1,024 were not used in this report.

Peak identification was accomplished by using the MATLAB program peakID.m. PeakID.m loaded the processed PSD vibration or current data and first graphed the original results. The PSD could then visually be inspected for the appropriate threshold value. The threshold value determined the minimum magnitude of either the current (in dB scale) or vibration (in g scale) under which a peak would not be identified. This allowed for peaks of small magnitudes to be unidentified. The frequencies were identified using motor current and vibration theory that predict them using motor characteristics and other known variables.

To identify interesting frequencies within the spectrum for any signal, spectra were visually examined for each cycle and also the output from peakID.m was also used. Then, interesting frequencies or frequency ranges were determined from this information. For an interesting frequency range, with a magnitude that appears to be changing, determination of the area under the frequency range (in the spectrum) should quantify the change. Quantification is discussed in the section on wavelet transform and multi-resolution analysis.

The coherence functions were generated using the MATLAB program ch1.m. This program loaded the two specified raw motor signals (as identified from the correlation coefficient) for processing. The coherence functions use the same processing constants as the PSD. Therefore, the coherence has the following processing constants.

nfft = 8,192

Fs	= 12,000
Noverlap	= 0
Window	= "Hanning".

Ch1.m also graphed the initial resulting spectrum. The initial spectrum was then used to determine a threshold value for peak identification in the same method as in peakID.m. The spectrum is then replotted with the appropriate peaks identified. The frequency resolution for the coherence function is 1.46 Hz.

5.3. Sub-Banded RMS Values Using 1-D Wavelet Transform and Multi-Resolution Analysis

Short-time Fourier transform (STFT) is often used to process non-stationary and transient signals. The STFT has a fixed window length and hence a fixed frequency resolution. This restriction can be overcome by sweeping the signal with varying size windows and thus providing frequency resolution at various levels. This in effect results in viewing the signal at a given point in time with different frequency resolutions. This procedure allows us to identify either low-frequency or high-frequency anomalies that may occur in a signal at a given point.

Wavelet transform-based multi-resolution analysis of signals was used to decompose the signals into various frequency sub-bands. This provides an accurate recovery of sub-band data without distortion caused by filters. The discrete wavelet transform (DWT) facilitates this procedure and is applied to both motor current and vibration signals. The decomposition into multi-levels is performed in one pass through the data and the resulting time-series are used to calculate their respective RMS values.

The following material is taken from reference [31].

5.3.1. Continuous Wavelet Transform (CWT)

The functions that may be transformed using wavelets are those that are square integrable on the real line. This class is denoted as $L^2(R)$.

$$f(x) \in L^2(R) \Rightarrow \int_{-\infty}^{+\infty} |f(x)|^2 \, dx < \infty \tag{5.16}$$

The set of functions that are generated in the wavelet analysis are obtained by dilating (scaling) and translating (time shifting) a single prototype function, which is called the mother wavelet. The wavelet function $\psi(x) \in L^2(R)$ has two characteristic parameters, namely, dilation (a) and translation (b), which vary continuously. A set of wavelet basis function $\psi_{a,b}(x)$ is defined as

$$\psi_{a,b}(x) = \frac{1}{\sqrt{|a|}} \psi\left(\frac{x-b}{a}\right) \qquad a, b \in R \,;\, a \neq 0 \tag{5.17}$$

Here, the translation parameter, "b", controls the position of the wavelet in time. A "narrow" wavelet can access high-frequency information, while a more dilated wavelet can access low-frequency information. This means that the parameter "a" varies for different frequencies. The continuous wavelet transform is defined by

$$W_{a,b}(f) = < f, \psi_{a,b} > = \int_{-\infty}^{+\infty} f(x) \, \psi_{a,b}(x) \, dx \,. \tag{5.18}$$

The wavelet coefficients are given as the inner product of the function being transformed with each basis function [31].

5.3.2. Discrete Wavelet Transform (DWT) and Multi-Resolution Analysis (MRA)

The calculation of wavelet coefficients at every possible value of the scale parameter (a) and the translation parameter (b) entails a large amount of computational effort. Furthermore, it may not be necessary to compute the wavelet coefficients with a high resolution of parameters a and b. The discrete wavelet transform (DWT) is performed by choosing scales (a) and translations (b) based on powers of two, often called the dyadic scales and translations.

The wavelet basis function $\Psi(t)$ is generated in terms of the so-called scaling function $\phi(t)$ in the form [32]

$$\Psi(t)=\sum_{n} h_1(n)\sqrt{2}\phi(2t-n) \qquad (5.19)$$

where $h_1(n)$ is a set of coefficients and the scaling function is generated recursively as

$$\phi(t)=\sum_{n} h(n)\sqrt{2}\phi(2t-n) \qquad (5.20)$$

Again h(n) is a set of parameters and $\sqrt{2}$ "maintains the norm of the scaling function with the scale of two" [32]. One may combine Eqs. (5.19) and (5.20) and express f(t) as an approximation in terms of the basis function. This yields

$$f(t)=\sum_{k} c(k)\phi(t-k)+\sum_{j}\sum_{k} d_j(k)2^{j/2}\Psi(2^j t-k) \tag{5.21}$$

From this the coefficients c(k) and $d_j(k)$ are calculated as the approximations and details of the time function f(t). Thus

$$d_j(k)=\int_{-\infty}^{\infty} f(t)\Psi_{jk}(t)dt \tag{5.22}$$

Note that the coefficients $h_1(n)$ and h(n) in Eqs. (5.19) and (5.20), respectively, may be considered as the coefficients of finite impulse response filters. Thus the discrete wavelet transform and the multi-resolution analysis are dual to each other, giving rise to multiple level decomposition of signals.

Figure 5.1 shows the various branches of this decomposition. At each stage the signal can be reconstructed to generate the raw signal and its components. The low-frequency component is often referred to as the approximation and the high-frequency components as the details [33].

The main application of wavelet transform in this thesis was to separate the vibration and motor current signal into frequency bands, or details (high frequency) and approximations (low frequency) in wavelet terminology. RMS calculations were then made on each of the sub-banded time series.

Details and approximations are the two outputs from a 1-D Wavelet decomposition. The original signal is divided into two parts (details and approximations) as determined by frequency for each level of decomposition.

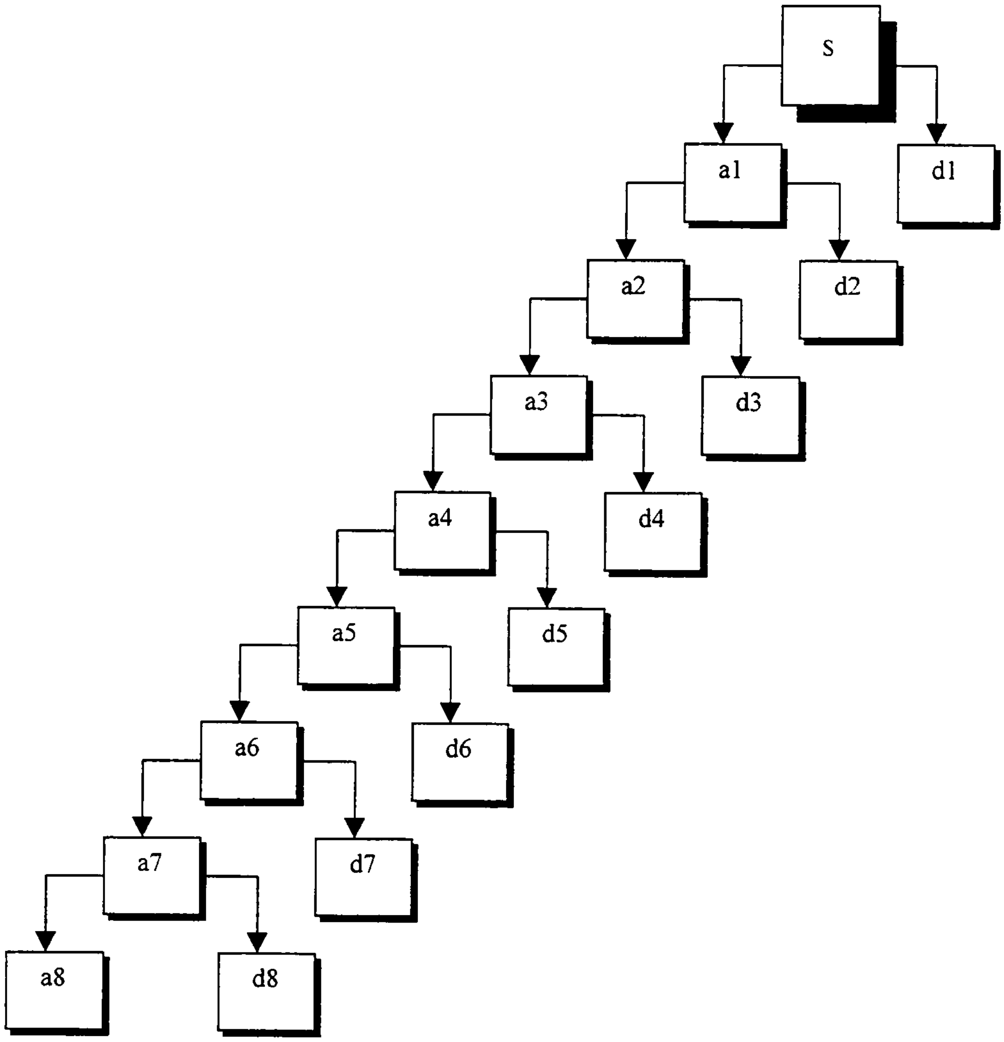

Figure 5.1. Multi-resolution analysis (MRA) of a signal (s) showing eight levels of approximations (a_i) and details (d_i).

For example, if the original signal has a frequency range of 0-6,000 Hz, the first level of decomposition divides the signal into 0-3,000 Hz (the approximation component or a1) and 3,000-6,000 Hz (the details component or d1). Now, if the same signal as before is used, but a two level 1-D wavelet decomposition is performed, the signal is split into four components. The approximation components are 0-3,000 (a1) and 0-1,500 Hz (a2). The second level of decomposition is determined by the first level approximation bandwidth. Meaning, the first level approximation bandwidth is subdivided into two equal parts, d2 and a2. The two detail frequency components are 6,000-3,000 (d1) and 3,000-1,500 Hz (d2). However, although there are four sub-bands of information, only look at three of the bands, d1, d2 and a2 for sub-banded information.

Because, sub-band a1 has been split into two parts and is just an overlap of information found in d2 and a2. This process may be repeated as many times as needed until the decomposition process depletes the needed number of points for analysis of a subdivided bandwidth. This decomposition by DWT is shown schematically in Figure 5.1.

Now by using the above approach with a 0-6,000 Hz frequency range and 8 levels of decomposition, the following frequency ranges are obtained in Table 5.1. Thus, the levels are defined by frequency bands in this application.

5.3.3. Wavelet Data Processing Procedure

The processing was accomplished using wmpro.m, rmswp.m and wrmspros.m. Wmpro.m processed the raw signals using a 1-D Wavelet decomposition with 8 levels using 6,000 data points and 'Daubechies 20' wavelet decomposition filter. The decomposition processing coefficients were to give the best results [reference]. A minimum entropy program on a subset of the same data was used in this experiment and determined that the above procedure

Table 5.1. Details and approximations frequency ranges for an 8-level decomposition

Level Number	Details (d)	Approximations (a)
1	6,000 - 3,000	3,000 - 0
2	3,000 - 1,500	1,500 - 0
3	1,500 - 750	750 - 0
4	750 - 375	375 - 0
5	375 - 187.5	187.5 - 0
6	187.5 - 93.75	93.75 - 0
7	93.75 - 46.875	46.875 - 0
8	46.875 - 23.4375	23.4375 - 0

was the best.

The output of this program (Wmpro.m) was the details and approximations for each decomposition level. The output of Wmpro.m was saved to a .mat file. This output was then processed using RMSwp.m.

To quantify the wavelet-processed signal, RMSwp.m was developed. RMSwp.m calculates RMS values for each level of the saved decomposed detail signal. These RMS values of the detail signals were then saved. The saved RMS values were then plotted by level, signal (vibration or current) and cycle using the program wrmspros.m. This output graph is used for the heuristic trending evaluation.

The frequency band of interest for motor current signals (Ix, Iy, and Iz) is between 50 and 70 Hz, thus containing main frequency component of a 60 Hz power supply. The band was identified as level #7. Once this band has been separated from the total signal, a RMS value on this band was calculated. This calculated RMS value was trended from cycle to cycle. But to be thorough, all levels were trended using the calculated RMS value as obtain using the DWT procedure.

The interesting frequency bands for the vibration signals were determined by a visual inspection of a final cycle linear spectrum plot and by using the peakID.m graphed output. But, the RMS values have been plotted for each signal and level versus cycle. The RMS values for each level have been trended. In addition to trending the RMS values, statistical line fitting (regression analysis) of the first and second order are applied to further assist in the trending of the 1-D wavelet sub-banded RMS values.

5.4. Data Fitting (Regression Analysis) Section

The data fitting (regression analysis) is divided into two section, theory and data processing procedures. Theory and MATLAB implementation are presented.

5.4.1. Regression Theory

Linear Regression fitting of the 1-D wavelet decomposed motor signals and the original RMS values were accomplished in the following manner by MATLAB programs wRMSfit8.m and RMSplot.m. Both the programs use a first order least-square fit for the RMS values. The first order least-squares approximation is given by

$$y = a + b*x \tag{5.23}$$

The equation for least-squares regression coefficients (a and b) are given by the following:

$$\mathrm{b} = \frac{n\sum_{i=1}^{n} x_i y_i - \sum_{i=1}^{n} x_i \sum_{i=1}^{n} y_i}{n\sum_{i=1}^{n} x_i^2 - \sum_{i=1}^{n} x_i} \tag{5.24}$$

and

$$\mathrm{a} = \frac{\sum_{i=1}^{n} y_i - b\sum_{i=1}^{n} x_i}{n} \tag{5.25}$$

where: x_i and y_i = variables

n = number of samples [34].

The original data and the least-squares data were then plotted together. The original and fitted data were then analyzed for error of fit using fractional RMS Error. Fractional RMS Error (FRMSE) is defined as

$$FRMSE = \{ \frac{1}{n} [(e1/y1)^2 + (e2/y2)^2 + \ldots + (en/yn)^2] \}^{(0.5)} \tag{5.26}$$

with: n = number of data points

e1 … en = error between fitted and original points

y1 … yn = original data points.

FRMSE ranges from 0 to infinity. A good fit between the original data and the least-squares generated data should approximately provide error of less than 0.20.

5.4.2. Regression Analysis Processing

Wavelet analysis may be used to separate the signals by frequency in order to obtain the interesting frequency bands. Each of these bands can be used to determine a RMS value. This value may be compared for each cycle to quantify an increase or decrease in the power spectrum for that particular frequency range. This increase or decrease may then be trended.

The program wRMSfit8.m accomplishes the task of fitting the RMS values generated by the 1-D wavelet decomposition by cycle and signal. First by grouping the decomposed motor data by motor number and signal type, then combining all the cycles into an 8 by cycle # matrix. Each row corresponds to a decomposition level. This matrix was plotted by row using all cycles. The plotted RMS values are then fitted by least-squares regression. The original data and the least-squares data were then plotted together. The plot is similar to the output of wrmspros.m except for the addition of least-squares line fit and the associated slope and fractional RMS error values.

RMSplot.m accomplished the same tasks by using previously processed whole-signal data. Since the RMS values had already been calculated by motpro.m and saved to a processed motor file, the RMS values only needed to be plotted and a regression analysis with fractional RMS error to be applied.

5.5. Generated Motor Current and Vibration Frequencies

Motor current and vibration frequencies were generated using mathematical formulas (in Chapter 4) that utilize motor characteristics. These frequencies were generated using the MATLAB program usemvb.m and are listed in section 7.1.1.1.

Chapter 6

PRELIMINARY ANALYSIS OF MOTOR TEST DATA

6.0. Summary of Preliminary Analysis of Data

A preliminary analysis of the data was performed for two reasons. It was necessary to narrow the amount of data to be analyzed. The second reason was to get an understanding of the spectral characteristic of the signals. The preliminary analysis of data is divided into three parts.

1) Specification of motors and signals for analysis

2) Spectral results

3) General results from wavelet transform.

6.1. Specification of Motors and Signals for Analysis

The motors are divided into three aging groups. The first group consists of bearing thermal aging, the second insulation thermal aging, and the third group consists of bearing fluting. The data used in this thesis consist of only two motor aging groups, the bearing fluting group and the insulation-aging group. Thus, there were data from load testing of six motors.

Once the three groups had been narrowed to two motor aging data sets, the load must be specified. There were seven different steady-state load settings: 0% uncoupled, 0% coupled, 25%, 50%, 75%, 100%, and 115%. All data presented in this thesis corresponds to 100% load tests.

For the group of motors (6) that were aged in the bearing fluting process or the insulation aging process, only current and vibration data were analyzed. There were six independent vibration and three phase current data sets taken for each load for each motor for each aging cycle. The amount of data must be narrowed in order to achieve the project goals.

The vibration data can be narrowed to three signals (out of six) very quickly for the following reason. Three of the vibration sensors were mounted on the fan cover that is bolted to the motor cover. These three were not used because they were not attached directly to the motor casing, thus allowing for additional vibration caused by the attachment between the accelerometer and the fan casing and then the fan casing and the motor.

For the both bearing fluting and stator aging cases, motor current and vibration signals were analyzed. The analysis includes time domain, spectral domain and wavelet processing for each of the three-phase currents and the three vibration signals.

Since all the induction motors that were aged have the same specifications, they should be physically identical. The characteristics exhibited by any one motor would be very similar to any motor that was aged in the same manner.

6.2. General Results of Spectral Analysis

This section is divided into three parts: general observation for all motors, observation from the stator aged group and observation from the fluting aged group. The signals that were processed for each motor were the three currents (Ix, Iy and Iz) and three vibration sensors mounted directly on the motor at the pulley end. These are cover vibration (Vc), vibration at 10:00 position (V10:00 or V10 or V1) and vibration at 2:00 position (V2:00 or V2). The first section is titled "General Observations and/or Results for each Aging Group" which is then subdivided first into each aging type and then again for each specific motor.

6.2.1. General Observations and/or Results for each Aging Group

1. When graphing motor current spectra we may need only to extend our frequency axis to 3,000 Hz.

2. Logarithmic representation of the vibration signals may give clues as to how an accelerometer is operating.

3. We may need to explore instantaneous motor power instead of instantaneous current. Instantaneous current does not seem to give any spectral information using the motor data.

6.2.2. General Observations made from the Analysis of the Stator Aged Motor Data

1. The RMS values for vibration do not appear to be trendable. But, the RMS values may trend for specific frequency bands.

2. All three current spectral signatures for motors 1 and 2 have no components past 3,000 Hz. Therefore, we may graph the currents to 3,000 Hz instead of 6,000 Hz.

3. The RMS values for the currents do not appear to be trendable.

4. Motor #1 is a special case. The motor probably could have been classified as failed well before the 12th cycle.

5. High frequency componets in the motor current spectra can be related to bearing vibration.

6.2.2.1. General Observations and/or Results for Motor #1

1. For Ix and Iy, there seems to be little change in the spectra as the cycles progress until the last cycle. From the 11^{th} to the 12^{th} cycle, there seems to be a significant change in the magnitude (drop) of the 60 Hz peak. Also, there seems to be more high frequency harmonics of 60 Hz in the 12^{th} cycle above 2,000 Hz.

2. For Iz, the same results apply except the magnitude of the 60 Hz peak increases from the 11^{th} to the 12^{th} cycle. Also, note that more high frequency harmonics are present in the Iz spectrum than in the Ix or Iy spectrum.

3. The linear spectral plots of vibration for the motor cover (Vc), 10:00 position at the pulley end (V10) and the 2:00 position at the pulley end (V2) show very distinct frequency peaks that appear to be easily identifiable from a physical point of view.

4. There seems to be a general trend of increased high frequency vibration (above 3,000 Hz) for all three spectra as the cycles increase.

5. The logarithmic spectral plots only show a large change in the spectra between the 11^{th} and 12^{th} cycles. From the 11^{th} to 12^{th} cycle, large seemingly harmonic peaks

appear in the spectra.

6. The RMS values for Ix and Iy stay approximately constant from the 0^{th} until the 11^{th} cycle. From the 11^{th} to the 12^{th} cycle, there is a large drop in the RMS value. Iz is the same except the RMS value increases from the 11^{th} to the 12^{th} cycle.

7. RMS values for vibration appear constant until the 12^{th} cycle, and then all three vibration signals show an increase in RMS magnitudes.

6.2.2.2. General Observations and/or Results for Motor #2

1. For Ix, Iy and Iz, there seems to be little change in the spectra as the cycles progress. There appears to be no motor current components above 3,000 Hz. The RMS values for Ix, Iy and Iz may trend.

2. The linear spectral plots of vibration for the motor cover (Vc), 10:00 position at the pulley end (V10) and the 2:00 position at the pulley end (V2) show very distinct frequency peaks that appear to be easily identifiable as to the frequency of the peak.

3. There seems to be a general trend of increased high frequency vibration (above 1,000 Hz) for V10 spectra as the cycles increase.

4. For V2 and Vc the spectra show very little activity over 1,000 Hz. Also note that for certain cycles the magnitude of vibration is very high for specific

frequencies.

5. RMS values for vibration appear constant.

6.2.2.3. General Observations and/or Results for Motor #3

1. For Ix, Iy and Iz, there seems to be little change in the spectra as the cycles progress. There seems to be no information about the currents above 3,000 Hz.

2. The linear spectral plots of vibration for the motor cover (Vc), 10:00 position at the pulley end (V10) and the 2:00 position at the pulley end (V2) show very distinct frequency peaks that appear to be easily identifiable as to the frequency of the peak.

3. There seems to be a general trend of increased high frequency vibration (above 1,000 Hz) for all three spectra as the cycles increase although the magnitude is small.

4. The RMS values for Ix, Iy and Iz are the same. The RMS values do not show an increase or decrease from the initial to the final cycle.

5. RMS values for vibration appear constant and non-trendable.

6.2.3. General Observations made from the Analysis of the Fluting-Aged Motor Data

1. Interesting frequency bands are defined well in the linear vibration plots. The bands are generally 1,000 +/- 200 Hz, 1,500 +/- 150 Hz, 2,500 +/- 200 Hz, 2,800 +/- 200 Hz and 3,900 +/- 100 Hz.

2. Logarithmic representation of the vibration signals may provide clues to the bandwidth of accelerometers. Example: m13c0L1 for V2 or m13c0L1 for Vc, there is a very low spectral energy past 3,500 Hz. Another example is m11c6L1 for V10, the signal from 2,500 Hz up looks low considering the previous and next cycles. The best example is m12c6L1 for Vc. The high-frequency spectrum above 1,200 Hz looks suspect.

3. There are large variations in vibration magnitudes from one cycle to the next for a specific signal (Vc, V10 or V2) that is not caused by observation #2 above.

4. High frequency vibration components (up to 4,000 Hz) seen in this study are unique in their characteristics.

6.2.3.1. General Observations and/or Results for Motor #11

1. For Ix, Iy and Iz there seems to be little change in the spectra as the cycles progress. There seems to be no significant change in the magnitude of the 60 Hz peak or any other peak in the spectrum.

2. There seems to be no peaks past 3,000 Hz for any cycle for any current.

3. The linear spectral plots of vibration for the motor cover (Vc), 10:00 position at the pulley end (V10) and the 2:00 position at the pulley end (V2) show very distinct frequency peaks that appear to be easily identifiable as to the frequency of the peak.

4. The interesting frequency (Hz) ranges for signal V1 are 900-1,100, 1,900, 2,100, 2,300-2,500, 2,600-2,900 and 3,100-4,100. For signal V2 the interesting frequency ranges are 900-1,100, 2,300-2,500, 2,600-2,900 and 3,100-4,100. The interesting frequency ranges for signal Vc are 900-1,100, 1,900-2,100, 2,300-2,500, 2,600-2,900 and 3,100-4,100.

5. There seems to be a general trend of increased high-frequency vibration (above 1,000 Hz) for all three spectra as the cycles increase.

6. The RMS values for Ix, Iy and Iz stay approximately constant for all cycles. There may be a small trend upward.

7. RMS values for vibration appear to trend for all three vibration signals. They show an increase in RMS magnitudes as the cycles progress.

8. There seems to be a problem with the signal for V10 during cycle 6.

6.2.3.2. General Observations and/or Results for Motor #12

1. For Ix, Iy and Iz there seems to be little change in the spectra as the cycles progress. There seems to be no significant change in the magnitude of the 60 Hz peak or any other peak in the spectrum.

2. There seems to be no peaks past 3,000 Hz for any cycle for any current.

3. The linear spectral plots of vibration for the motor cover (Vc), 10:00 position at the pulley end (V10) and the 2:00 position at the pulley end (V2) show very distinct frequency peaks that appear to be easily identifiable as to the frequency of the peak.

4. The interesting frequency (Hz) ranges for signal Vc are 600-1,100, 1,200-1,700 and 2,600-2,900. The interesting frequency (Hz) ranges for signal V1 are 600-1,100, 2,300-2,500, 2,600-2,900 and 3,400-4,100. For signal V2 the interesting frequency (Hz) ranges are 600-1,100, 2,200-2,400, 2,600-2,900 and 3,500-4,100 (very small).

5. There seems to be a general trend of increased high frequency vibration (above 1,000 Hz) for all three spectra as the cycles increase.

6. The RMS values for Ix, Iy and Iz stay approximately constant for all cycles. There may be a small trend upward.

7. RMS values for vibration appear to trend for all three vibration signals. They show an increase in RMS magnitude as the cycles progress.

8. Check the vibration spectrum for signal Vc for cycles 6 and 7. For V10, check cycles 3 and 6. For signal V2 check cycle 7.

6.2.3.3. General Observations and/or Results for Motor #13

1. For Ix, Iy and Iz there seems to be little change in the spectra as the cycles progress. There seems to be no significant change in the magnitude of the 60 Hz peak or any other peak in the spectrum.

2. There seems to be no peaks past 3,000 Hz for any cycle for any current.

3. The linear spectral plots of vibration for the motor cover (Vc), 10:00 position at the pulley end (V10) and the 2:00 position at the pulley end (V2) show very distinct frequency peaks that appear to be easily identifiable as to the frequency of the peak.

4. The interesting frequency ranges for signal Vc are 800-1,100, 1,800-2,200, 2,600-3,000 and 3,200-4,000. The interesting frequency ranges for signal V1 are 900-1,100, 1,800-2,000, 2,300-2,500, 2,600-2,900, 3,100-3,500 and 3,800-4,000. For signal V2 the interesting frequency ranges are 900-1,100, 1,800-2,100, 2,300-2,500, 2,600-2,900, 3,100-3,500 and 4,000-4,100 (very small).

5. There seems to be a general trend of increased high-frequency vibration (above 1,000 Hz) for all three spectra as the cycles increase.

6. The RMS values for Ix, Iy and Iz stay approximately constant for all cycles other than at cycle 5. There may be some sort of physical problem.

7. RMS values for vibration <u>do not</u> appear to trend for any of the three vibration signals.

8. Check all current spectra for cycle 5. There are some unusual 60 Hz harmonics. Check signal Vc for cycle 1, 3 and 5. For V10, check cycles 0, 3 and 4. Finally, for V2, check cycle 5.

6.3. General Observations and/or Results for Wavelet Decomposition

Using an eight-level decomposition, the 60 Hz sub-band was isolated (actually 93.75 - 46.88 Hz). The other detail sub-bands using an eight-level decomposition are given as 6,000-3,000, 3,000-1,500, 1,500-750, 750-375, 375-187.5, 187.5-93.75, 93.75-46.88, and 46.88-23.44 Hz. The decomposition was applied to motors #1, 2 and 3 (motor currents only), 11, 12 and 13 (vibration signals only) for initial and final cycles.

For the motor current data, the 60 Hz peak is isolated (seventh details sub-band) and has a large magnitude compared to the other bands. There seems to be no or very little change in the magnitudes of the sub-bands from the initial to final cycle for any current. This will be checked by RMS calculations using the sub-banded data.

For the vibration data, the same process was used as above. The detail plots showed large changes in magnitude in the first four sub-bands from the initial to final cycles for motor #11, 12, and 13. This will be checked by RMS calculations using the sub-banded data for all cycles.

Chapter 7

RESULTS OF MOTOR LOAD TEST DATA ANALYSIS AND DISCUSSION

7.0. Introduction to Results and Discussion

The results and discussion section is divided into two main sections: spectral characterization and wavelet 1-D RMS analysis. Spectral characterization includes the results of identifying salient frequency bands and comparison to theoretical values. The wavelet 1-D analysis section contains the 1-D wavelet-processed RMS values that are generated by signal decomposition and used for trending as a function of aging cycle.

It should be noted that there was an error in recording motor #2 data. When motor #2 data were extracted from the motor data CD, an error was made in naming the files for compression onto the zip disk. No data were saved for the second cycle. This caused programming problems throughout data processing. The zip disk data were used for all the processing. The problem was solved by setting cycle #2 data equal to cycle #1 data. This solved the programming problems but distorted the results that involve using cycle #2. Therefore, the results of motor #2, cycle #2 data may not be used always. This is also stated at the point of usage.

7.1. Spectral Characterization

The spectral characterization section is divided into three parts. The first part consists of power spectra of vibration and current signals and comparison with generated frequencies. The second part contains the identification of spectral frequency ranges within the current signal for motors #1, 2 and 3, and the vibration spectrum for motors #11, 12 and 13. The third part describes correlation and coherence calculations.

7.1.1. Spectral Peak Identification

In the first part, the generation of frequencies that should be seen in both the vibration and current spectra using known mechanical and electrical theory, was accomplished. Using the theoretically generated frequencies, the motor signal spectra were analyzed and pertinent peaks were identified. Some spectral peaks cannot be matched between theory and signal spectra.

7.1.1.1. Generated Motor Current and Vibration Frequencies

Each section contains the motor current and vibration frequencies from induction motor theory calculated within the MATLAB framework using the program usemvb.m.

The motor current frequencies predicted by theory used the following characteristics and variables to determine the needed frequencies.

Electrical line frequency = 60 Hz

Number of poles in the Motor = 4

RPM @ 100 % load = 1,740

The first two are treated as fixed motor characteristics. As seen in the motor current spectra, the electrical line frequency is usually 60.03 Hz. The RPM of operation at 100% load varied from motor to motor. The speed was an RMS value calculated over the time of the test. Below are the RMS RPMs obtained from the data. The RMS RPM data for the stator-aged motors are given in Table 7.1. The fluted bearing motor RPM data are shown in Table 7.2.

Since the average value of the RPM is approximately 1,740 the following electrical and vibration characteristic frequencies were calculated. The results were generated by USEMVB.m.

Synchronous frequency = 30 Hz.

Shaft frequency = 29 Hz.

Slip frequency = 1 Hz.

Table 7.1. RPM Values for motors # 1, 2 and 3

Cycle # / Motor #	1	2	3
0	1744.26	1724.37	1746.90
1	1744.09	1724.03	1746.72
2	1744.75	1722.51	1743.76
3	1743.20	1722.24	1746.19
4	1744.53	1721.55	1746.37
5	1742.92	1722.71	1745.64
6	1744.46		1743.45
7	1738.45		1744.85
8	1744.00		1745.07
9	1743.04		
10	1743.34		
11	1742.57		
12	NA*		
Average RPM	**1743**	**1723**	**1745**

*NA : This motor test, motor #1, cycle #12 was not used in this report. It was determined that the motor had failed during a previous cycle and the data were not used.

Table 7.2. RPM values for motors # 11, 12 and 13

Cycle # / Motor #	11	12	13
0	1743.13	1743.38	1748.37
1	1743.58	1741.77	1748.14
2	1744.84	1741.14	1746.45
3	1742.01	1742.30	1748.74
4	1743.59	1741.70	1746.21
5	1741.85	1738.06	**1726.87**
6	1740.37	1739.84	1745.61
7	1741.39	1739.30	1745.38
Average RPM	**1742**	**1740**	**1744**

Side-bands of shaft rotation and synchronous frequency = 48, 52, 56, 64, 68, 72 Hz.

Imbalance frequency = 29 Hz.

Misalignment or Looseness frequencies = 29, 58, 87, 116, 145, 174, 203, 232, 261, 290, 319, 348, 377, 406, 435, 464, 493, 522, 551, 580 Hz.

Oilwhirl frequencies = 11.02, 14.21, 22.04, 28.42 Hz.

Electrical line (60 Hz) harmonics frequencies = 60, 120, 180, 240, 300, 360, 420, 480, 540, 600, 660, 720, 780, 840, 900, 960, 1,020, 1,080, 1,140, 1,200, 1,260, 1,320, 1,380, 1,440 Hz.

The first 20 harmonics of the fundamental vibration frequencies for the SKF model 6505 bearing are given in Table 7.3. Harmonics of the fundamental bearing frequencies for the SKF model 6506 (European) are given in Table 7.4. Vibration frequencies, caused by the bearing, that may be seen in the motor current spectra are given in Tables B.1 and B.2. These generated frequencies are used in the next section to identify the spectral peaks in the motor data.

7.1.1.2. Motor Current Spectral Peak Identification for the Stator-Aged Cases

The test data were divided into three sections corresponding to each motor in a particular aging group. Threshold values were visually set such that only major magnitude peaks would be seen.

A spectral plot of Motor #1, current Ix for the initial cycle is shown in Figure 7.1 with the final cycle shown in Figure 7.2. The unidentifiable peaks for motor #1, given in Table 7.5, using all three currents are 1,216 and 1,336 Hz. Notice there is no change in the spectra from the initial to the final cycles. This result is common for the other two stator-aged motors. The unidentifiable peak for motor #2, found in Table 7.6, using all the three current signals is 50 Hz. The unidentifiable peaks for motor #3, given in Table 7.7, are 380, 1,220, 1,340 and 1,460. All other peaks were identified as motor current line harmonics or vibration harmonics.

Thus, the unidentified peaks for all three stator-aged motors are at 50, 380, 1,216, 1,220, 1,335, 1,340 and 1,460 Hz. We also notice many high frequency line harmonics within

Table 7.3. Bearing harmonics for SKF model 6505

SKF Bearing 6505	**Defect Type**			
Harmonic	**Cage Train**	**Ball**	**Outer Race**	**Inner Race**
1	11.55	137.6	104.0	157.0
2	23.10	273.5	207.9	314.1
3	34.66	410.2	311.9	471.1
4	46.20	546.9	415.9	628.1
5	57.76	683.6	519.8	785.2
6	69.31	820.4	623.8	942.2
7	81.86	957.1	727.8	1099
8	92.41	1094	831.7	1256
9	104.0	1231	935.7	1413
10	115.5	1367	1040	1570
11	127.1	1504	1144	1727
12	138.6	1641	1248	1884
13	150.2	1778	1352	2042
14	161.7	1914	1456	2199
15	173.3	2051	1560	2356
16	184.8	2188	1663	2513
17	196.4	2324	1767	2670
18	207.9	2461	1871	2827
19	219.5	2598	1975	2984
20	231.0	2735	2079	3141

Table 7.4. Bearing harmonics for SKF 6506 European

Bearing 6506 (European)	**Defect Type**			
Harmonic	**Cage Train**	**Ball**	**Outer Race**	**Inner Race**
1	11.50	134.0	103.5	157.5
2	23.00	268.1	207.0	315.0
3	34.49	402.1	310.4	472.6
4	45.99	536.2	413.9	630.1
5	57.49	670.2	517.4	787.6
6	68.99	804.3	620.9	945.1
7	80.49	938.3	724.3	1103
8	91.98	1072	327.8	1260
9	103.5	1206	931.3	1418
10	115.0	1341	1035	1575
11	126.5	1475	1138	1733
12	138.0	1609	1242	1890
13	149.5	1743	1345	2048
14	161.0	1877	1449	2205
15	172.5	2011	1552	2363
16	184.0	2145	1656	2520
17	195.5	2279	1759	2678
18	207.0	2413	1863	2835
19	218.5	2547	1966	2993
20	230.0	2681	2070	3150

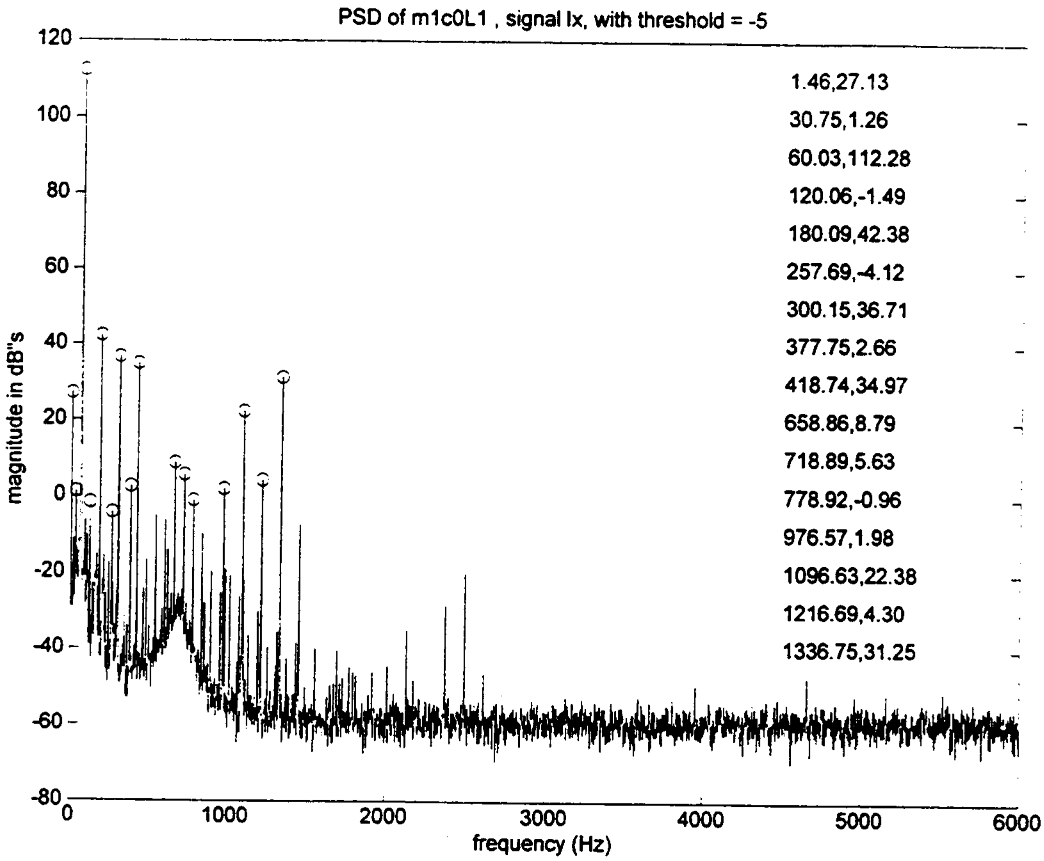

Figure 7.1. PSD of motor #1, signal Ix, initial cycle, with threshold value = -5 dB.

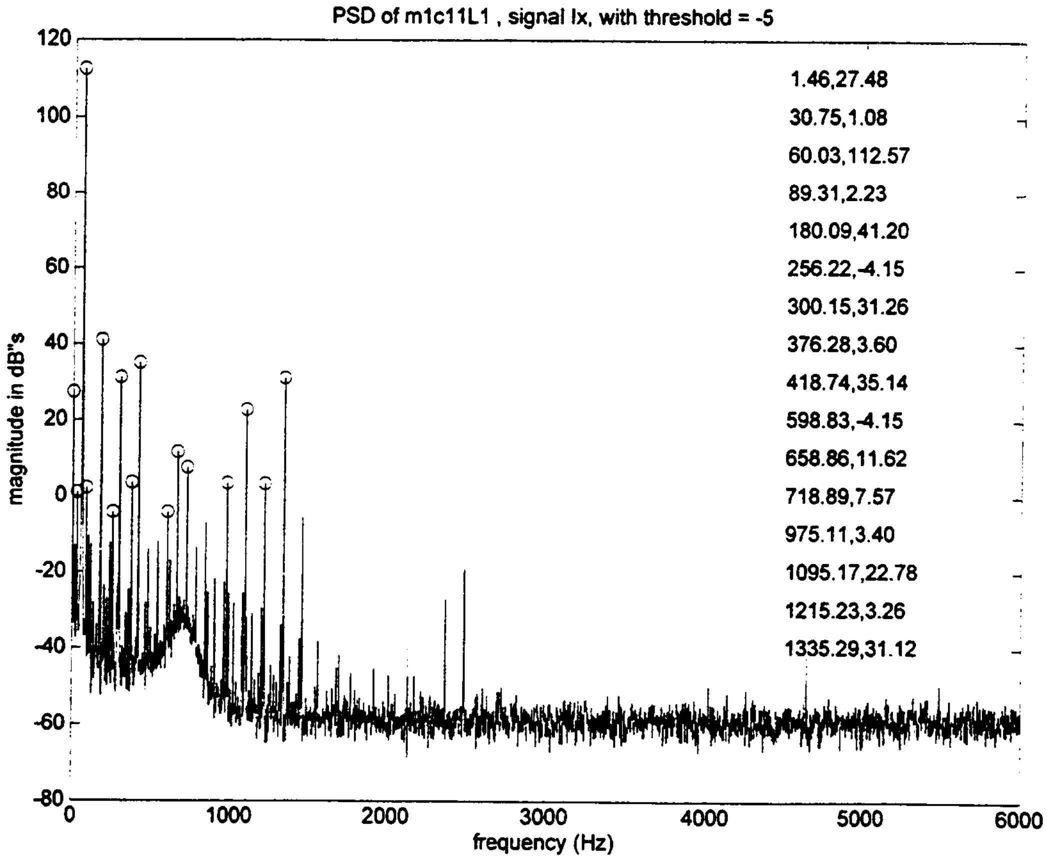

Figure 7.2. PSD of Motor #1, signal Ix, final cycle, with threshold = -5 dB.

Table 7.5. Current spectrum peaks for motor #1 with threshold = -5 dB
Bold values indicate line current or harmonic, * indicates bearing induced frequency

	Current Ix		**Current Iy**		**Current Iz**	
	Initial	**Final**	**Initial**	**Final**	**Initial**	**Final**
Peak Frequency (Hz)	1.46	1.46	1.46	1.46	1.46	1.46
	30.75*	30.75*	30.75*	30.75*	30.75*	30.75*
	60.03	**60.03**	**60.03**	**60.03**	**60.03**	**60.03**
	120.06	**89.31**	**180.09**	**89.31**	**180.09**	**89.31**
	180.09	**180.09**	**300.15**	**180.09**	**240.12**	**180.09**
	257.69*	256.22*	377.75*	256.22*	**300.15**	**300.15**
	300.15	**300.15**	**418.74**	**300.15**	377.75*	376.28*
	377.75*	376.28*	**658.86**	376.28*	**418.74**	**418.74**
	418.74	**418.74**	**778.92**	**418.74**	**658.86**	**658.86**
	658.86	**598.83**	**898.98**	**658.86**	**718.89**	**718.89**
	718.89	**658.86**	976.57*	**778.92**	**778.92**	**778.92**
	778.92	**718.89**	1096.63*	**898.98**	**838.95**	**838.95**
	976.57*	975.11*	1336.75	975.11*	976.57*	975.11*
	1096.63*	1095.17*		1095.17*	1096.63*	1095.17*
	1216.69	1215.23		1335.29	1336.75	1335.29
	1336.75	1335.29				

Table 7.6. Current spectrum peaks for motor #2 with threshold = -10 dB
Bold values indicate line current or harmonic, * indicates bearing induced frequency

	Current Ix		Current Iy		Current Iz	
	Initial	**Final**	**Initial**	**Final**	**Initial**	**Final**
	0	0	0	0	0	0
	50	30*	50	30*	50	30*
	60	50	**60**	50	**60**	50
	180	**60**	**180**	**60**	**120**	**60**
	240	90*	**240**	90*	**180**	90*
	290	**120**	290*	**180**	**240**	**180**
	300	**180**	**300**	**240**	**290**	**240**
Peak Frequency (Hz)	**360**	**240**	**360**	290*	**300**	290
	420	290*	**420**	**300**	**360**	**300**
	540	**300**	**660**	**360**	**420**	**360**
	600	**360**	**780**	**420**	**600**	**420**
	660	**420**	**900**	**660**	**660**	**600**
	720	**540**	**960**	**780**	**720**	**660**
	780	**600**	**1080**	**900**	**780**	**720**
	960	**660**	**1090**	**960**	**840**	**780**
	1080	**720**	**1320**	**1080**	**1080**	**840**
	1090	**780**		**1320**	**1090**	**900**
	1200	**840**		**1440**	**1320**	**960**
	1320	**960**				**1080**
	1440	**1080**				**1320**
		1200				**1440**
		1320				
		1440				

Table 7.7. Current spectrum peaks for motor #3 with Threshold = -5 dB
Bold values indicate line current or harmonic, * indicates bearing induced frequency

	Current Ix		**Current Iy**		**Current Iz**	
	Initial	**Final**	**Initial**	**Final**	**Initial**	**Final**
	0	0	1.46	1.46	0	1.46
	30*	30*	30.75*	30.75*	30*	30.75*
	60	**60**	**60.03**	**60.03**	**60**	**60.03**
	90*	**180**	89.31*	**180.09**	90*	89.31*
	120	260*	**120.06**	259.15*	**120**	**180.09**
	180	290*	**180.09**	292.83*	**180**	292.83*
	260*	**300**	260.61*	**300.15**	290*	**300.15**
	290*	380	292.83*	379.21	**300**	379.21
Peak Frequency (Hz)	**300**	**420**	**300.15**	**418.74**	380	**418.74**
	380	**600**	380.67	**658.86**	**420**	**658.86**
	420	**660**	**418.74**	**778.92**	**660**	**718.89**
	540	**720**	**658.86**	898.98	**720**	**778.92**
	660	980*	**778.92**	1098.10*	**780**	**838.95**
	720	1100*	1098.10*	1336.75	**840**	1098.10*
	780	1220	1338.21		1100*	1336.75
	1100*	1340			1340	
	1220	1460				
	1340					

the spectra. The stator current frequencies at the higher end are indicative of bearing vibration and are identified using the relationship in Equation (4.2). Identification of the source of unknown peaks may provide better accuracy in the determination of motor characteristics and degradation.

7.1.1.3. Peak Identification for the Vibration Spectra of the Fluted Motors

Unlike the current spectrum where one threshold level could usually be set for both the initial and final cycles, the vibration spectra required different threshold levels for different cycles. This was caused by large changes in the magnitudes of vibration as the motor experienced fluting.

In Table 7.8-7.10, as well as the example data in Figures 7.3-7.8 (Motor #11, signals V1, V2 and Vc, initial and final cycles), many peaks above the threshold were observed. The peak values of the final spectra in Figures 7.4, 7.6 and 7.8, seem to fall into certain frequency bands. Similar results were found for motors #11 and 12.

Tables 7.8-7.10 give an idea of the complexity of a fluted-bearing vibration signal. Very few spectral peaks could be matched with theoretical frequencies. Thus, it is of importance to determine the source of interesting frequency ranges (or IFRs) for fluted motors. The IFRs are determined in Section 7.1.2.

A close inspection of the bearing races and balls indicate damage in the form of pitting and frosting. The large spread of frequencies in the vibration spectrum might be due to these numerous surface imperfections. This finding is presented for the first time in this research. The high frequency components (above 1 kHz) are characteristic of bearing fluting degradation.

7.1.2. Identification of Interesting Frequency Regions (IFRs)

The frequency ranges found in the preliminary results sections (6.2.2.1-6.2.2.3 and 6.2.3.1-6.2.3.3), the spectral plots using logarithmic scale for motor current and linear scales for vibration (examples given in Figures 7.1-7.8) and the tabulated values (Tables 7.5-7.10) were

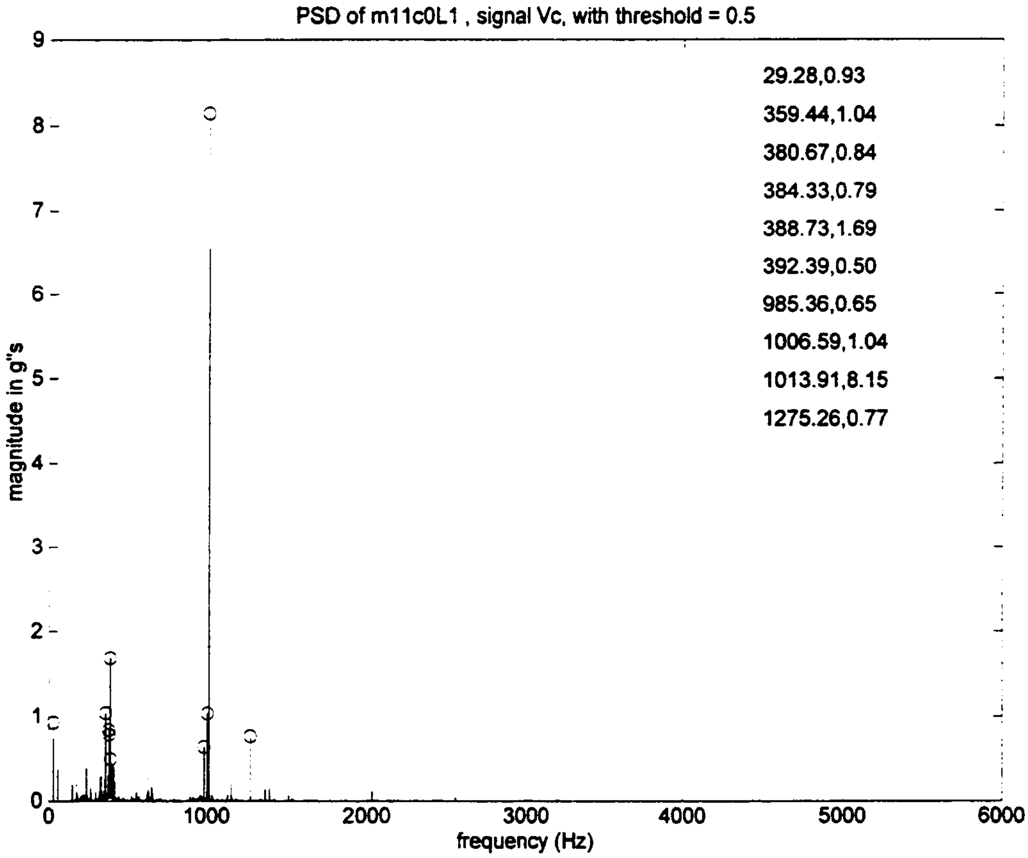

Figure 7.3. PSD of Motor #11, signal Vc, initial cycle, with a threshold of 0.5 g.

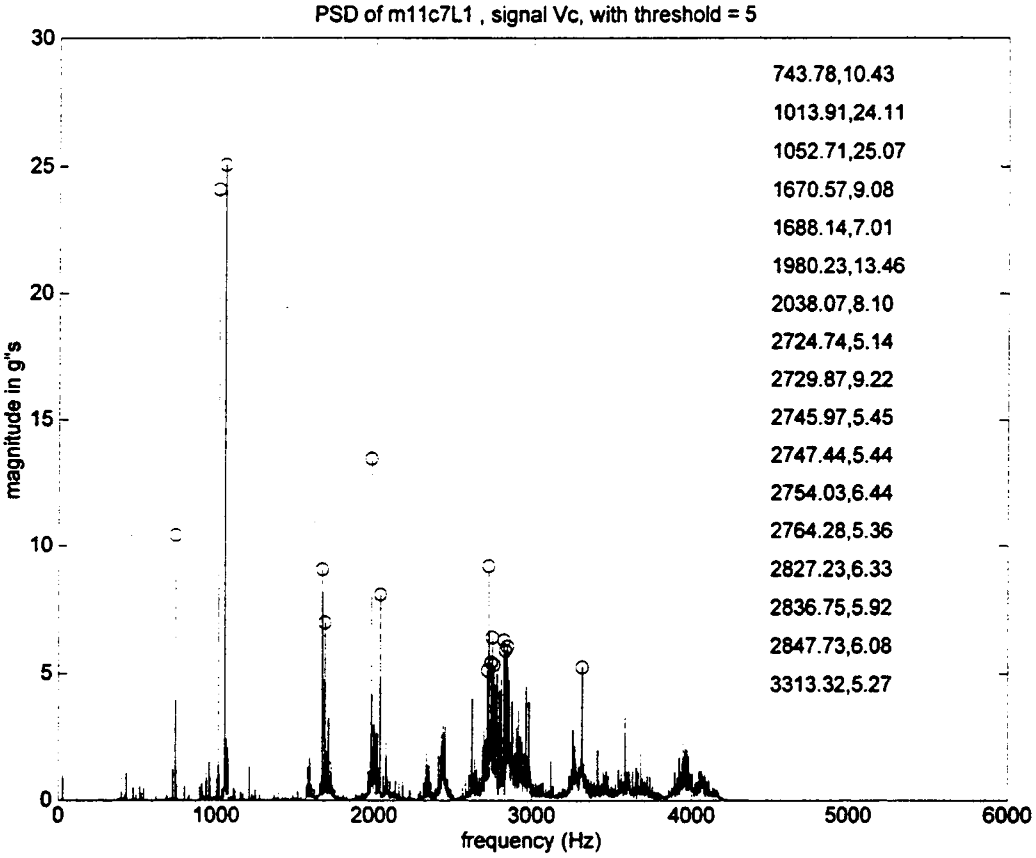

Figure 7.4. PSD of Motor #11, signal Vc, final cycle, with a threshold of 5 g.

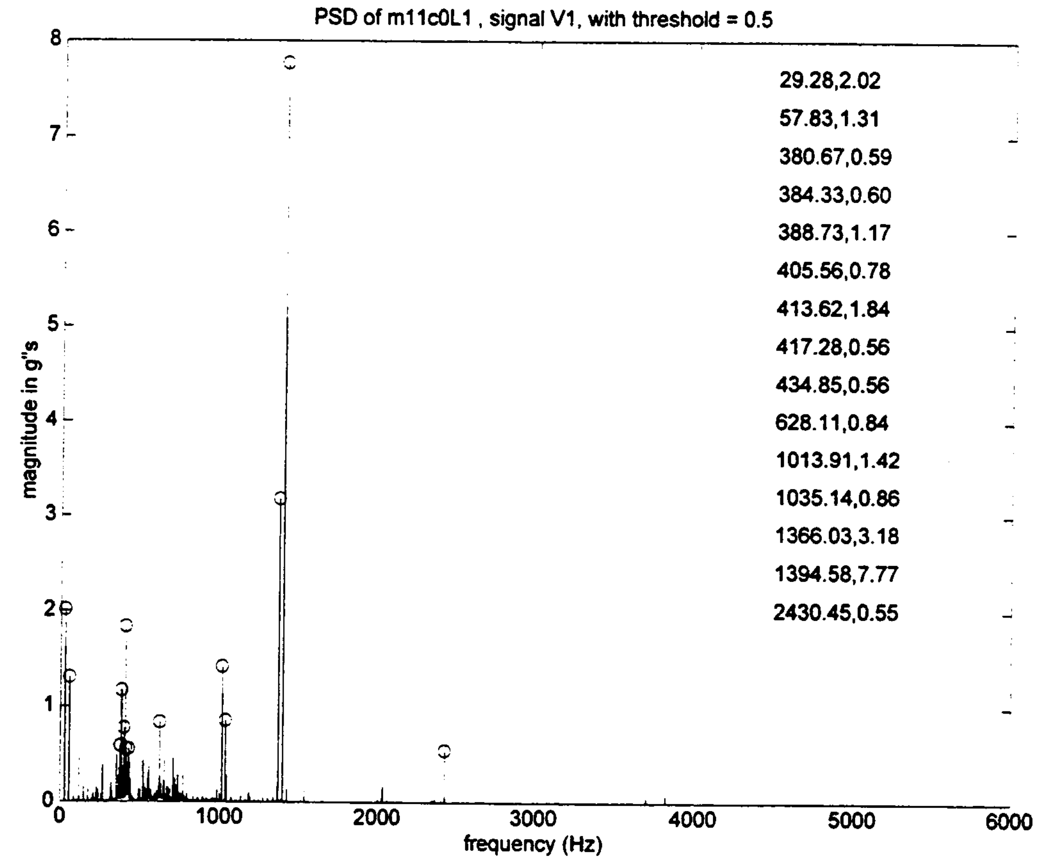

Figure 7.5. PSD of Motor #11, signal V1, initial cycle, with a threshold of 0.5g.

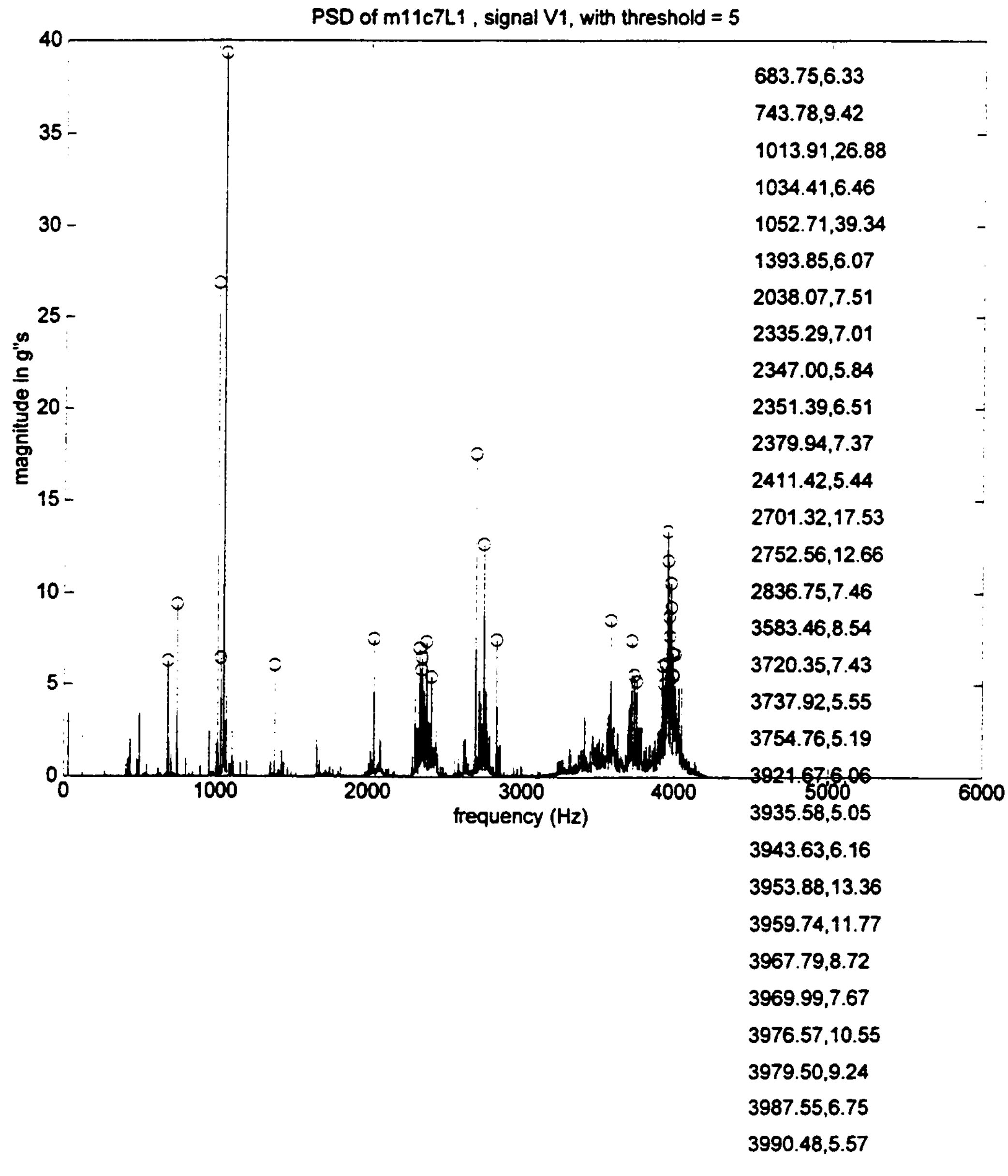

Figure 7.6. PSD of Motor #11, signal V1, final cycle, with a threshold of 0.5g.

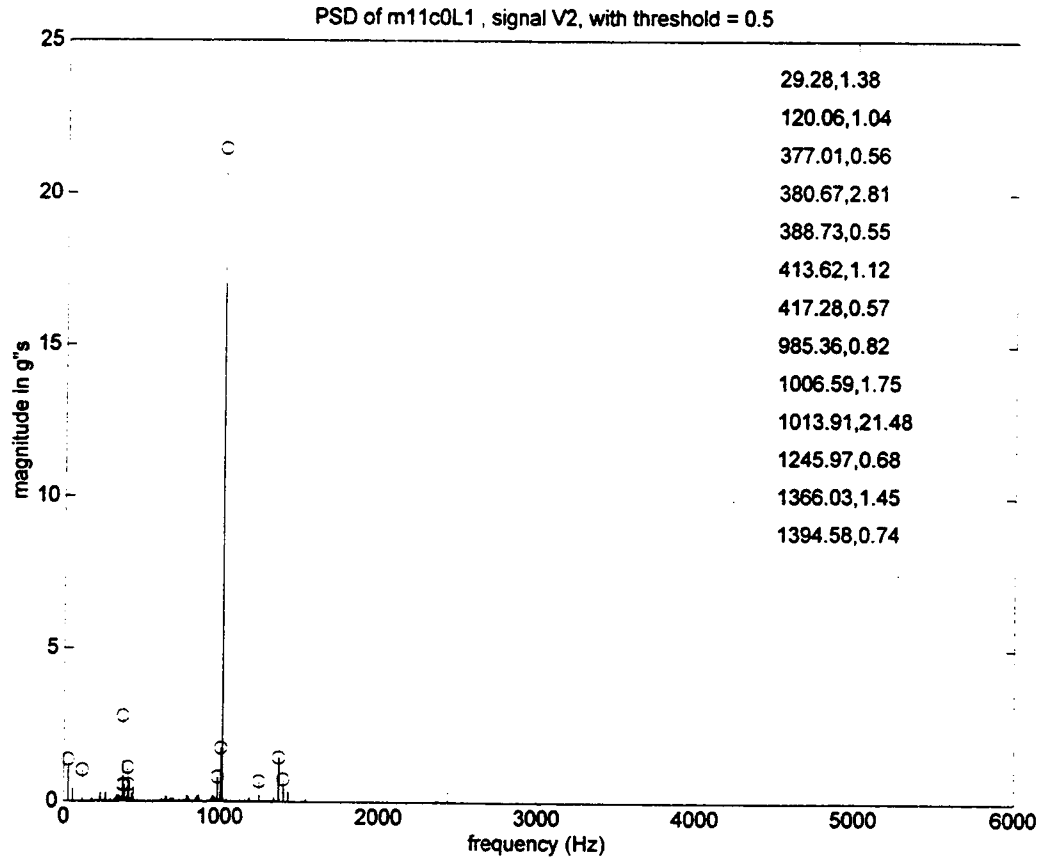

Figure 7.7. PSD of Motor #11, signal V2, initial cycle, with a threshold of 0.5g.

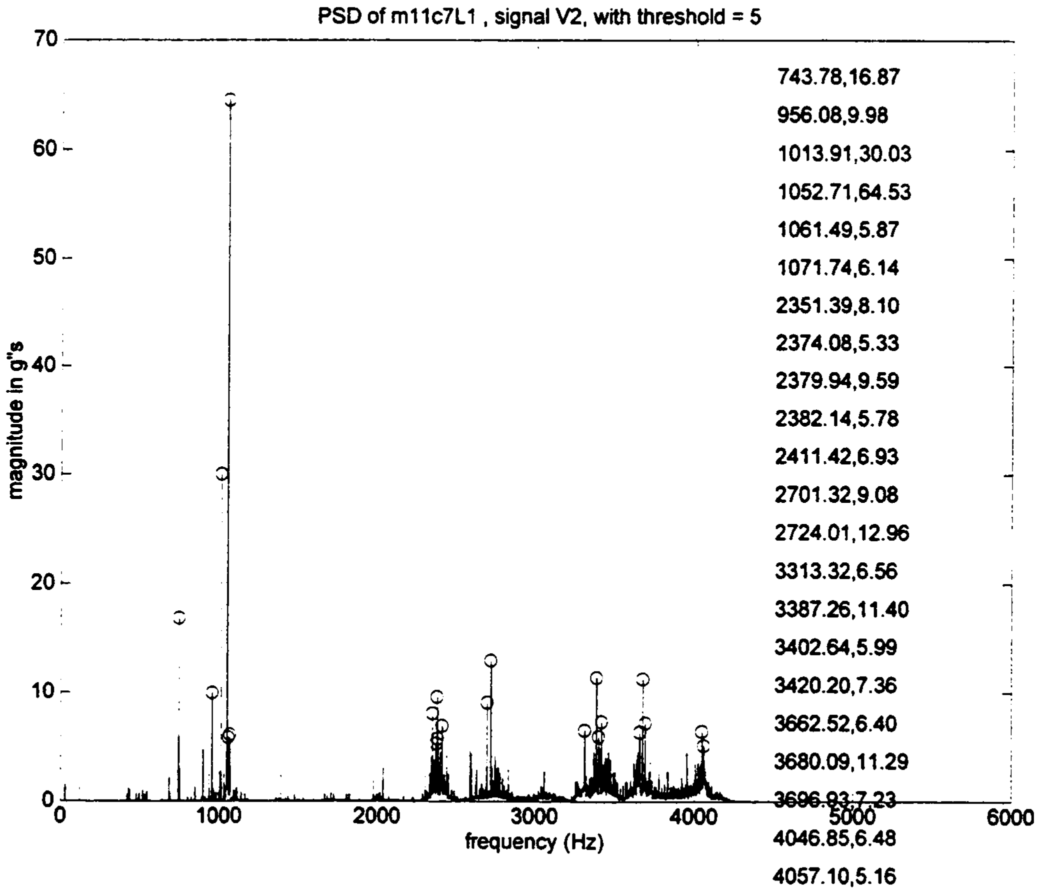

Figure 7.8. PSD of Motor #11, signal V2, final cycle, with a threshold of 0.5g.

Table 7.8. Vibration spectrum peaks for motor #11 with initial threshold = 0.5 and final threshold = 5

	Cover Vibration (Vc)		**Vibration at 10:00 (V1)**		**Vibration at 2:00 (V2)**	
	Initial	**Final**	**Initial**	**Final**	**Initial**	**Final**
	29.28	743.78	**29.28**	683.75	**29.28**	743.78
	359.44	1013.91	**57.83**	743.78	**120.06**	956.08
	380.67	1052.71	**380.67**	1013.91	**377.01**	1013.91
	384.33	1670.57	384.33	1034.41	**380.67**	1052.71
	388.73	1688.14	388.73	1052.71	388.73	1061.49
	392.39	1980.23	405.56	1393.85	**413.62**	1071.74
	985.36	2038.07	**413.62**	2038.07	417.28	2351.39
	1006.59	2724.74	417.28	2335.29	985.36	2374.08
Peak Frequency (Hz)	1013.91	2729.87	**434.85**	2347.00	1006.59	2379.94
	1275.26	2745.97	628.11	2351.39	1013.91	2382.14
		2747.44	1013.91	2379.94	1245.97	2411.42
		2754.03	1035.14	2411.42	**1366.03**	2701.32
		2764.28	**1366.03**	2701.32	1394.58	2724.01
		2827.23	1394.58	2752.56		3313.32
		2836.75	2430.45	2836.75		3387.26
		2847.73		3583.46		3402.64
		3313.32		3720.35		3420.20
				3737.92		3662.52
				3754.76		3680.09
				3921.67		3696.93
				3935.58		4046.85
				3943.63		4057.10
				3953.88		
				3959.74		
				3967.79		
				3969.99		
				3976.57		
				3979.50		
				3987.55		
				3990.48		

Table 7.9. Vibration spectrum peaks for motor #12 with initial threshold = 0.25 and final threshold [-]

	Cover Vibration (Vc), [0.25]		Vibration at 10:00 (V1), [20]		Vibration at 2:00 (V2)), [10]	
	Initial	**Final**	**Initial**	**Final**	**Initial**	**Final**
Peak Frequency (Hz)	**29.28**	306.0	**115.67**	306.0	**177.89**	306.0
	120.06	641.3	**120.06**	612.0	268.67	612.0
	177.89	669.8	**206.44**	640.6	359.44	640.6
	206.44	699.1	293.56	669.8	**413.62**	669.8
	235.72	736.5	**413.62**	678.6	417.28	6742.2
	351.39	765.0	417.28	793.6	1013.91	736.5
	359.44	793.6	718.89	888.7	**1366.03**	765.0
	413.62	822.8	1013.91	918.0		794.3
	1013.91	851.4	1035.14	946.6		822.8
	1035.14	855.1	1184.48	2291.4		860.2
	1101.02	860.2	1394.58	2295.0		888.7
	1155.20	865.3	2430.45	2296.5		918.0
		882.9		2299.4		2291.4
		888.7		2301.6		2293.6
		918.0		2306.7		2295.0
		946.6		2601.8		2296.5
		1377.0		3539.5		2299.4
		1499.3		3543.9		2301.6
		1501.5		3546.1		2303.1
		2598.8		3552.7		2306.7
		2601.8		3641.3		2309.7
		2604.7		3816.3		2601.8
		2607.6		3827.2		
		2631.0		3833.1		
		2896.8		3835.3		
		2899.7		3837.5		
		2907.8		3844.1		
				3846.3		
				3850.7		
				3854.3		
				3857.2		
				3859.4		
				3862.4		
				3865.3		
				3867.5		
				3869.0		
				3871.9		
				3874.1		

Table 7.9 (continued)

	Cover Vibration (Vc), [0.25]		Vibration at 10:00 (V1), [20]		Vibration at 2:00 (V2)), [10]	
	Initial	**Final**	**Initial**	**Final**	**Initial**	**Final**
Peak Frequency (Hz)				3875.5		
				3879.9		
				3882.1		
				3884.3		
				3888.0		
				3891.7		
				3894.6		
				3896.8		
				3904.1		
				3906.3		
				3926.1		

Table 7.10. Vibration spectrum peaks for motor #13 with threshold = [-]

	Cover Vibration (Vc)		**Vibration at 10:00 (V1)**		**Vibration at 2:00 (V2)**	
	Initial [1.0]	**Final_[5.0]**	**Initial [1.5]**	**Final_[5.0]**	**Initial [1.0]**	**Final_[5.0]**
	29.28	814.1	**29.28**	**29.30**	**29.28**	521.2
	1013.91	834.6	**120.06**	500.0	**120.06**	540.3
	1017.57	912.9	**381.41**	678.6	**381.41**	954.6
	1020.50	954.6	439.97	954.6	959.00	1115.7
	1039.53	1016.1	1017.57	1016.1	1010.25	1122.3
	1158.86	1122.3	1020.50	1064.4	1013.91	1127.4
		1147.1	1039.53	1122.3	1017.57	1147.1
		1782.6	1071.74	1147.1	1020.50	1773.1
		1920.9	1075.40	1441.4	1039.53	1854.3
		1944.4	1398.98	1782.6	1075.40	2060.0
		2001.5	2333.82	1854.3	2333.82	2336.7
		2060.0		1912.9		2343.3
		2343.3		2226.2		2354.3
Peak Frequency (Hz)		2620.8		2343.3		2371.9
		2622.3		2354.3		2375.5
		2655.2		2371.9		2377.7
		2691.1		2375.5		2383.6
		2759.9		2377.7		2387.3
		2823.6		2383.6		2389.5
		2836.7		2387.3		2395.3
		2854.3		2395.3		2399.0
		2893.1		2399.0		2401.2
		2921.7		2407.0		2407.0
		2939.2		2639.1		2620.8
		3267.2		2726.2		2749.6
				2749.6		2784.8
				2761.3		2836.7
				2778.9		2854.3
				2784.8		3110.5
				2814.1		3127.4
				2836.7		3267.2
				2854.3		3325.0
				3249.6		3511.7
				3267.2		3980.2
				3284.8		4052.0
				3290.6		4069.5
				3292.1		

Table 7.10 (continued)

	Cover Vibration (Vc)		Vibration at 10:00 (V1)		Vibration at 2:00 (V2)	
	Initial [1.0]	**Final [5.0]**	**Initial [1.5]**	**Final [5.0]**	**Initial [1.0]**	**Final [5.0]**
Peak Frequency (Hz)				3325.0		
				3953.1		
				3968.5		
				3980.2		

used to identify the IFRs in the various power spectra.

Using the graphed spectra (also used in the preliminary results), the IFRs were identified. But, when using the graphed spectra, there may be some error when assigning a value along the frequency axis. Using tabulated values, we can precisely identify the range of frequency, but it is a range that is above a specified threshold value. Thus, this may not represent the total span of the interesting frequency range. By using both, the IFRs were identified. Notice that the IFRs are at high frequencies.

Section 7.1.2 is divided into two parts, one to deal with motor current frequency ranges and the other to deal with vibration signal frequency ranges.

7.1.2.1. Interesting Frequency Ranges (IFRs) within the Motor Current Spectra

Within the motor current spectra, using the stator-aged data, no IFRs were identified. None of the peaks or regions of frequencies within the spectra seemed to change from the initial cycle to final cycle. Examples of the initial and final motor current spectra for motor #1, current Ix are given in Figures 7.1 and 7.2. As seen later in section 7.2.2.2, the 60Hz region RMS values do change as the cycles progress.

7.1.2.2. Interesting Frequency Ranges (IFRs) within the Vibration Spectra

The vibration spectra, using the bearing fluted data, have a different behavior compared to the motor current spectra. The vibration signals showed many IFRs in the final spectra (an example shown in Figure 7.4, Figure 7.6 or Figure 7.8) as compared to one for the initial cycle (Figure 7.3, Figure 7.5 or Figure 7.7). The IFRs are listed for each motor and for the three signals in Tables 7.11-7.13. The IFRs represent a change (or degradation) in the motor condition, specifically the bearings in this case.

Table 7.11. IFRs for motor #11

Motor #11 signal type / frequency range	Vc	V10:00	V2:00
Frequency Ranges (Hz)	950-1050	950-1050	950-1050
	1600-1700	1900-2100	2300-2400
	1900-2100	2300-2400	2600-2900
	2500-3000	2600-2900	3400-4100
	3250-3350	3400-4100	

Table 7.12. IFRs for motor #12

Motor #12 signal type / frequency range	Vc	V10:00	V2:00
Frequency Ranges (Hz)	700-1000	600-1000	600-1050
	2500-3000	2300-2400	2300-2400
		2600-2700	2600-2900
		3500-4100	

Table 7.13. IFRs for motor #13

Motor #13 signal type / frequency range	Vc	V10:00	V2:00
Frequency Ranges (Hz)	900-1100	900-1100	1000-1150
	1900-2100	1800-1900	2300-2400
	2600-3100	2300-2400	2600-2900
	3200-3300	2600-2800	3000-3500
		3100-3400	4000-4100
		3800-4100	

7.1.3. Correlation and Coherence Between Signals

Coherence functions were calculated for pairs of current signals, pairs of vibration signals and between current and vibration signals. The frequency-domain signature was calculated for cases when the correlation coefficient has a high value. Therefore, the correlation coefficients were first calculated in order to establish signal pairs for computing coherence functions.

7.1.3.1. Correlation Coefficients

As stated in section 5.2.2, the correlation coefficients were plotted using the sum of the absolute value of the correlation coefficients for all the cycles divided by the number of cycles. Example plots of the correlation coefficients for Motor #3 are shown in Figures 7.9-7.13. The combination of summed signal pair correlation coefficient values (SSPCC) are listed in Table 7.14 for all motors.

The highest overall correlation coefficient (in bold) for a signal group was used for each aging motor group. The resulting signal combinations for coherence calculations are shown in Table 7.15. Note that all six signals, with 20 different pair combinations, were used in each motor aging group.

7.1.3.2. Coherence Function

The coherence functions were calculated using the above combination of signals for the specified motor for the initial and final cycles. The results are divided into stator aged and bearing fluting aged groups. Note that the threshold values can change from one cycle to another. Coherence plots for the various combinations are shown in Appendix C.

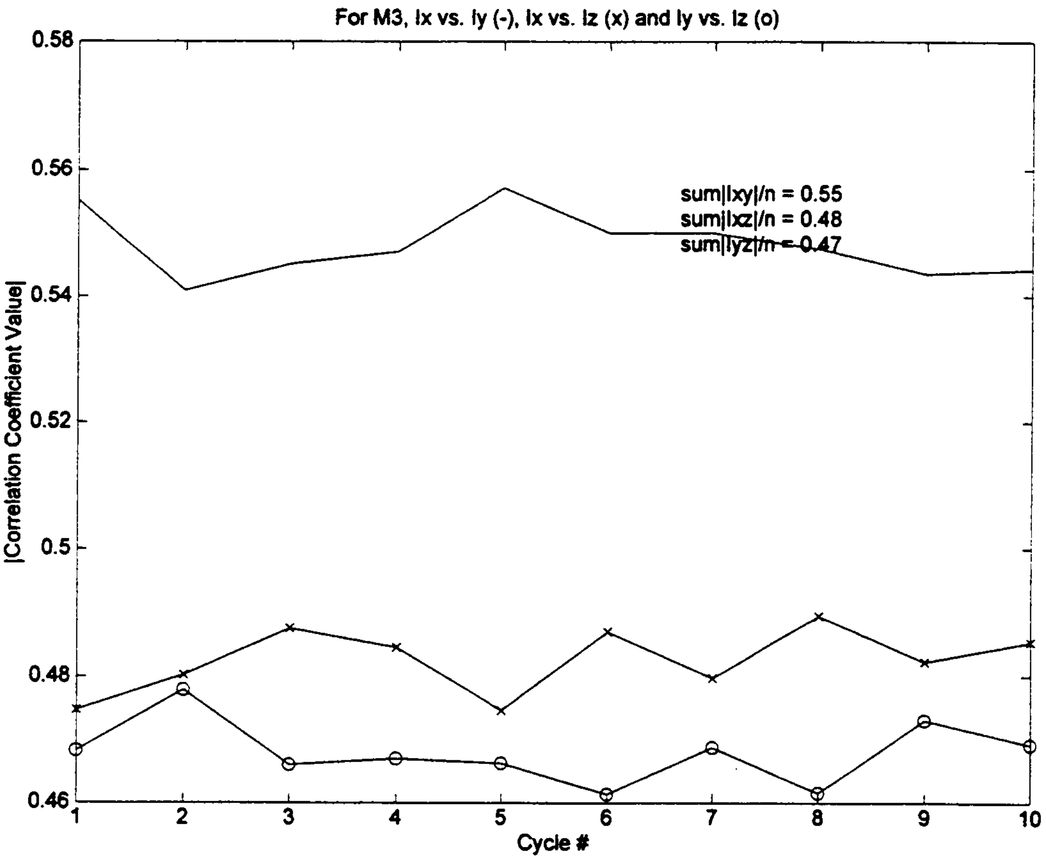

Figure 7.9. Motor #3 signal pair correlation coefficient values for specified pairs.

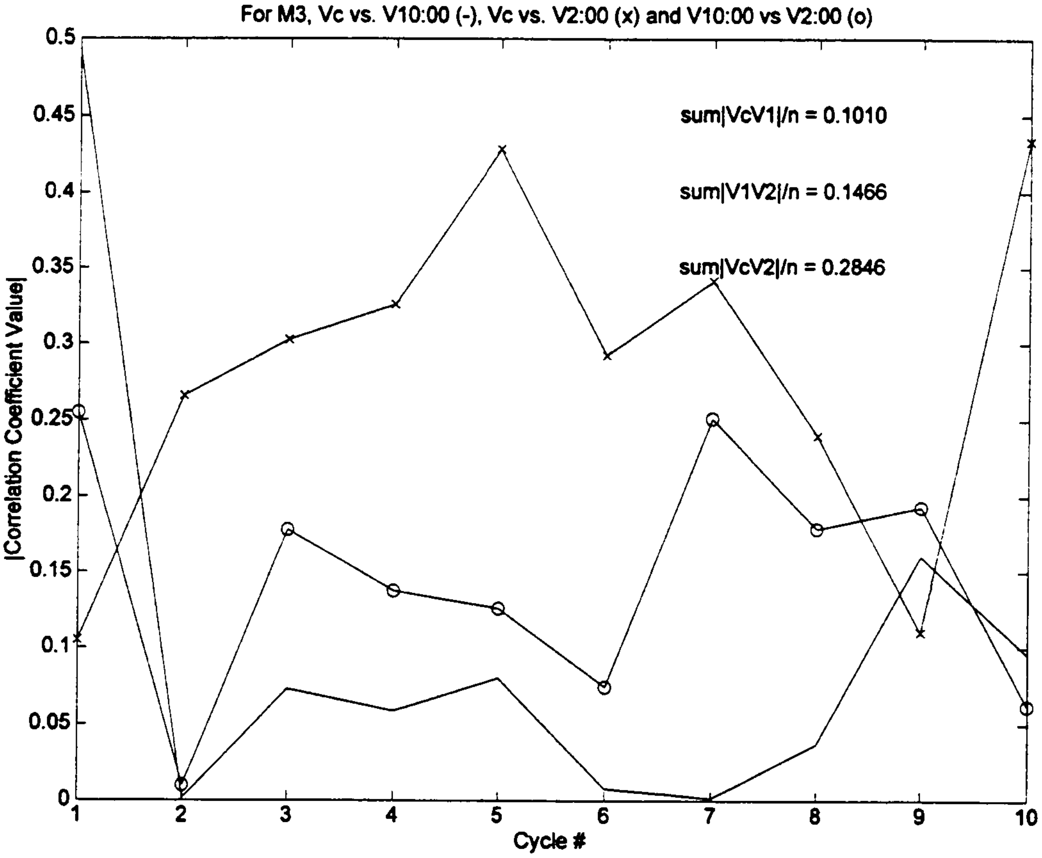

Figure 7.10. Motor #3 signal pair correlation coefficient values for specified pairs.

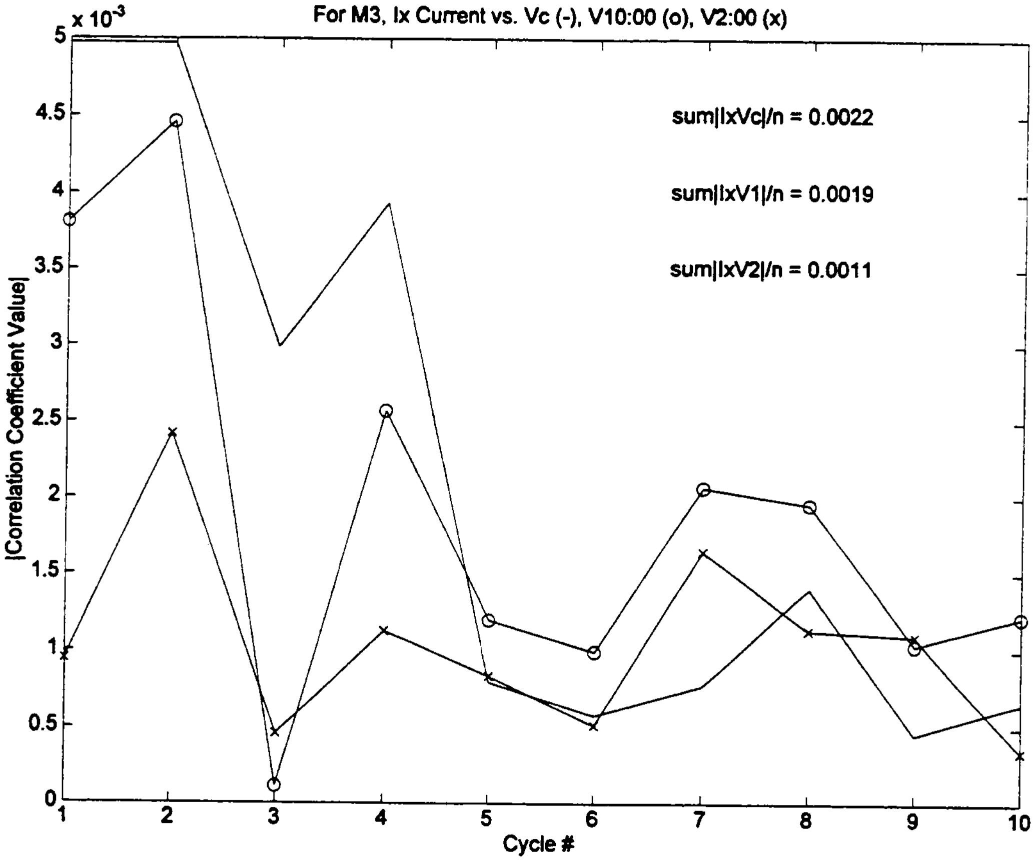

Figure 7.11. Motor #3 signal pair correlation coefficient values for specified pairs.

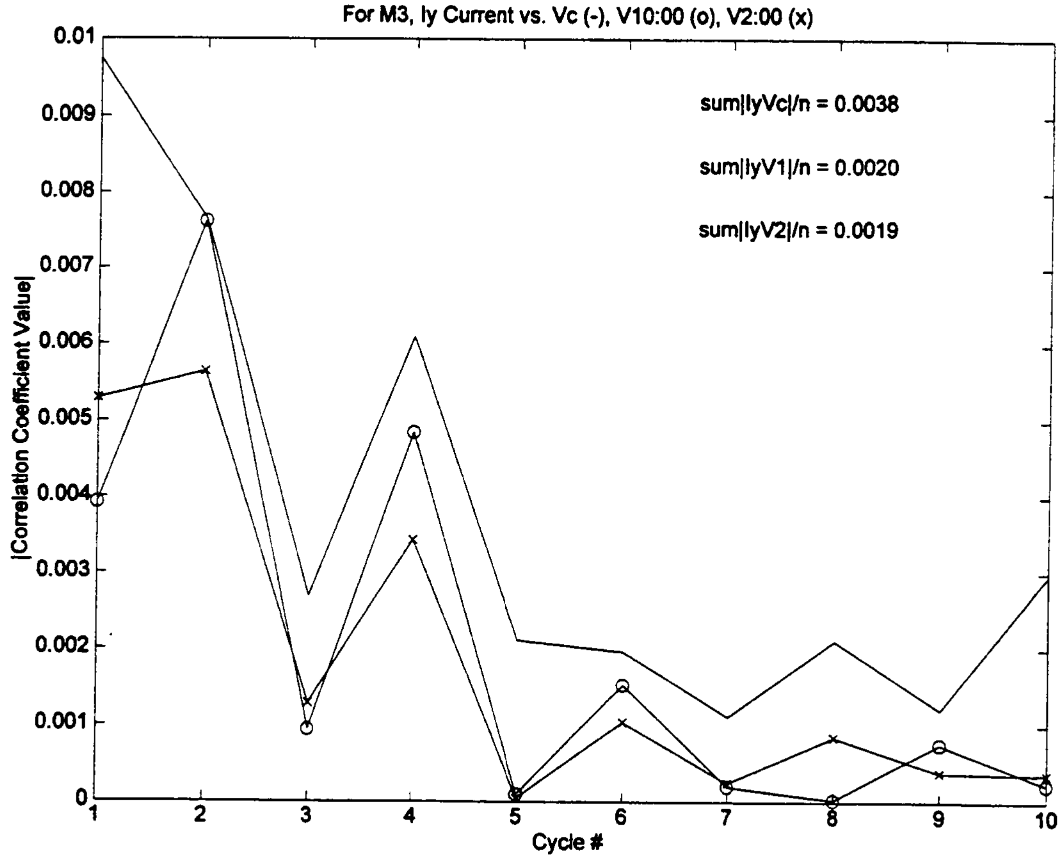

Figure 7.12. Motor #3 signal pair correlation coefficient values for specified pairs.

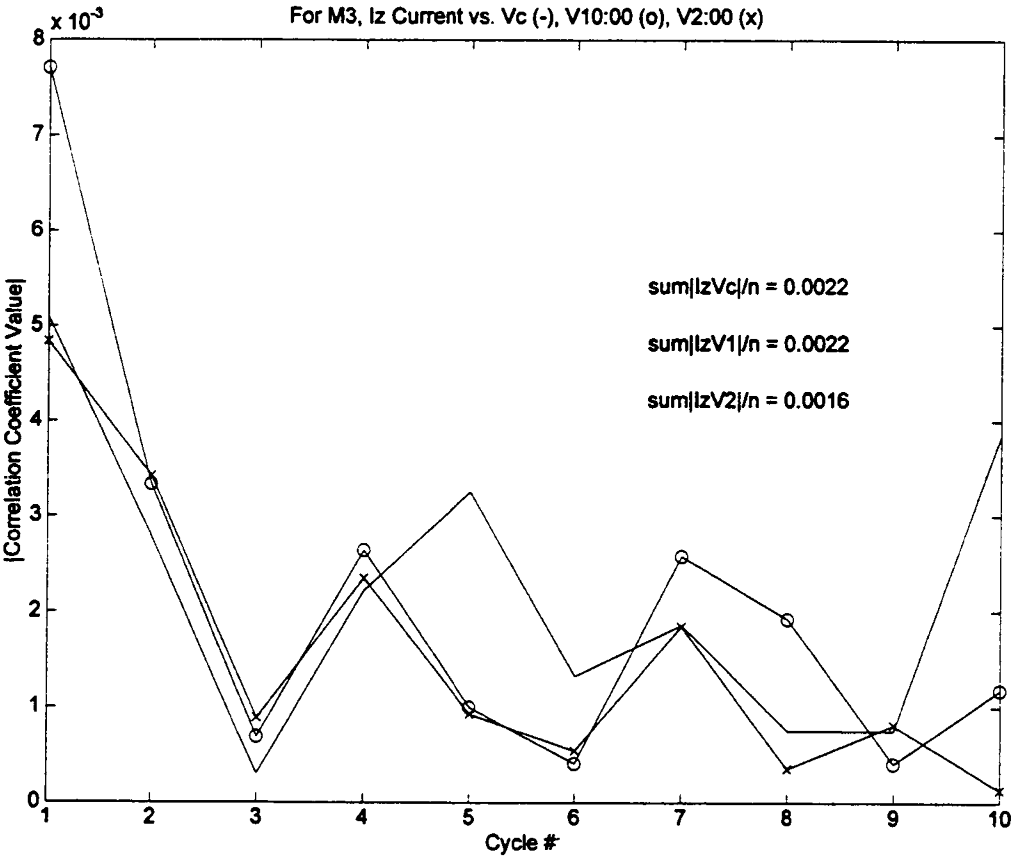

Figure 7.13. Motor #3 signal pair correlation coefficient values for specified pairs.

Table 7.14. SSPCC values for all motors and signal combinations
Highest value in **bold**.

Signal Comb/ Motor #	**1**	**2**	**3**	**11**	**12**	**13**
Vc-V1	0.1677	0.3443	0.1010	0.1089	0.1279	0.1750
V1-V2	0.1271	0.3492	0.1466	0.1298	0.0960	0.1755
V2-Vc	0.1239	**0.5420***	**0.2846**	0.2651	0.2324	**0.4079**
Ix-V1	0.0015	0.0036	0.0019	0.0010	0.0004	0.0009
Ix-V2	0.0011	0.0027	0.0011	0.0007	0.0007	0.0004
Ix-Vc	0.0020	0.0024	0.0022	0.0008	0.0012	0.0007
Iy-V1	0.0017	0.0036	0.0020	0.0011	0.0007	0.0011
Iy-V2	0.0013	0.0013	0.0019	0.0007	0.0005	0.0003
Iy-Vc	0.0014	0.0030	**0.0038**	0.0009	**0.0013**	0.0008
Iz-V1	0.0014	0.0030	0.0022	0.0006	0.0004	0.0010
Iz-V2	0.0014	0.0021	0.0016	0.0006	0.0005	0.0005
Iz-Vc	0.0020	0.0021	0.0022	0.0003	0.0005	0.0006
Ix-Iy	0.54	0.54	**0.55**	0.54	**0.55**	0.53
Iy-Iz	0.47	0.47	0.47	0.47	0.47	0.51
Iz-Ix	0.49	0.49	0.48	0.49	0.48	0.46

* This value includes motor #2 cycle #2 data. Therefore, it will not be used.

Table 7.15. Coherence function signal pair combinations

Motor # / Signals	Current vs. Current	Vibration vs. Current	Vibration vs. Vibration
1	none	none	none
2	none	none	none
3	Ix ,Iy	Vc , Iy	Vc , V2:00
11	none	none	none
12	Ix , Iy	Vc , Iy	none
13	none	none	V2:00 , V10:00

7.1.3.2.1. Coherence Results for Stator-Aged Motors

For motor #3, the coherence between the currents Ix and Iy is generally above 0.6 for both the initial and final spectra in the range 0-2,500 Hz. After 2,500 Hz there is a significant drop-off, to 0.35, in the coherence. The initial and final spectra look approximately the same behavior. Since there is little change in the coherence function spectra for the signal pair Ix and Iy from initial to final cycle, the aging process does not seem to affect the relationship between these two signals. These results are shown in Figures 7.14 and 7.15.

For motor #3, the coherence function between Vc and Iy is generally below 0.35 for all frequencies for the initial cycle. There are peaks above 0.5, with these peaks occurring at harmonics of 60 Hz. at 120, 240, 360, 480, 600, etc. But as the motor is aged, the coherence function changes. There are more peaks above 0.35 in the final cycle than in the initial cycle. Some of these peaks seem to be 60 Hz harmonics. Therefore, the aging process causes a minor change in the relationship between these two signals. These results are shown in Figures C.1 and C.2.

For motor #3, the coherence function between Vc and V2 is very high (> 0.6) up to 5,000 Hz, for both the initial and final cycles. But, there is a large difference in the coherence above 2,000 Hz between the initial and final cycle spectra. The final cycle exhibits extremely high coherence in the range 2,500-3,500 Hz and also at 4,500 Hz, whereas the initial cycle does not exhibit this. Thus, the aging process causes a significant change in the relationship between these two signals. These results are shown in Figures C.3 and C.4.

7.1.3.2.2. Bearing Fluting Coherence Data

For motor #12, the coherence function between signals Ix and Iy (both initial and final cycles shown in Figures C.5 and C.6) acts similarly to that of motor #3. Therefore, the bearing fluting aging process does not affect the relationship for this signal pair.

But, for motor #12, the coherence between Vc and Iy (shown in Figures C.7 and C.8) drops from the initial to final cycle. For the initial cycle, there are many peaks above 0.5, but the

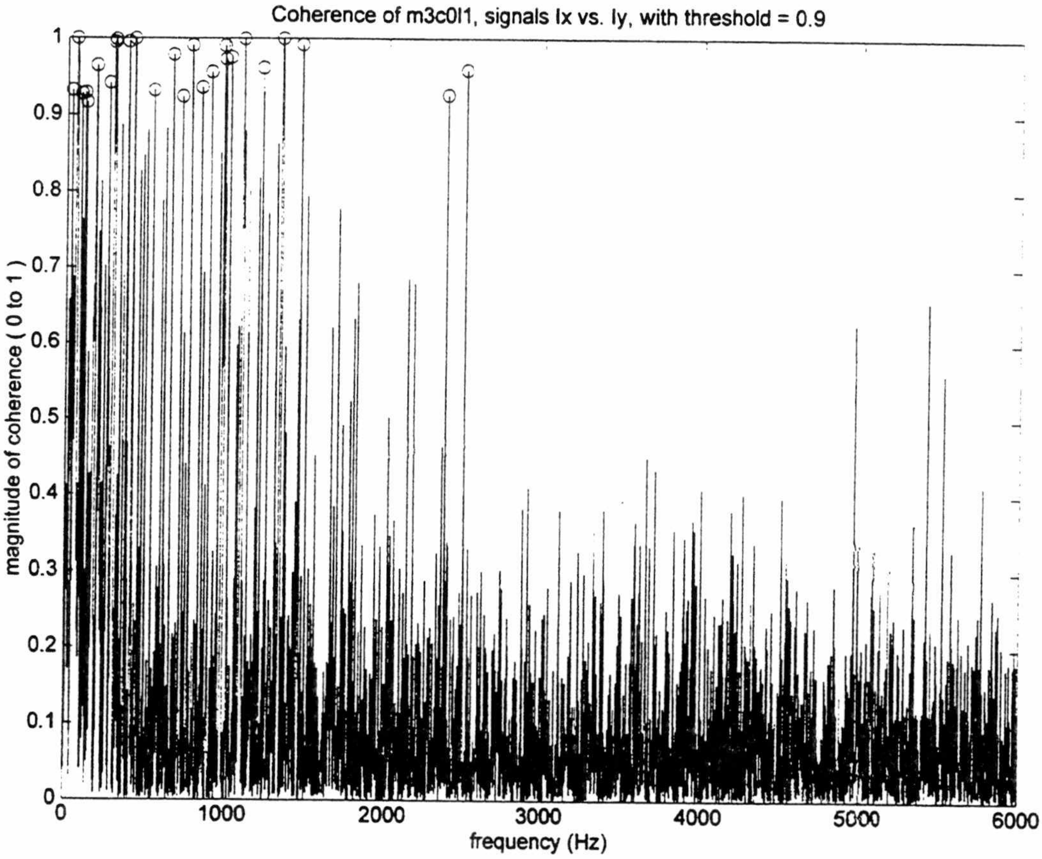

Figure 7.14. Initial coherence function for motor #3 using signals Ix and Iy.

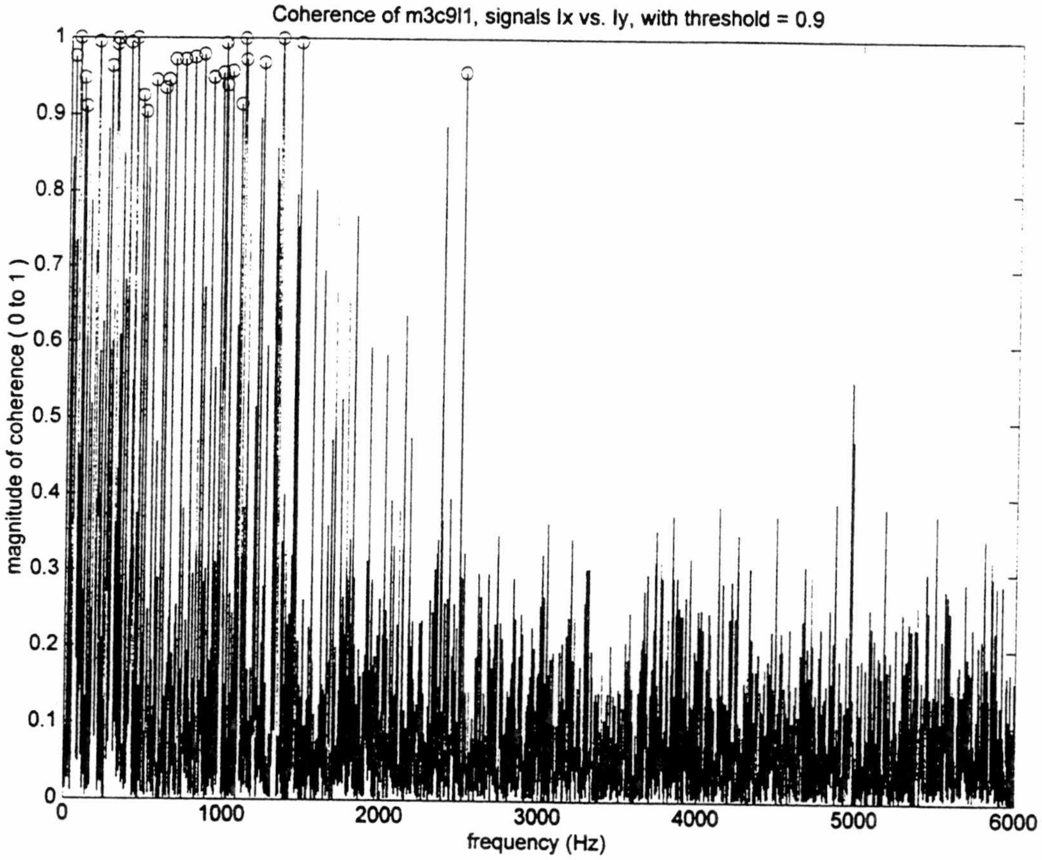

Figure 7.15. Final coherence function for motor #3 using signals Ix and Iy.

final cycle has only two peaks above that value. The bearing fluting aging process causes a significant decrease in the relationship between these two signals.

The coherence between signals Vc and V2 for motor #13 (Figures C.9 and C.10) has similar results to motor #3 Vc and V2. There is extremely high coherence (> 0.8) in the initial spectrum from 0-4,000 Hz, with a drop-off at 4000 Hz to 0.3. The final coherence spectrum exhibits extremely high coherence (> 0.8) from 0-5,500 Hz, with many more peaks above the threshold value of 0.95 than the initial cycle. Thus the bearing fluting aging process contributes a significant increase in the relationship between these two signals.

The coherence function provides a qualitative assessment of the causal relationship between any two signals. This could be specifically applied to determine if bearing vibrations cause motor current spectral peaks and quantify the correlation.

7.2. Wavelet 1-D Decomposition of the Signals and Signature Trending

The wavelet 1-D decomposition section is divided into two parts. The first part presents general observation or visual trending from the wavelet-processed signals. The second part deals with trending the RMS values for each level of the wavelet-decomposed signals.

7.2.1. Wavelet 1-D Sub-banded RMS Visual Trending

The results for the 1-D Wavelet Decomposition is divided first into two sections, one for the motor currents (using motors #1, 2 and 3) and the other for the vibration (using motors #11, 12 and 13). These signals are divided into the eight levels used for the decomposition with each level representing a specific frequency range. The results are classified as very trendable, trendable, questionable or not trendable for each signal at each level. The terms are defined as follows

- Very trendable means that there is no decrease (or increase for a decreasing trend) in values as the cycles progress. A value assigned to this classification will be 3.

- Trendable is interpreted as a small changes in the RMS value as the cycles progress with the overall values generally increasing. A value assigned to this classification will be 2.
- Questionable means that there is more than one decrease in RMS values as the cycles progress, but there is a general increase in the RMS values. A value assigned to this classification will be 1.
- Not trendable encompasses plots with many peaks and valleys and very little increase (or decrease) in RMS values as the cycles progress. A value assigned to this classification will be 0.

The total of the points will give a general idea of the trendability of each level. The rating method is done heuristically, for either an increasing or a decreasing trend. Note that motor #2 cycle #2 is used in this section, but the results should not be skewed since this procedure is heuristic in nature.

7.2.1.1. Motor Current

None of the motor currents (for the stator-aged motors) for any level appear to trend. Only level 7 (containing the 60 Hz peak) may trend. This is a very weak trend if any.

7.2.1.2. Vibration Signals

All vibration signals (Vc, V1 and V2) for each motor (#11, 12 and 13) for each level are considered and rated. The value given in parenthesis is the number of signals, in that level, that exhibit that grade of trendability. The value is the number of total points of that rating given the number of trendable signals in that range. Only the first row calculation is shown.

The results, in Table 7.16, indicate that the third level representing 1,500 – 750 Hz. has the most trendable values with 3,000 – 1,500 and 750 - 375 Hz as the second most trendable of the levels and level one the third. These results correspond to the IFR results found in section 7.1.2.2.

Table 7.16. Heurisitic (or Visual) evaluation of trendability

Level # (Hz) \ Rating	Very Trendable	Trendable	Questionable	Not Trendable	Total Points
1 (6,000 - 3,000)	(0) 0	(2) 4	(7) 7	0 (0)	0+4+7+0 = 11
2 (3,000 - 1,500)	1	6	2	0	14
3 (1,500 - 750)	1	4	3	1	15
4 (750 -375)	0	5	4	0	14
5 (375 -187.5)	0	2	4	3	8
6 (187.5 - 93.8)	0	0	3	8	3
7 (93.8 - 46.9)	0	2	2	6	6
8(46.9 - 23.4)	0	0	7	2	7

7.2.2. Regression Fitting for the 1-D Wavelet Decomposition RMS Values

The results are grouped for each motor, with the motor signals RMS slope and error values listed by level. The level RMS values were plotted by cycle (x-axis) verus RMS value (y-axis). A criteria was established, using both the slope and the fractional RMS error values, to determine if the signal and level were trendable.

The fractional RMS error criteria for a good fit of data is approximately 0.2. Therefor, if the value for the fractional RMS error was greater than 0.2, the fit was not good and was rejected. Also, the slope of the line must be above a certain value or essentially, the signal value was not changing. The value established was ± 0.01. It should be noted that these are not general since the values may be skewed because of a 'bad' point in the trend.

7.2.2.1. Regression Fitting for the 1-D Wavelet Decomposed Motor Current RMS Values

As detailed in the wavelet section in the data processing chapter, the region of concern for motor current signatures was level 7. Level 7 corresponds to frequencies between 93.75 and 46.875 Hz, thus containing the 60 Hz frequency peak. An example using the three phase currents (Ix, Iy and Iz) for motor #1, level 7 can be seen in Figures 7.16 - 7.18. From Tables 7.17 - 7.19,

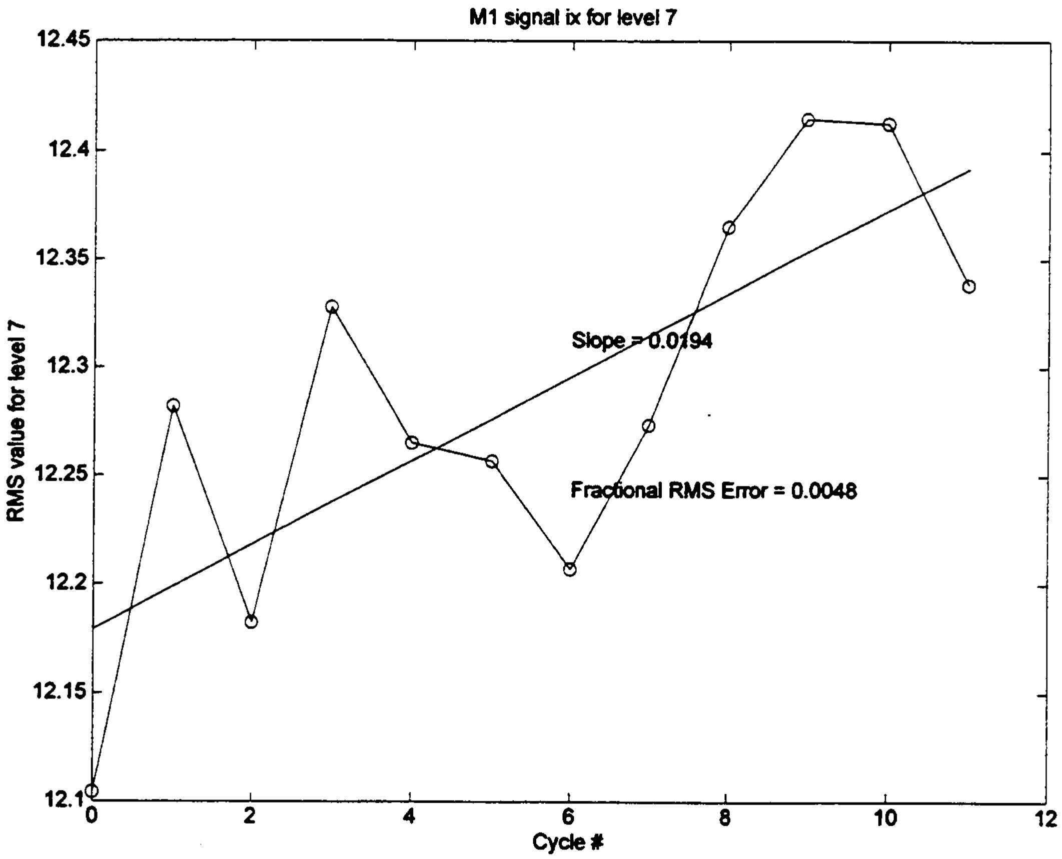

Figure 7.16. Trending plot for motor #1, signal Ix, level #7.

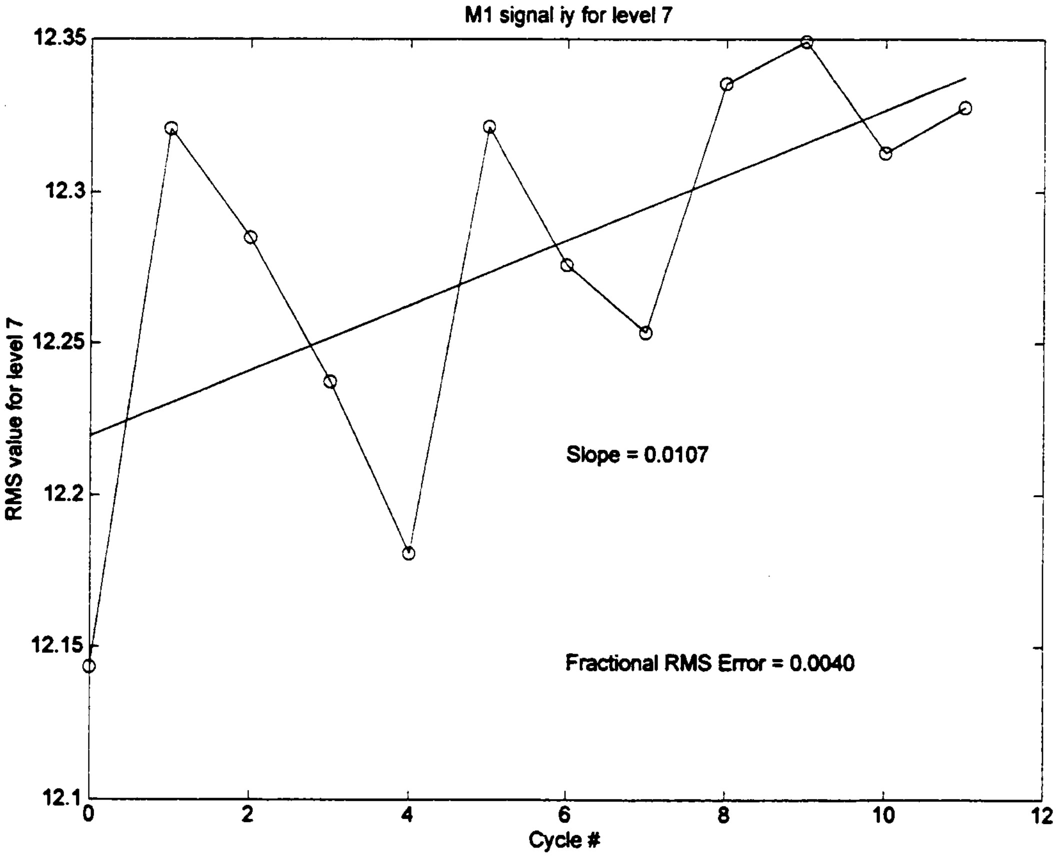

Figure 7.17. Trending plot for motor #1, signal Iy, level #7.

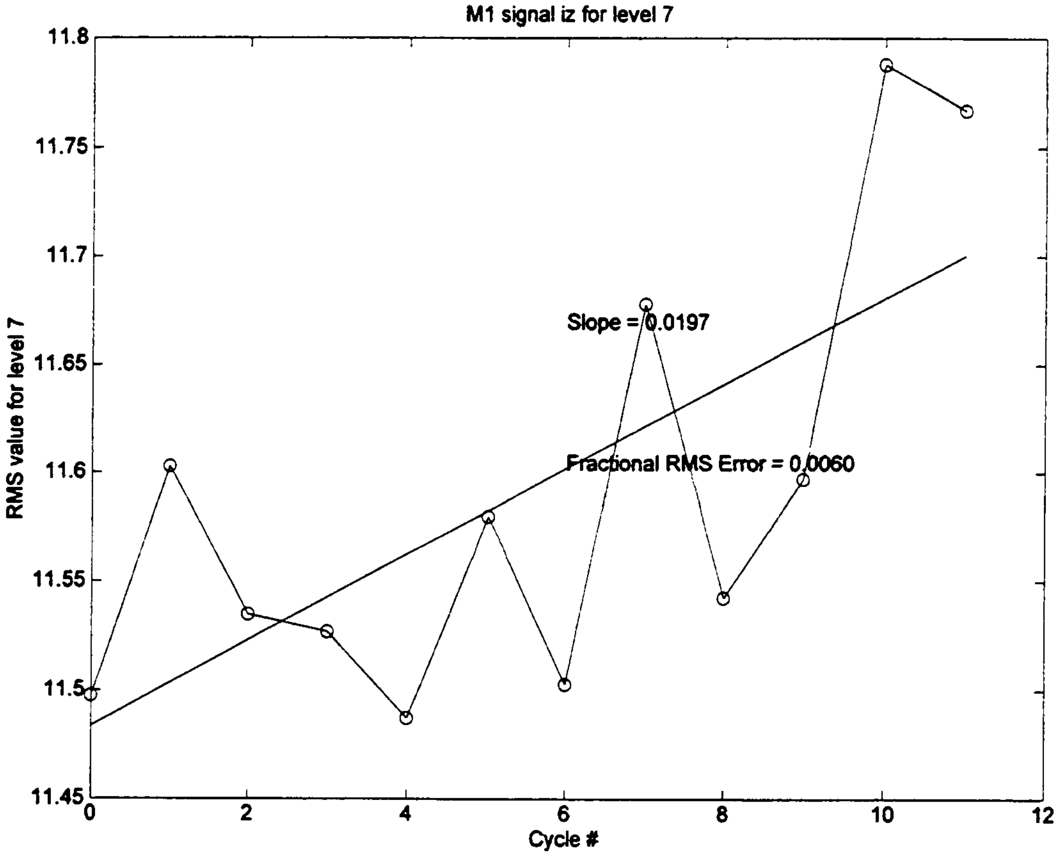

Figure 7.18. Trending plot for motor #1, signal Iz, level #7.

Table 7.17. Regression analysis for motor #1

Motor #1	Ix		Iy		Iz	
level	Slope	Error	Slope	Error	Slope	Error
8	-0.0099	0.117	0.0102	0.0707	0.0008	0.1210
7	**0.0194**	**0.0048**	**0.0107**	**0.0040**	**0.0197**	**0.0060**
6	-0.0073	0.1323	0.0058	0.2150	0.0048	0.2323
5	-0.0005	0.0948	-0.0033	0.2067	-0.0002	0.1629
4	-0.0030	0.1099	-0.0026	0.1956	0.0040	0.1242
3	-0.0013	0.0709	-0.0008	0.1462	0.0026	0.0946
2	-0.0012	0.1365	-0.0009	0.2779	0.0018	0.1768
1	-0.0015	0.2358	-0.0012	0.5940	0.0028	0.3758

Table 7.18. Regression analysis for motor #2

Motor #2	Ix		Iy		Iz	
level	Slope	Error	Slope	Error	Slope	Error
8	-0.0191	0.1497	-0.0070	0.1091	0.0389	0.0620
7	**0.0941**	**0.0068**	**0.0834**	**0.0082**	**0.0759**	**0.0093**
6	-0.0016	0.2712	-0.0206	0.1183	0.0263	0.2279
5	0.0154	0.0458	-0.0003	0.1537	0.0020	0.2330
4	0.0132	0.1037	-0.0081	0.1387	0.0058	0.2218
3	0.0074	0.1217	-0.0062	0.1536	0.0043	0.2103
2	0.0058	0.1803	-0.0051	0.2796	0.0029	0.3616
1	0.0069	0.2470	-0.0062	0.4604	0.0032	0.5194

Table 7.19. Regression analysis for motor #3

Motor #3	Ix		Iy		Iz	
level	Slope	Error	Slope	Error	Slope	Error
8	0.0232	0.0899	-0.0220	0.1090	0.0229	0.1141
7	**0.0149**	**0.0138**	**0.0236**	**0.0130**	**0.0264**	**0.0146**
6	0.0190	0.1212	-0.0099	0.1173	-0.0052	0.1325
5	0.0016	0.1740	0.0051	0.2085	-0.0096	0.1791
4	0.0069	0.1707	0.0028	0.1732	-0.0070	0.1392
3	0.0038	0.1643	0.0023	0.1395	-0.0045	0.1122
2	0.0022	0.3158	0.0017	0.2477	-0.0034	0.1960
1	0.0032	0.5693	0.0022	0.47.89	-0.0045	0.4153

only level 7 (the region of concern) has a slope greater than |0.01| and an error less than 0.20, thus meets the criteria set for trendability.

7.2.2.2. Regression Fitting for the 1-D Wavelet Decomposed Vibration RMS Values

For the fluting aged motors, the levels of concern, as established from the peak identification section (Tables 7.11, 7.12 and 7.13), were 1, 2, 3 and 4. These levels can be compared to the IFRs found in section 7.1.2.2 to determine which IFRs were contained in which level.

The regression analysis for motor #11 is shown in Table 7.20 and a graphical representation of the four levels of concern for signal Vc, V1 and V2 are shown in Figures 7.19 - 7.30. For motor #11, many levels exceed the minimum slope value (levels 3, 2 and 1), but also exceed the maximum error values as well. These line trend well, but show considerable error. The regression analysis for motor #12 is shown in Table 7.21.

The same is true for motor #12, as is true for motor #11, levels 4, 3, 2 and 1 exceed the minimum slope value and also exceeds the error requirement. Level 3 seems to fit the criteria the closest.

The regression analysis for motor #13 is shown in Table 7.22. The analysis for motor #13 indicate that only levels 4, 2 and 1 meet the slope requirements but they fail the error requirement. This may be due to the FRMSE definition. The FRMSE defined causes small value points to contribute large amounts of error in what would be trendable values. Visual trending results (section 7.2.1.2) support this point.

For comparison, the full signal least-squares regression trending will be discussed for the three current phases for motors #1, 2 and 3, then for the three vibrations of motors #11, 12 and 13.

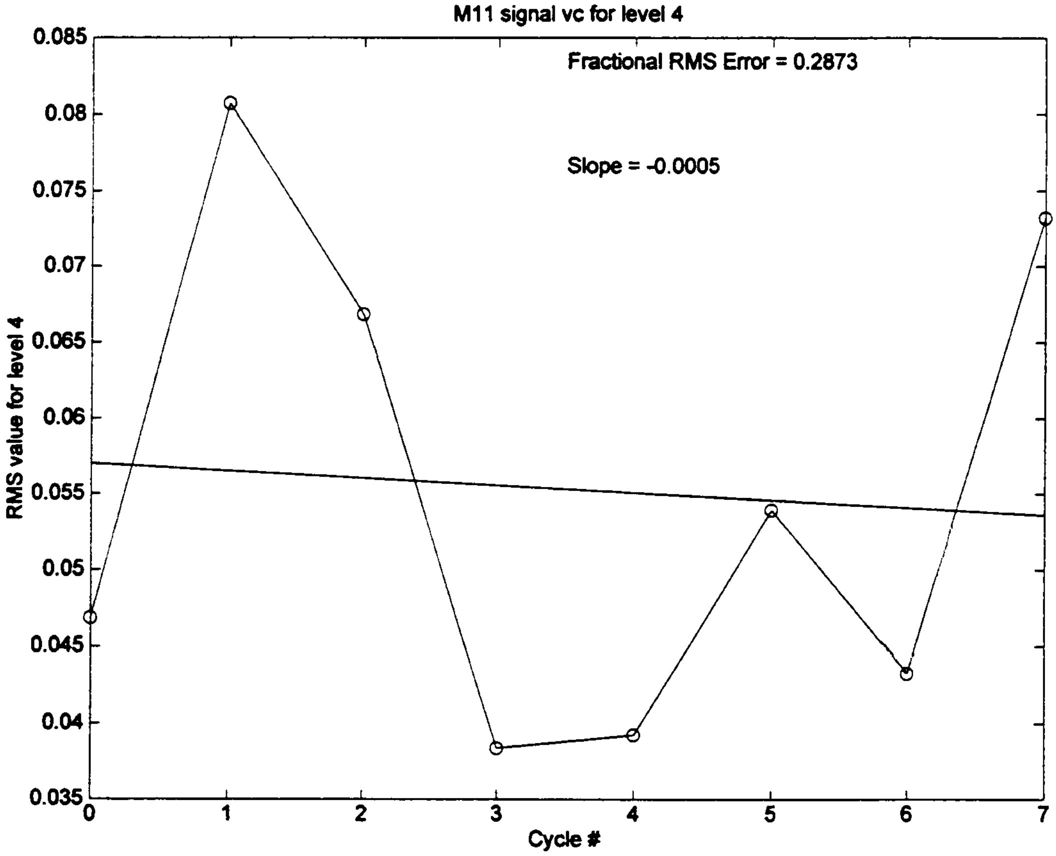

Figure 7.19. Trending plot for motor #11, signal Vc, level #4.

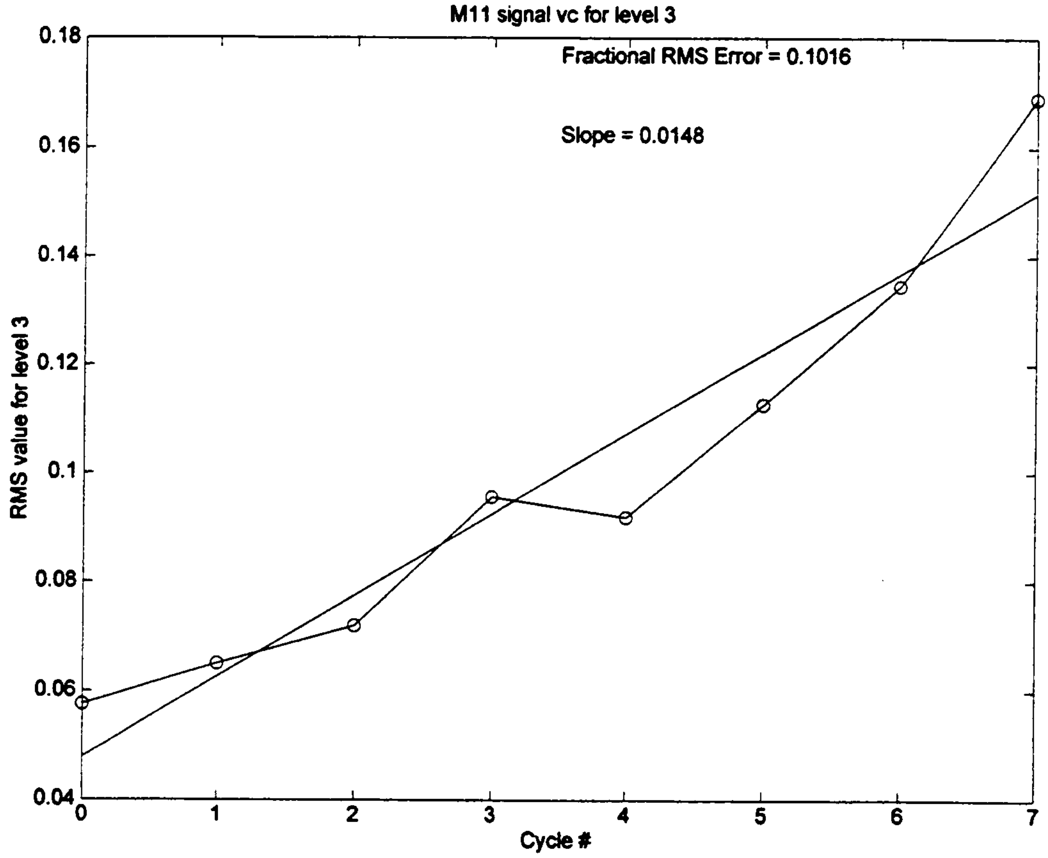

Figure 7.20. Trending plot for motor #11, signal Vc, level #3.

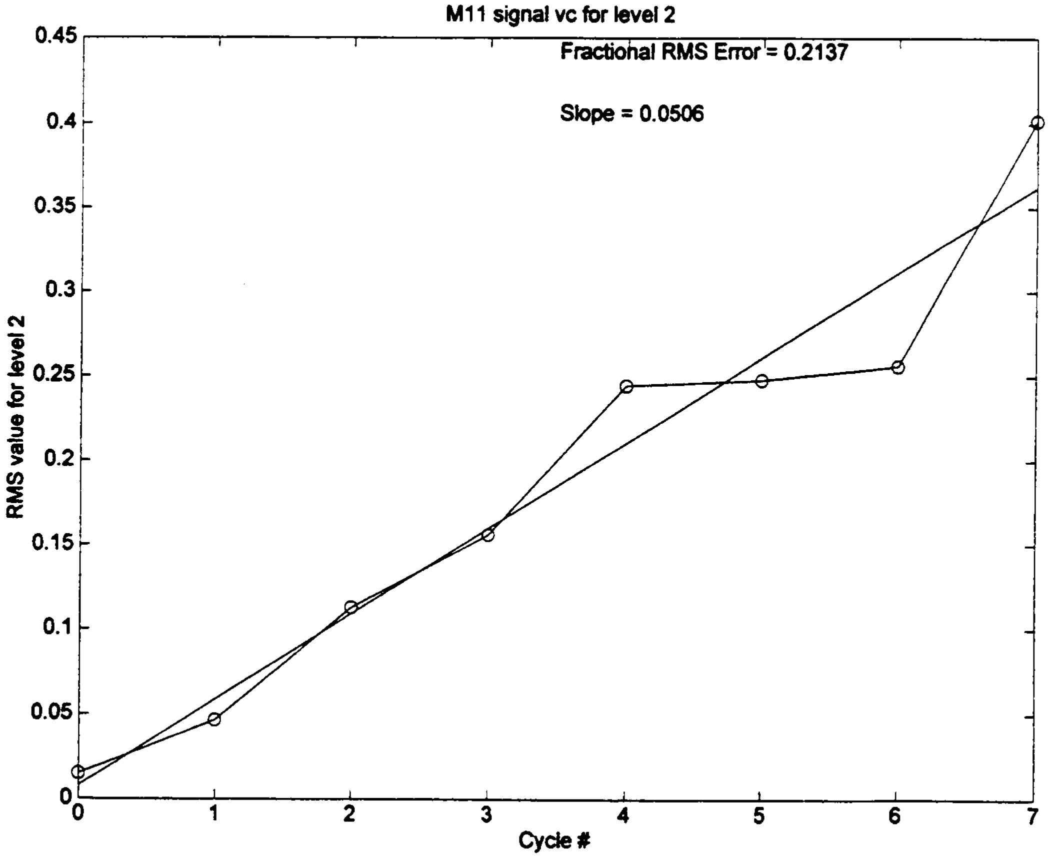

Figure 7.21. Trending plot for motor #11, signal Vc, level #2.

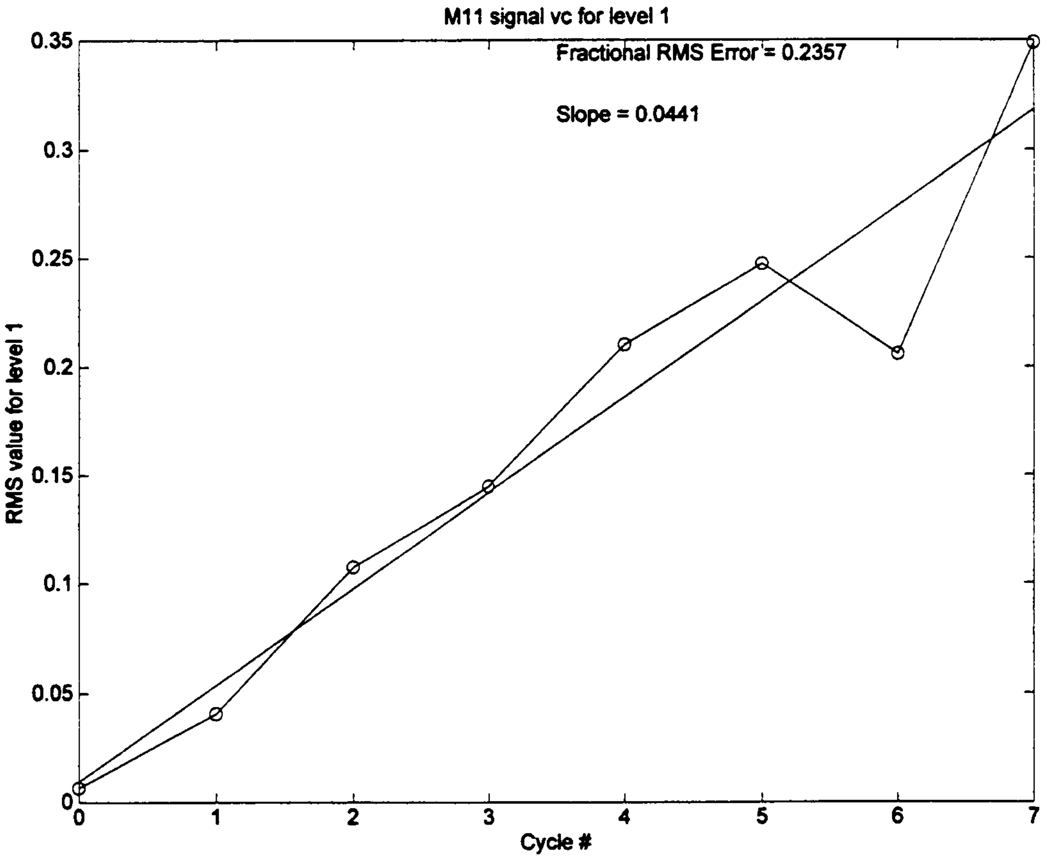

Figure 7.22. Trending plot for motor #11, signal Vc, level #1.

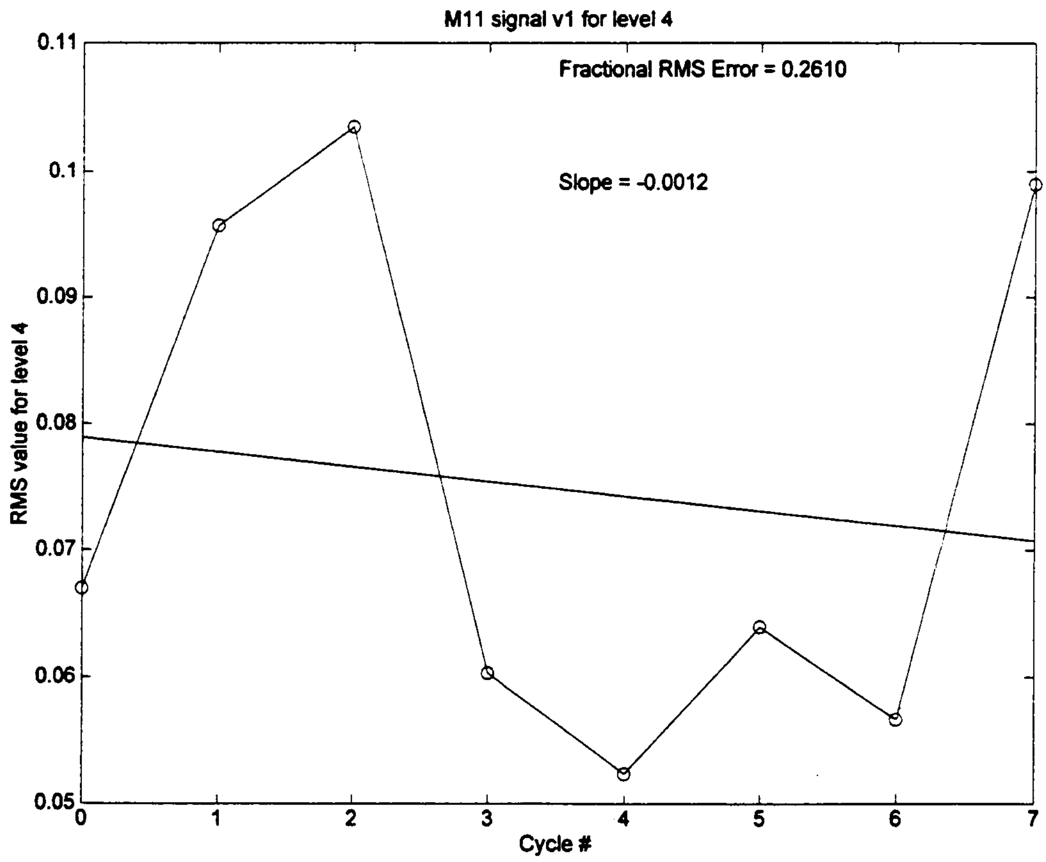

Figure 7.23. Trending plot for motor #11, signal V1, level #4.

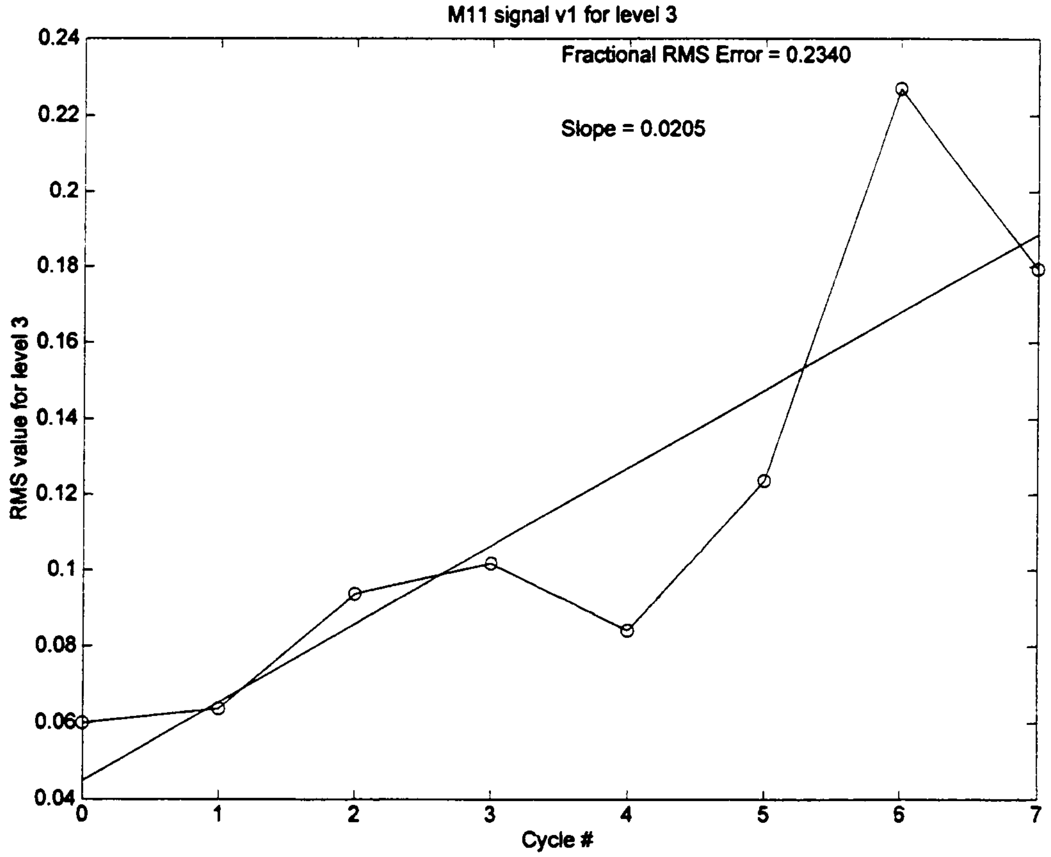

Figure 7.24. Trending plot for motor #11, signal V1, level #3.

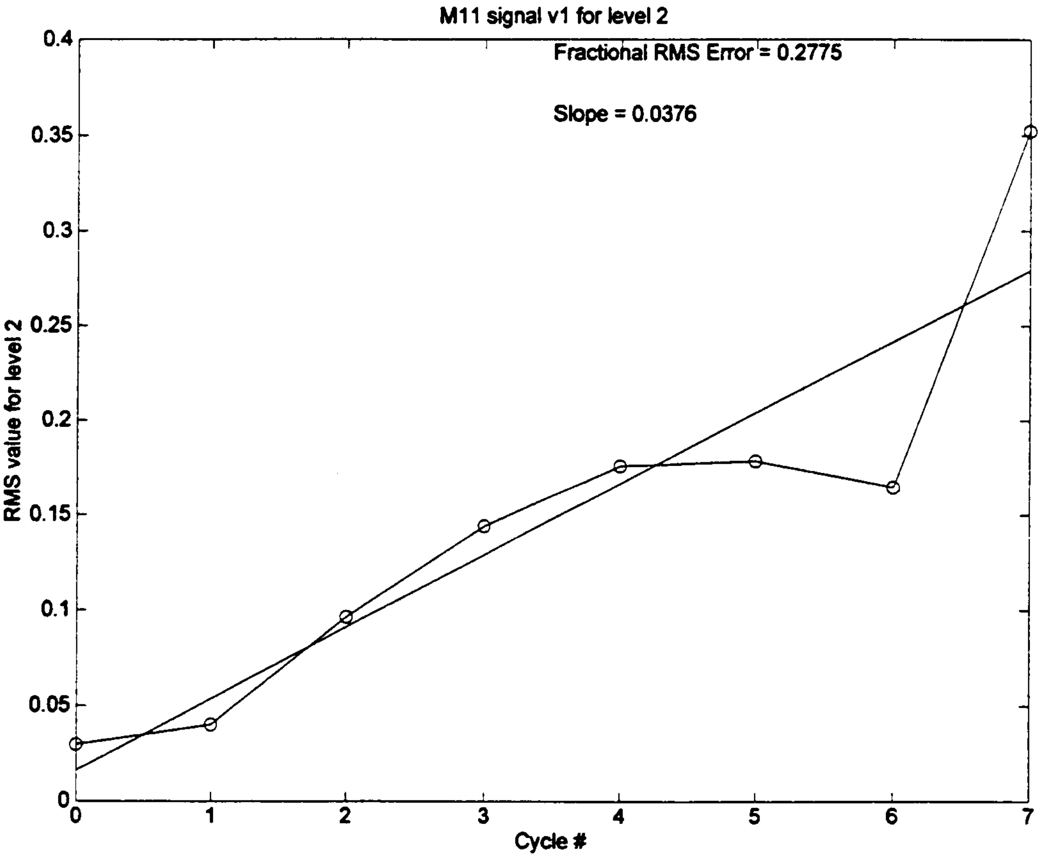

Figure 7.25. Trending plot for motor #11, signal V1, level #2.

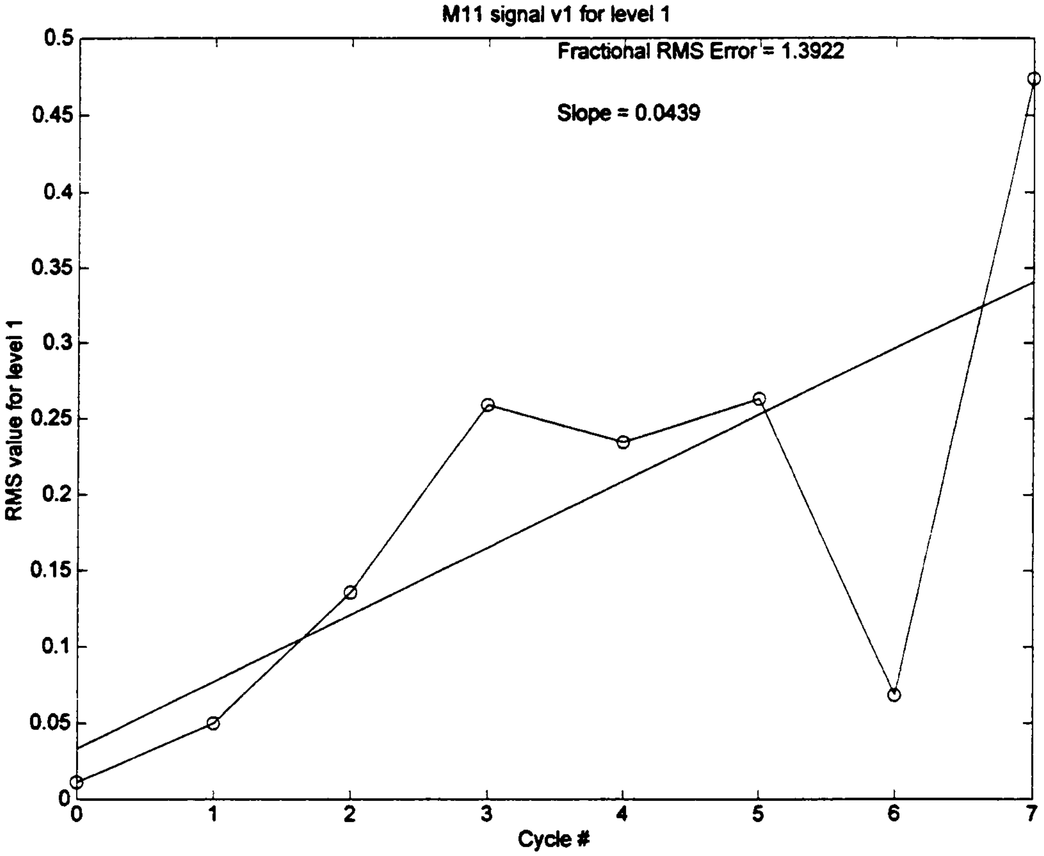

Figure 7.26. Trending plot for motor #11, signal V1, level #1.

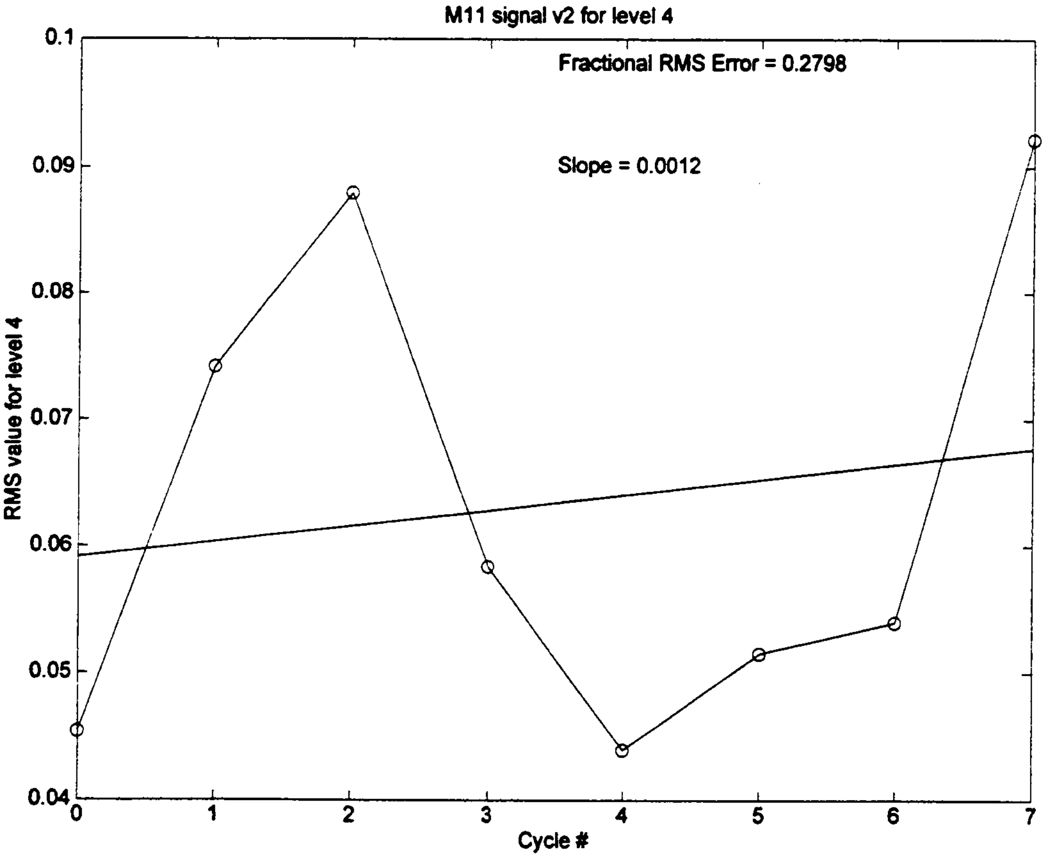

Figure 7.27. Trending plot for motor #11, signal V2, level #4.

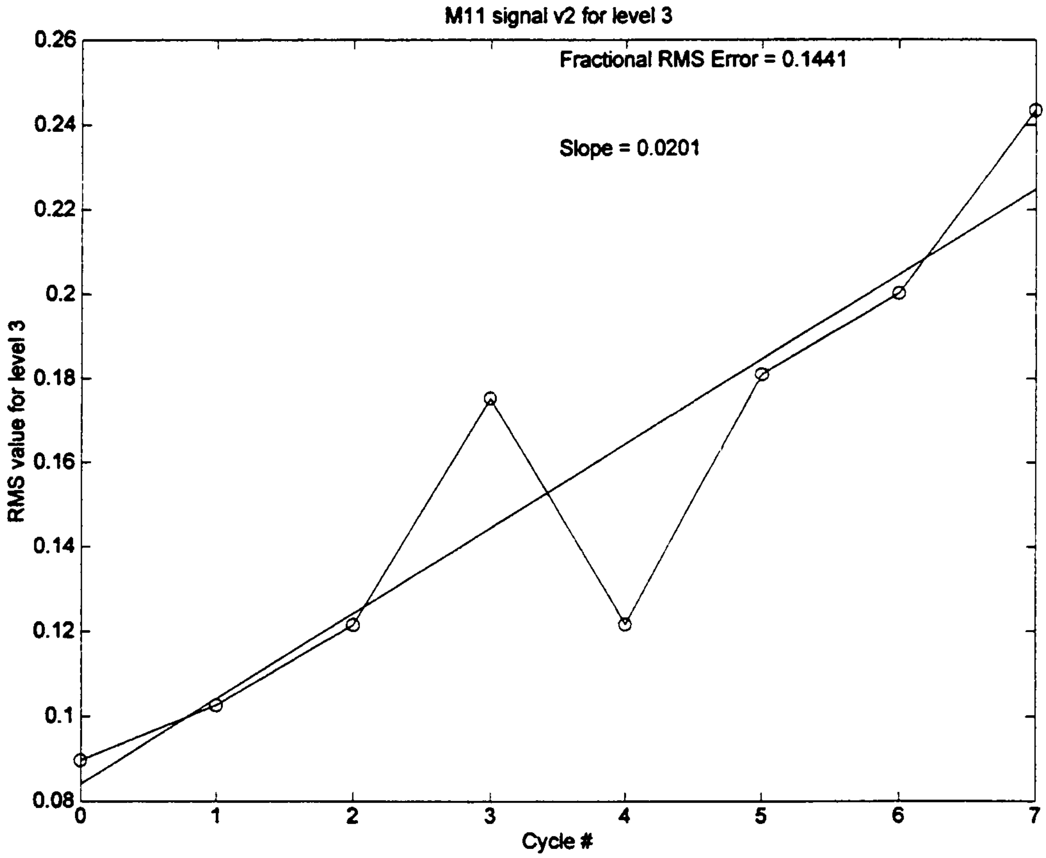

Figure 7.28. Trending plot for motor #11, signal V2, level #3.

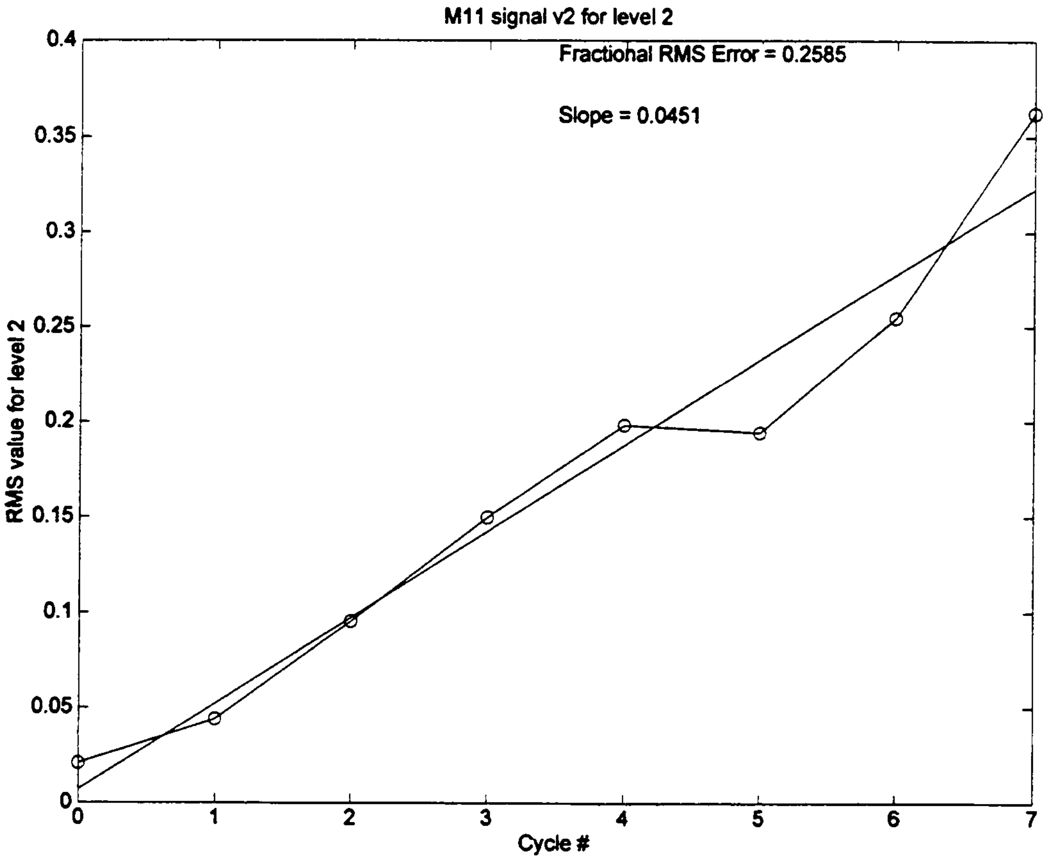

Figure 7.29. Trending plot for motor #11, signal V2, level #2.

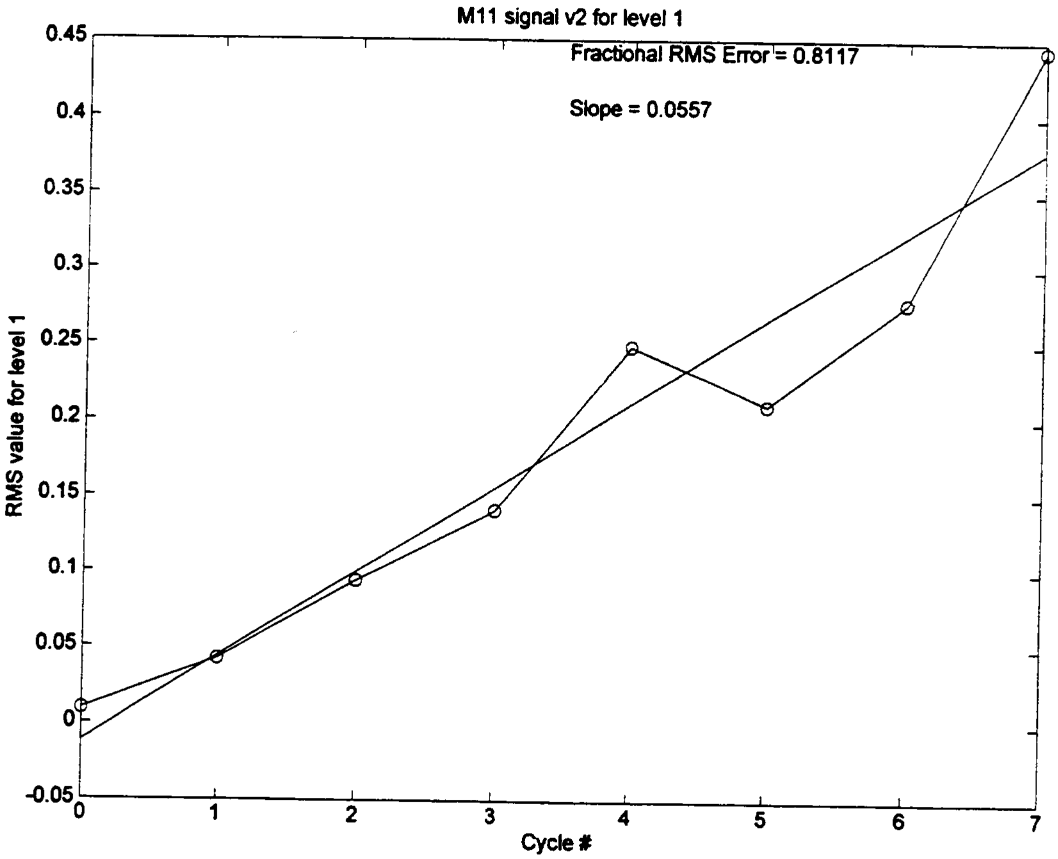

Figure 7.30. Trending plot for motor #11, signal V2, level #1.

Table 7.20. Regression analysis for motor #11

Motor #11	Vc		V10:00		V2:00	
level	Slope	Error	Slope	Error	Slope	Error
8	0.0001	0.0714	0.0015	0.0933	0.0005	0.0582
7	-0.0009	0.4634	-0.0013	0.5882	-0.0008	0.2722
6	-0.0006	0.3254	0.0038	0.4817	0.0015	0.4294
5	-0.0046	0.3847	-0.0023	0.3031	-0.0046	0.3082
4	-0.0005	0.2873	-0.0012	0.2610	0.0012	0.2798
3	0.0148	0.1016	0.0205	0.2340	0.0201	0.1441
2	0.0506	0.2137	0.0376	0.2775	0.0451	0.2585
1	0.0441	0.2357	0.0439	1.3922	0.0557	0.8117

Table 7.21. Regression analysis for motor #12

Motor #12	Vc		V10:00		V2:00	
level	Slope	Error	Slope	Error	Slope	Error
8	0.0004	0.1160	0.0017	0.7016	0.0006	0.8897
7	0.0010	1.0750	-0.0001	0.3074	0.0007	0.4879
6	0.0015	0.2677	0.0017	0.3762	0.0017	0.3766
5	0.0093	0.2235	0.0148	0.3380	0.0083	0.3649
4	0.0325	0.5683	0.0277	0.5520	0.0243	0.5589
3	0.0645	0.4931	0.0468	0.3610	0.0407	0.2767
2	0.0551	0.6205	0.0840	0.4850	0.0542	0.4841
1	0.0379	1.7902	0.1476	3.1112	0.0540	0.6827

Table 7.22. Regression analysis for motor #13

Motor #13	Vc		V10:00		V2:00	
level	Slope	Error	Slope	Error	Slope	Error
8	0.0003	0.0735	0.0018	0.1034	0.0011	0.1570
7	0.001	0.3170	0.0002	0.3040	0.0004	0.4643
6	0.0029	1.0737	0.0041	0.5376	0.0061	0.6622
5	0.0019	0.4948	0.0016	0.4129	0.0014	0.3479
4	0.0074	0.2802	0.0118	0.3705	0.0095	0.2010
3	0.0064	0.5144	0.0012	0.4682	0.0001	0.5185
2	0.0151	0.6102	0.0359	0.3165	0.0352	0.3079
1	0.0112	1.4205	0.0256	0.7187	0.0190	0.8693

7.2.2.3. Comparison of the Trended 1-D Wavelet Decomposed RMS Values with the Full-signal RMS Values

First, the results for full-signal motor current RMS least-squares trended values for each motor current phase for motors #1, 2 and 3 are shown in Table 7.23. An example trend for motor #1 current Ix is shown in Figure 7.31.

Table 7.23. Full-signal regression analysis for motor currents

Motor # / Current	Ix		Iy		Iz	
	Slope	Error	Slope	Error	Slope	Error
1	0.0152	0.0041	0.0120	0.0044	0.0234	0.004
2	NA	NA	NA	NA	NA	NA
3	0.0237	0.0130	0.0173	0.0115	0.0251	0.142

In comparison with the level 7 wavelet decomposed, the full-signal approach meets the requirements but the wavelet decomposed signal has a larger slope value and as small error. Therefore, the wavelet decomposed current at level 7 trends better than the full-signal data and may be used to monitor similarly aged motor degradation with a higher precision than the full-spectrum signal.

The full-signal RMS least-squares trended values for motors #11, 12 and 13 for each vibration signal is found in Table 7.24. An example trend for motor #11, signal Vc is shown in Figure 7.32.

Table 7.24. Full-signal regression analysis for motor vibrations

Motor # / Vibration	Vc		V10:00		V2:00	
	Slope	Error	Slope	Error	Slope	Error
11	0.0586	0.0966	0.0543	0.1925	0.0620	0.1062
12	0.1020	0.3788	0.1833	0.4873	0.0936	0.2664
13	0.0219	0.2887	0.0400	0.2707	0.0350	0.3041

In Table 7.24, the slope and error values of the full-signal vibrations were closer to the established criteria than the wavelet decomposed vibration signals at any level of concern (1, 2, 3

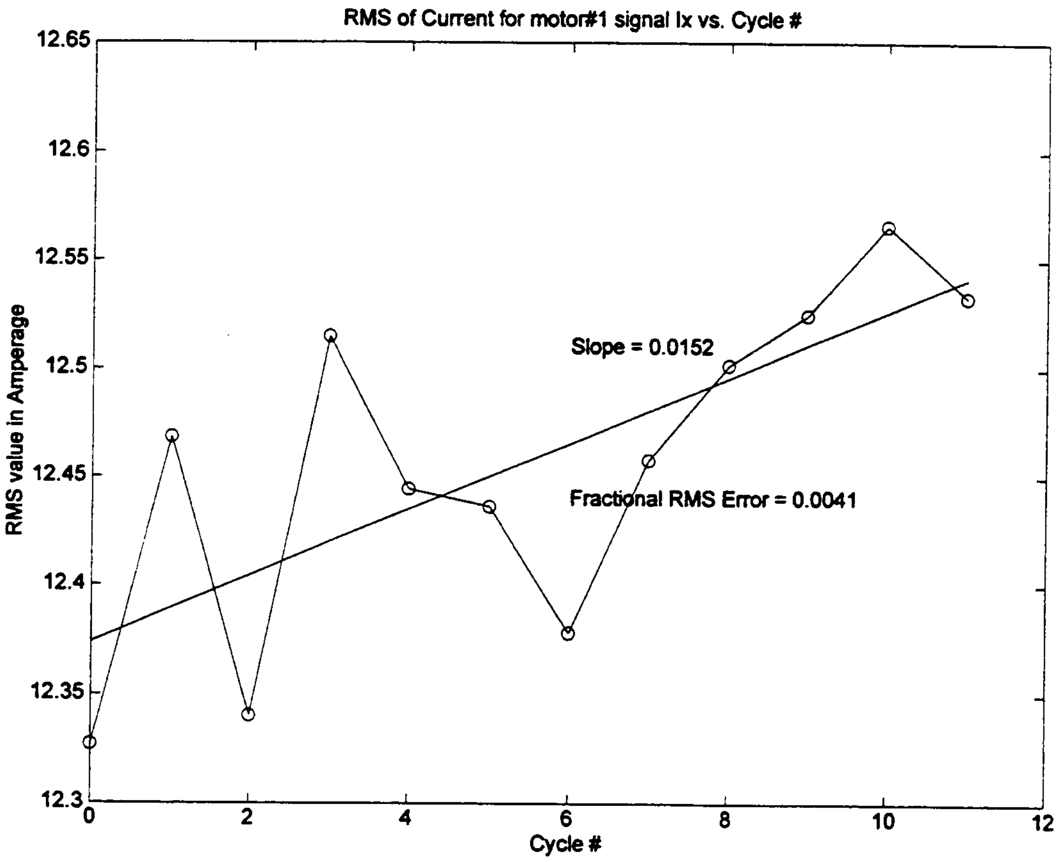

Figure 7.31. Full-signal trending plot for motor #1, signal Ix.

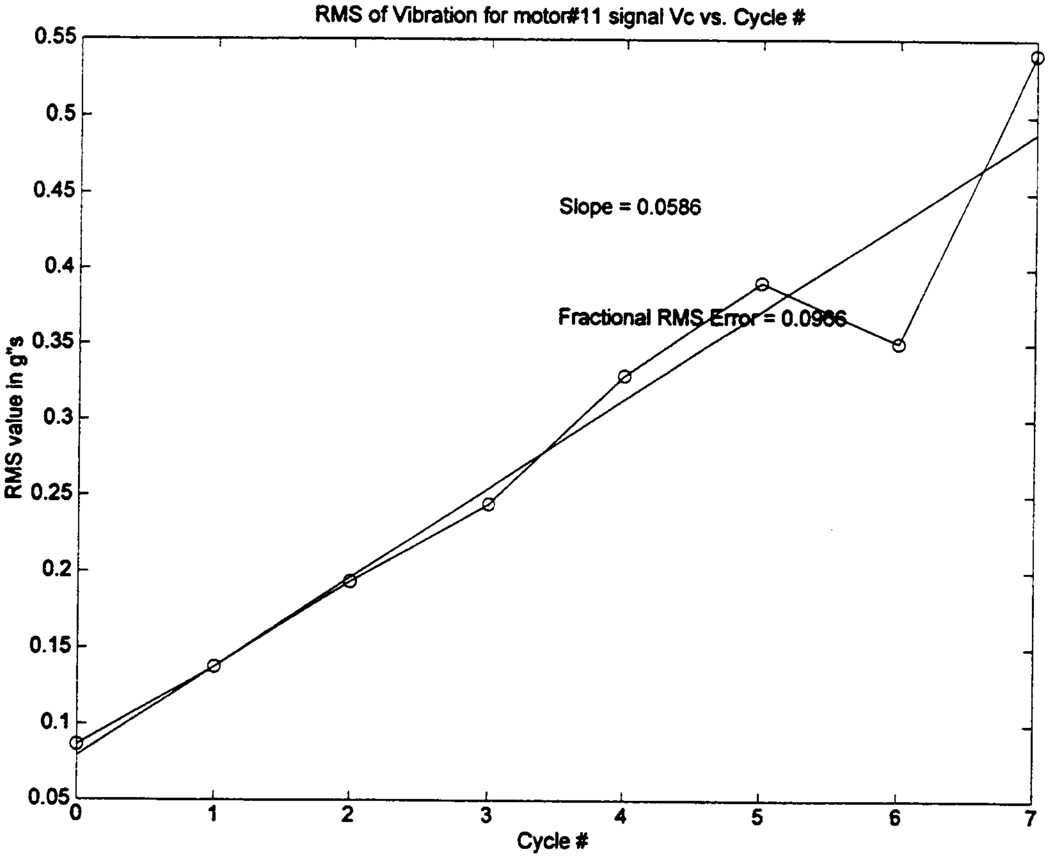

Figure 7.32. Full-signal trending plot for motor #11, signal Vc.

and 4). Therefore, the full-signal vibration data trends better than the wavelet decomposed signal at any level using the trending criteria, regression method and error estimation. The trending of RMS values of decomposed signal corresponding to specific frequency ranges indicate that certain sub-bands dominate the contribution to overall RMS value. A different approach such as defining different decomposition levels or regression method and error estimation may yield better trending results for the wavelet sub-banded signal. This concludes the regression and results section.

Chapter 8

CONCLUDING REMARKS AND RECOMMENDATIONS FOR FUTURE WORK

8.0. Introduction

A complete spectral characterization of vibration and motor current signals from load testing of 5-HP induction motors subjected to aging experiments, is presented in this thesis. The data were acquired from progressive aging cycles corresponding to stator insulation aging and bearing electrical (fluting) aging. The trending of important frequency ranges in the signals was accomplished by computing RMS values of signal components decomposed using 1-D wavelet transform and multi-resolution analysis. The identification of characteristic signal frequency bands and their degradation trending have been successfully accomplished in this thesis.

8.1. Concluding Remarks

The significant contributions of this research include a thorough review of induction motor faults and detection methods, a better understanding of the motor current and vibration spectral characteristics by peak identification and quantification of the relationship between signals before and after the aging processes and a better trending method, and using characteristic frequency ranges and wavelet decomposition when analyzing vibration or motor current signals for motors that are aged in similar processes.

The significant achievements are summarized as follows.

- There are many ways to determine the condition and mode of failure of an induction motor. The literature review of this thesis gives an in-depth look at many of the techniques.

- Few unidentifiable peaks within the stator-aged motor current spectra and no IFRs. Many high-frequency line harmonics and some bearing induced frequency peaks are seen.

- Many unidentifiable peaks within the bearing fluted vibration spectra and many IFRs. The IFRs are also at high frequencies. The high frequency components (above 1kHz) are characteristic of bearing fluting degradation.

- The large spread of frequencies in the vibration spectrum for the bearing fluted motors may be due to numerous surface imperfections such as pitting and frosting on the bearing races and rolling elements.

- The 60 Hz region of the motor current signature trends better than the full-spectrum signal for the stator-aged motors.

- The vibration signal IFRs also trend well for the bearing fluted motors.

- The wavelet decomposition provides a technique for identifying most influential frequency bands in a complex signal.

- The coherence functions showed causal relationship in certain pairs of motor vibration signals throughout the signal spectrum. The relationships between motor currents were also high, with the relationship between motor current and vibration much lower.

- Many of the frequency components in the stator current signal correspond to bearing vibration signals. This indicates that motor current analysis can be used to monitor many bearing related frequencies.

- The coherence relationships between the signal pairs were also affected as the motors were aged using either process.

8.2. Recommendations for Future Work

Identification of the unknown peaks within the spectra may yield a better accuracy in the determination of motor characteristics and degradation. There may be a correlation between the number of surface imperfection on the inner and outer races of the bearing and the frequencies where IFRs appear at high frequency bands. The use of the 60 Hz region of the motor current signal and not the full spectrum for condition monitoring of stator-aged motors should yield better trending results for improved degradation monitoring. Other trending techniques or redefining the decomposition levels may yield even better results and enable improved condition monitoring when using vibration signals for bearing fluted motors. The coherence functions should be examined closely with an emphasis on the identification of peaks and their nature as they pertain to each type of aging process. This should be especially useful in further identifying bearing vibration peaks that were seen in the motor current spectra. The motor current could be used for bearing vibration monitoring. The motor power signature should be investigated for bearing vibration induced spectral peaks. The use of multivariate time series analysis for relating various signals will also yield better results.

References

1. P.F. Albrecht, J.C. Appiarus, D.W. Houghtaling, R.M. McCoy, E.L. Owen and D.K. Sharma, "Assesment of the reliability of motors in utility applications", IEEE Transactions on Energy Conversion, Vol. EC-2, No. 3, September 1987.

2. Improved Motors for Utility Applications, Vol.1, EL-2678, EPRI Research Project 1763-1, Final Report, October 1982.

3. R. K. Cho, J. H. Lang and S. D. Umas, "Detection of Broken Rotor Bars in Induction Motors Using State and Parameter Estimation", IEEE Transaction on Industry Applications, Vol. 28, No. 3, May/June 1992, p. 702-709.

4. B. Raychaudhuri, "Fault Monitoring and Residual Life Estimation of Electric Motors", MS Thesis, The University of Tennessee, Knoxville, 1995.

5. G. A. Bisbee, "Why do motor shaft and bearings fail", Tappi Journal, September 1994.

6. "Motor Bearing Damage Detection Using Stator Current Monitoring", IEEE Transaction on Industry Applications, Vol. 1, No. 1, pp. 110-116, 1994.

7. "Reliability Based Maintenance: How to Improve Plant Performance by Reducing Downtime Maintenance Costs", Presented by: Alex Bradley, CSI, pp.3.1-5.25, 1992.

8. "Motor Current Signature Analysis as a Predictive Maintenance Tool", Proceedings of the American Power Conference, pp. 65-66.

9. S. F. Legowski, A. H. M. Sadrul and A. M. Trzynadlowski, "Instantaneous Power as a Medium for the Signature Analysis of Induction Motors, IEEE Transactions on Industry Applications, Vol. 32, No. 4, July/August 1996, p. 905.

10. B. R. Upadhyaya, A. S. Erbay and J. P. McClanahan, "Accelerated Aging Studies of Induction Motors and Fault Diagnosis," The University of Tennessee, Knoxville, MRC/BRU/96-03, Sept. 1997.

11. R. Maier, "Protection of squirrel-cage induction motors utilizing instantaneous power and phase information", IEEE Trans. Industry Application, Vol. 28, pp. 376-380, 1992.

12. S.V. Bowers and K.R. Piety, "Proactive Motor Monitoring Through Temperature, Shaft Current, and Magnetic Flux Measurements", CSI 1993 Users Conference, September 20-24, 1993, p. 2-3.

13. A. H. Bonnett and G. C. Soukup, "Rotor Failures in Squirrel Cage Induction Motors", IEEE Transactions on Industry Applications, Vol. IA-22, No. 6, pp. 1165-1173, Nov/Dec 1986.

14. J. R. Nicholas, Jr., "Motor Electrical Monitoring and Condition Analysis", Maintenance Technology; pp. 22-28, September 1996.

15. J. E. Traister, "Handbook of Electric Motors: Use and Repair", second edition, p. 149.

16. J. Kochensparger, "Applying Predictive Maintenance Testing to Minimize Motor Failure Downtime", Plant Engineering, March 12, 1987, p. 186-190.

17. P. Walker, "Preventing Motor Shaft–Current Bearing Failures", Plant Engineering, December 12, 1992, p. 100-103.

18. S. F. Farag, R. G. Bartheld and T. G. Habetler, "An Integrated On-Line Motor Protection System", IEEE Industry Applications Magazine, March/April 1996, p. 23.

19. V. Lyon, "Transient Analysis of Alternating-Current Machinery, An Application of the Method of

Symmetrical Components", MIT, 1954.

20. J. R. Nicholas Jr., "Arriving at a New Way to Analyze Resistance to Ground", P/PM Technology, October 1996, p. 56.

21. J. Tranter, "Combining Spectra, Cepstra and Demodulated Spectra in an Expert System", P/PM Technology, August 1997, pp. 68-74.

22. R.B. Randall, "Cepstrum Analysis", Digital Signal Analysis, B & K Technical Review, pp. 161-190.

23. R.B. Randall, "Gearbox Fault Diagnosis Using Cepstrum Analysis", Proc. IVth World Cong. Theory of Machines and Mechanisms, Vol. 1, pp. 169-174, I. Mesh. E., London 1968.

24. S.W. Bowers, K.R. Piety, R.W. Piety and R.J. Colsher, "Evaluation of the Field Application of Motor Current Analysis".

25. R.R. Scheon, T.G. Habetler, F. Kamran and R.G. Bartheld, "Motor Bearing Damage Detection Using Stator Current Monitoring", IEEE Transaction on Industry Applications, Vol. 1, No. 1, pp. 110-116, 1994.

26. R.K. Mobley, "An Introduction to Predictive Maintenance", New York: Van Nostrand Reihold, 1990.

27. D. Kowal, "Bearing Damage Resulting from Voltages and Currents", CSI, 1997.

28. This information was verbally transmitted to myself from Austin Bonnet at MARCON in 1998.

29. B. R. Upadhyaya, NE522 Notes, Chapter 3, 1996.

30. R. E. Uhrig, Random Noise Techniques in Nuclear Reactor Systems, 1970.

31. S. Seker, B. R. Upadhyaya, A. S. Erbay and J. P. McClanahan, "Application of Wavelet Transforms and Multi-resolution Analysis to Monitor Bearing Damage in Induction Motors", Journal of Sound and Vibration, submitted 1998.

32. C. S. Burns, R. A. Gopinath and H. Guo, "Introduction to Wavelets and Wavelet Transforms: A Primer", Prentice-Hall, Upper Saddle River, NJ, 1998.

33. MARLAB Wavelet Toolbox, The Math Works, Inc., 1997.

34. G. R. Cooper, C. D. McGillem, Probabilistic Methods of Signal and System Analysis, Harcourt Brace Jovanovich College Publishers, pp. 163-164, 1986.

Appendixes

Appendix A MATLAB Codes

USEMVB.m

```
% The predicted stator current frequencies
% (febng) caused by bearing vibrations which induce rotor
% movement are:  febng = | fe +- m*fvbng |

%  where: m = 1, 2, 3, ...
%  fe = electrical supply frequency
%  fvbng = characteristic vibration frequencies

% There are also current spectrum frequencies generated by
% the difference in the frequency of rotation
% of the shaft and the motor's synchronous frequency:
%  fecc = fe * [1 +- (k * fslip * P)]

%  where: fe = electrical supply frequency
%      P = number of poles wound in stator = 4
%      fsynch = 2*fe / P
%      fshaft = shaft turn frequency = 30
%      fslip = slip frequency = fsynch - fshaft
%      k = 1, 2, 3, ...

fe = 60;
P = 4;
rpm=1740
fshaft = rpm/60;
fsynch = 2*fe/P
fslip = fsynch-fshaft     % slip frequency    %
k = [1:1:5];        % harmonics     %
feccp = fe+k*fslip*P
feccn = fe-k*fslip*P

% The motion within the motor could be caused by imbalance, bearings,
% and looseness.  Where: fshaft = fundamental frequency of
% rotation.

N =[1:40];
M =[1:5];

finbal = 1*fshaft
fmisalign = N*fshaft
floose = 0.5*N*fshaft
foilwhirl = [0.38;0.49]*M*fshaft

% We can obtain some of the frequencies that are caused by
% the bearing vibration.  For example, we use a specific
% bearing, the SKF 6205.  The precalculated frequency
% problems for the inner and outer ring, cage train, and
% ball defect occur at the following frequencies (in Hz):

fvIR5 = 90.25
fvOR5 = 59.75
fvCT5 = 6.639
fvBall5 = 78.580

% The SKF bearing defect frequencies were calculated at 1000 RPM, thus we
% must correct for our usage speed.  The correction is given by:

% Actfrq (Hz) = 0.001*(RPM)*(Precalculated frequency)

% Thus by using the recommended correction, the bearign frequencies for
% the SKF 6205 are given as the following:
```

```
fvIR5 = 0.001*rpm*90.25
fvOR5 = 0.001*rpm*59.75
fvCT5 = 0.001*rpm*6.639
fvBall5 = 0.001*rpm*78.580

% It has the following characteristic frequencies. They are applied below:

m = [1:1:20];              % First 20 harmonics       %
fvCTh5 = m*fvCT5               % fundamental train    %
fvBallh5 = m*fvBall5               % ball spin        %
fvORh5 = m*fvOR5           % outer ball pass      %
fvIRh5 = m*fvIR5           % inner ball pass      %

% We must now use the same process for the SKF 6206 (European) bearing.
% Thus, by using the recommended correction, the bearing
% frequencies for the SKF 6206 (European) are given as the following:

fvIR6 = 0.001*rpm*90.53
fvOR6 = 0.001*rpm*59.470
fvCT6 = 0.001*rpm*6.608
fvBall6 = 0.001*rpm*77.039

% It has the following characteristic frequencies.
% They are applied below:

m = [1:1:20];              % First 20 harmonics       %
fvCTh6 = m*fvCT6               % fundamental train          %
fvBallh6 = m*fvBall6               % ball spin                  %
fvORh6 = m*fvOR6           % outer ball pass            %
fvIRh6 = m*fvIR6           % inner ball pass            %

% Electrical Frequency Harmonics seen in a signal

electricalfz=60*[1:50]

% Electrical Frequencies Caused by Vibrations

feCTh5a = abs(60+fvCTh5)            % fundamental train    %
feCTh5s = abs(60-fvCTh5)
feBallh5a = abs(60+fvBallh5)        % ball spin                %
feBallh5s = abs(60-fvBallh5)
feORh5a = abs(60+fvORh5)            % outer ball pass      %
feORh5s = abs(60-fvORh5)
feIRh5a = abs(60+fvIRh5)            % inner ball pass          %
feIRh5s = abs(60-fvIRh5)

feCTh6a = abs(60+fvCTh6)            % fundamental train    %
feCTh6s = abs(60-fvCTh6)
feBallh6a = abs(60+fvBallh6)        % ball spin                %
feBallh6s = abs(60-fvBallh6)
feORh6a = abs(60+fvORh6)            % outer ball pass      %
feORh6s = abs(60-fvORh6)
feIRh6a = abs(60+fvIRh6)            % inner ball pass          %
feIRh6s = abs(60-fvIRh6)
```

MOTPRO.m

```
%
% M-file, "motpro.m" to process PSD and RMS for signals
%
%

clear;

m=input('Input motor data file extension (no .dat needed). ','s');
eval(['load ' m '.dat']);
[r,c]=eval(['size(' m ')'])

% Data from .dat file is loaded
% Next we will assign individual values of vibration and
%  current from the dat file.  The code is:

Ix=eval([m,'(1,:)']);
Iy=eval([m,'(2,:)']);
Iz=eval([m,'(3,:)']);
Vc=eval([m,'(4,:)']);  % vibration from sensor on cover
V1=eval([m,'(8,:)']);  % vibration from sensor at 10:00
V2=eval([m,'(9,:)']);  % vibration from sensor at 2:00

% RMS values from raw signal

RIx=((1/c)*(sum(Ix.^2)))^(0.5)
RIy=((1/c)*(sum(Iy.^2)))^(0.5)
RIz=((1/c)*(sum(Iz.^2)))^(0.5)
RVc=((1/c)*(sum(Vc.^2)))^(0.5)
RV1=((1/c)*(sum(V1.^2)))^(0.5)
RV2=((1/c)*(sum(V2.^2)))^(0.5)

% Calculation of mean of signals

mIx=mean(Ix)
mIy=mean(Iy)
mIz=mean(Iz)
mVc=mean(Vc)
mV1=mean(V1)
mV2=mean(V2)

% Convert to column vectors

Ix=Ix';
Iy=Iy';
Iz=Iz';
Vc=Vc';
V1=V1';
V2=V2';

% We will also subtract the mean value from the data so that it
%  will remove any gain in the signals.The code is be given as:

Ix=Ix-mIx;
Iy=Iy-mIy;
Iz=Iz-mIz;
Vc=Vc-mVc;
V1=V1-mV1;
V2=V2-mV2;

% RMS values without DC signal
```

```
RIx0=((1/c)*(sum(Ix.^2)))^(0.5)
RIy0=((1/c)*(sum(Iy.^2)))^(0.5)
RIz0=((1/c)*(sum(Iz.^2)))^(0.5)
RVc0=((1/c)*(sum(Vc.^2)))^(0.5)
RV10=((1/c)*(sum(V1.^2)))^(0.5)
RV20=((1/c)*(sum(V2.^2)))^(0.5)

% This procedure saves space with the MATLAB system.

eval(['clear ',m]);

% We will now load various constants that are determined
%  by the sampling procedure of the data and also the
%  fourier processing or PSD that will be done.
%  The code input is as follows:

nfft1=16392;     % Power of 2 for fft for vibration1
nfft2=1024;        % Power of 2 for fft for vibration2
nfft3=8196;        % Power of 2 for fft for current
Fs=12000;       % Sampling Frequency = 12000 Hz
window='hanning';      % Window of psd
noverlap=512;   % Overlap for psd
Fc=60;        % Carierier Frequency = 60 Hz

% For the high frequency data, the values obtained
%  in the current measurementwere sampled at 12,000 Hz
%  for 60 seconds.  Thus producing a file that is 1 MB
%  for each measurement.

% We can now process the psd & RMS of the individual
%  signals, for example:

[pIx,fIx]=psd(Ix,nfft3,Fs);
plot(fIx,20*log10(pIx))
title([' Power Spectrum for ' m ', current Ix'])
xlabel(' frequency ')
ylabel(' Magnitude in dB ')

[pIy,fIy]=psd(Iy,nfft3,Fs);
figure(2)
plot(fIy,20*log10(pIy))
title([' Power Spectrum for ' m ', current Iy'])
xlabel(' frequency ')
ylabel(' Magnitude in dB ')

[pIz,fIz]=psd(Iz,nfft3,Fs);
figure(3)
plot(fIz,20*log10(pIz))
title([' Power Spectrum for  ' m ', current Iz'])
xlabel(' frequency ')
ylabel(' Magnitude in dB ')

[pVcn1,fVcn1]=psd(Vc,nfft1,Fs);
figure(4)
plot(fVcn1,pVcn1)
title([' Power Spectrum for ' m ' Vc using nfft ' num2str(nfft1)])
xlabel(' frequency ')
ylabel(' Magnitude in g"s ')

[pVcn2,fVcn2]=psd(Vc,nfft2,Fs);
figure(5)
```

```
plot(fVcn2,20*log10(pVcn2))
title([' Spectrum for ' m ' Vc using nfft = ' num2str(nfft2)])
xlabel(' frequency ')
ylabel(' Magnitude in db ')

[pV1n1,fV1n1]=psd(V1,nfft1,Fs);
figure(6)
plot(fV1n1,pV1n1)
title([' Spectrum for ' m ' V10:00 using nfft = ' num2str(nfft1)])
xlabel(' frequency ')
ylabel(' Magnitude in g"s ')

[pV1n2,fV1n2]=psd(V1,nfft2,Fs);
figure(7)
plot(fV1n2,20*log10(pV1n2))
title([' Spectrum for ' m ' V10:00 using nfft = ' num2str(nfft2)])
xlabel(' frequency ')
ylabel(' Magnitude in db ')

[pV2n1,fV2n1]=psd(V2,nfft1,Fs);
figure(8)
plot(fV2n1,pV2n1)
title([' Spectrum for ' m ' V2:00 using nfft = ' num2str(nfft1)])
xlabel(' frequency ')
ylabel(' Magnitude in g"s ')

[pV2n2,fV2n2]=psd(V2,nfft2,Fs);
figure(9)
plot(fV2n2,20*log10(pV2n2))
title([' Spectrum for ' m ' V10:00 using nfft = ' num2str(nfft2)])
xlabel(' frequency ')
ylabel(' Magnitude in db ')

% Now we need to save the RMS values and the psd's

eval(['save ' m 'p RIx RIy RIz RVc RV1 RV2 pIx fIx pIy fIy pIz fIz pVcn1 fVcn1
pVcn2 fVcn2 pV2n1 fV2n1 pV2n2 fV2n2 pV1n1 fV1n1 pV1n2 fV1n2'])
```

PEAKID.m

```
%
% peakID.m Locates peaks within data set
%

clear;

% Input motor and cycle number, and signal type

motor=input('Input motor number. ');
cycle=input('Input cycle number. ');
s=input('Input signal. ','s');
eval(['load m' num2str(motor) 'c' num2str(cycle) '11p'])

% Input data

if cycle==0,
if s=='Ix'
   y=pIx;
   f=fIx;
 elseif s=='Iy'
   y=pIy;
   f=fIy;
 elseif s=='Iz'
   y=pIz;
   f=fIz;
 elseif s=='Vc'
   y=pVcn1;
   f=fVcn1;
 elseif s=='V1'
   y=pV1n1;
   f=fV1n1;
 elseif s=='V2'
   y=pV2n1;
   f=fV2n1;
end
else
 if s=='Ix'
   y=eval(['pIx' num2str(cycle)]);
   f=eval(['fIx' num2str(cycle)]);
 elseif s=='Iy'
   y=eval(['pIy' num2str(cycle)]);
   f=eval(['fIy' num2str(cycle)]);
 elseif s=='Iz'
   y=eval(['pIz' num2str(cycle)]);
   f=eval(['fIz' num2str(cycle)]);
 elseif s=='Vc'
   y=eval(['pVcn1c' num2str(cycle)]);
   f=eval(['fVcn1c' num2str(cycle)]);
 elseif s=='V1'
   y=eval(['pV1n1c' num2str(cycle)]);
   f=eval(['fV1n1c' num2str(cycle)]);
 elseif s=='V2'
   y=eval(['pV2n1c' num2str(cycle)]);
   f=eval(['fV2n1c' num2str(cycle)]);
end
end

% Plot of initial spectrum for threshold evaluation

clf;
```

```
if (s=='Ix')|(s=='Iy')|(s=='Iz')
    plot(f,20*log10(y))
    title(['PSD of m' num2str(motor) 'c' num2str(cycle) 'L1 , signal ' s])
    xlabel('frequency (Hz)')
    ylabel('magnitude in dB"s')
    thresholdB=input('Input threshold value. ');
    threshold=10^(thresholdB/20);
else
    plot(f,y)
    title(['PSD of m' num2str(motor) 'c' num2str(cycle) 'L1 , signal ' s])
    xlabel('frequency (Hz)')
    ylabel('magnitude in g"s')
    threshold=input('Input threshold value. ');
end

% zeroing of values in spectrum less than threshold level
%  (keep original signal y)

yt=y;
ind=(find(yt<threshold));
yt(ind)=threshold;

% finding local maxima

datasize = length(yt);

count = 0;
for i = 2 : datasize-1
   if ( (yt(i-1) < yt(i)) & (yt(i+1) < yt(i)) )
      count = count+1;
      maxima(count,:) = [ f(i) yt(i) ];
   end
end

['Peak values (frequency and Amplitude) for m' num2str(motor) 'c'
num2str(cycle) 'L1  signal ' s]
maxima

[rmax,cmax]=size(maxima);

if (s=='Ix')|(s=='Iy')|(s=='Iz')
   plot(maxima(:,1),20*log10(maxima(:,2)),'ro')
   hold
   plot(f,20*log10(y))
   aux=axis;
   if rmax<16
   for k=1:rmax
      sf=sprintf('%.2f,%.2f',maxima(k,1),20*log10(maxima(k,2)));
      text(aux(2)*4.5/6,aux(4)-10*k,sf)
   end
   end
   title(['PSD of m' num2str(motor) 'c' num2str(cycle) 'L1 , signal ' s ', with
threshold = ' num2str(thresholdB)])
   xlabel('frequency (Hz)')
      ylabel('magnitude in dB"s')

else
   plot(f,y)
   hold
   plot(maxima(:,1),maxima(:,2),'ro')
   aux=axis;
```

```
   if rmax<16
   for k=1:rmax
      sf=sprintf('%.2f,%.2f',maxima(k,1),maxima(k,2));
      text(aux(2)*4.5/6,aux(4)-aux(4)*k/20,sf)
   end
   end
 title(['PSD of m' num2str(motor) 'c' num2str(cycle) 'L1 , signal ' s ', with
threshold = ' num2str(threshold)])
 xlabel('frequency (Hz)')
 ylabel('magnitude in g"s')
end
```

RMSPLOT.m

```
%
% Group and plot RMS values determined for each cycle
%  for each  preprocessed signal for a motor
%
%         RMSplot.m
%

clear;

f=input('Input motor number for RMS plotting. ');
cycle=input('Input # of cycles. ');

eval(['RMSm' num2str(f) '=zeros(' num2str(cycle) ',6);']);

for i=0:cycle-1

   if (i==0)&(f==1)
   eval(['load m' num2str(f) 'c' num2str(i) 'llp']);
   eval(['RMSm' num2str(f) '(i+1,:)=[RIx RIy RIz RVc RV1 RV2];'])
   else
      eval(['load m' num2str(f) 'c' num2str(i) 'llp']);
       eval(['RMSm' num2str(f) '(i+1,:)=[RIx' num2str(i) ' RIy' num2str(i) '
RIz' num2str(i) ' RVc' num2str(i) ' RV1' num2str(i) ' RV2' num2str(i) '];'])
   end


end

eval(['RMSm' num2str(f)])

% For least-squares fit of data

Y=eval(['RMSm' num2str(f)]);
X=[0:cycle-1]';
N=1;

for j=1:6

   clear P S Y1 E EY SEY SSEY RMSerror;
   [P,S]=polyfit(X,Y(:,j),N);
   [Y1]=polyval(P,X,S);

   E=abs(Y(:,j)-Y1);
   EY=E./(Y(:,j));
   SEY=EY.^2;
   SSEY=sum(SEY);
   RMSerror=sqrt(SSEY/cycle);

% Plots data matrix and least squares fit by

figure(j)
plot(X,Y(:,j))
hold
plot(X,Y(:,j),'ro')
aux=axis;
plot(X,Y1)

if j==1
   sig='Ix';
elseif j==2
```

```
   sig='Iy';
elseif j==3
   sig='Iz';
elseif j==4
   sig='Vc';
elseif j==5
   sig='V10:00';
else
   sig='V2:00';
end

if (j==1)|(j==2)|(j==3)
   sf1=sprintf('Fractional RMS Error = %.4f',RMSerror);
   text(aux(2)*1/2,aux(4)-aux(4)/60,sf1)
   sf2=sprintf('Slope = %.4f',P(1));
   text(aux(2)*1/2,aux(4)-aux(4)/90,sf2)
   title(['RMS of Current for motor#' num2str(f) ' signal ' sig ' vs. Cycle
#'])
   xlabel('Cycle #')
   ylabel('RMS value in Amperage')
else
   sf1=sprintf('Fractional RMS Error = %.4f',RMSerror);
   text(aux(2)*1/2,aux(4)-aux(4)/50,sf1)
   sf2=sprintf('Slope = %.4f',P(1));
   text(aux(2)*1/2,aux(4)-aux(4)/10,sf2)
   title(['RMS of Vibration for motor#' num2str(f) ' signal ' sig ' vs. Cycle
#'])
   xlabel('Cycle #')
   ylabel('RMS value in g"s')
end

end
```

WMPRO.m

```
% Wavelet decomposition of the motor signals
%
%  PROGRAM : WMpro.m
%

% Motor Data Loaded

f=input('Input motor # and cycle # (no .dat needed). ','s');
s=input('Input signal type (I for current or V for vibration). ','s');
eval(['load ' f 'L1.dat']);

% Number of samples of signal to be examined

 N=6000;
 fs=12000;
 t=0:1/fs:(N-1)/fs;

% Specify Motor signals

if s=='I'
    Ix=eval([f 'l1(1,1:' num2str(N) ')']);
    Iy=eval([f 'l1(2,1:' num2str(N) ')']);
    Iz=eval([f 'l1(3,1:' num2str(N) ')']);
elseif s=='V'
   Vc=eval([f 'l1(4,1:' num2str(N) ')']);
   V1=eval([f 'l1(8,1:' num2str(N) ')']);
   V2=eval([f 'l1(9,1:' num2str(N) ')']);
end

eval(['clear ' f]);

% Wavelet parameters

 lev=8;
 wav='db20';

 % Wavelet Analysis

 % Analysis for Current

 if s=='I'
 [cx,lx]=wavedec(Ix,lev,wav);
 d='d';
 a='a';
 for i=1:lev
    detx(i,1:N)=wrcoef(d,cx,lx,wav,i);
    appx(i,1:N)=wrcoef(a,cx,lx,wav,i);
 end

 figure(1)
 for i=1:lev
    subplot(lev+1,1,i),plot(t,detx(i,1:N))
 if i==1
    title(['Details of ' f 'L1 , current Ix '])
    end
 if i==4
    ylabel('Amplitudes of Details')
    end
 if i==lev
```

```
        xlabel('time (sec)')
    end
 end

 figure(2)
 for i=1:lev
    subplot(lev+1,1,i),plot(appx(i,1:1000))
 if i==1
    title(['Approximations of ' f 'L1 , current Ix '])
    end
 if i==4
    ylabel('Amplitudes of Approximations')
    end
 if i==lev
         xlabel('time (# of data points)')
    end
 end

% Wavelet Analysis on Iy

 [cy,ly]=wavedec(Iy,lev,wav);
 d='d';
 a='a';
 for i=1:lev
    dety(i,1:N)=wrcoef(d,cy,ly,wav,i);
    appy(i,1:N)=wrcoef(a,cy,ly,wav,i);
 end

 figure(3)
 for i=1:lev
    subplot(lev+1,1,i),plot(t,dety(i,1:N))
 if i==1
    title(['Details of ' f 'L1 , current Iy '])
    end
 if i==4
    ylabel('Amplitudes of Details')
    end
 if i==lev
        xlabel('time (sec)')
    end
 end

 figure(4)
 for i=1:lev
    subplot(lev+1,1,i),plot(appy(i,1:1000))
 if i==1
    title(['Approximations of ' f 'L1 , current Iy '])
    end
 if i==4
    ylabel('Amplitudes of Approximations')
    end
 if i==lev
         xlabel('time (# of data points)')
    end
 end

% Wavelet Analysis on Iz

 [cz,lz]=wavedec(Iz,lev,wav);
 d='d';
 a='a';
 for i=1:lev
```

```
    detz(i,1:N)=wrcoef(d,cz,lz,wav,i);
    appz(i,1:N)=wrcoef(a,cz,lz,wav,i);
    end

 figure(5)
 for i=1:lev
    subplot(lev+1,1,i),plot(t,detz(i,1:N))
 if i==1
    title(['Details of ' f 'L1 , current Iz '])
    end
 if i==4
    ylabel('Amplitudes of Details')
    end
 if i==lev
        xlabel('time (sec)')
    end
 end

 figure(6)
 for i=1:lev
    subplot(lev+1,1,i),plot(appz(i,1:1000))
 if i==1
    title(['Approximations of ' f 'L1 , current Iz '])
    end
 if i==4
    ylabel('Amplitudes of Approxiamtions')
    end
 if i==lev
         xlabel('time (# of data points)')
    end
 end

% Calculations for motor vibration

%  Vibration Vc

elseif s=='V'

 [cx,lx]=wavedec(Vc,lev,wav);
 d='d';
 a='a';
 for i=1:lev
    detx(i,1:N)=wrcoef(d,cx,lx,wav,i);
    appx(i,1:N)=wrcoef(a,cx,lx,wav,i);
 end

 figure(1)
 for i=1:lev
    subplot(lev+1,1,i),plot(t,detx(i,1:N))
 if i==1
    title(['Details of ' f 'L1 , Cover Vibration '])
    end
 if i==4
    ylabel('Amplitudes of Details')
    end
 if i==lev
        xlabel('time (sec)')
    end
 end

 figure(2)
 for i=1:lev
```

```
    subplot(lev+1,1,i),plot(appx(i,1:1000))
  if i==1
    title(['Approximations of ' f 'L1 , Cover Vibration '])
    end
  if i==4
    ylabel('Amplitudes of Approximations')
    end
  if i==lev
          xlabel('time (# of data points)')
    end
  end

% Wavelet Analysis on V1

  [cy,ly]=wavedec(V1,lev,wav);
  d='d';
  a='a';
  for i=1:lev
    dety(i,1:N)=wrcoef(d,cy,ly,wav,i);
    appy(i,1:N)=wrcoef(a,cy,ly,wav,i);
  end

  figure(3)
  for i=1:lev
    subplot(lev+1,1,i),plot(t,dety(i,1:N))
  if i==1
    title(['Details of ' f 'L1 , V10:00 '])
    end
  if i==4
    ylabel('Amplitudes of Details')
    end
  if i==lev
        xlabel('time (sec)')
    end
  end

  figure(4)
  for i=1:lev
    subplot(lev+1,1,i),plot(appy(i,1:1000))
  if i==1
    title(['Approximations of ' f 'L1 , V10:00 '])
    end
  if i==4
    ylabel('Amplitudes of Approximations')
    end
  if i==lev
         xlabel('time (# of data points)')
    end
  end

% Wavelet Analysis on V2

  [cz,lz]=wavedec(V2,lev,wav);
  d='d';
  a='a';
  for i=1:lev
    detz(i,1:N)=wrcoef(d,cz,lz,wav,i);
    appz(i,1:N)=wrcoef(a,cz,lz,wav,i);
    end

  figure(5)
  for i=1:lev
```

```
   subplot(lev+1,1,i),plot(t,detz(i,1:N))
  if i==1
   title(['Details of ' f 'L1 , V2:00'])
   end
  if i==4
   ylabel('Amplitudes of Details')
   end
  if i==lev
       xlabel('time (sec)')
   end
  end

  figure(6)
  for i=1:lev
   subplot(lev+1,1,i),plot(appz(i,1:1000))
  if i==1
   title(['Approximations of ' f 'L1 , V2:00 '])
   end
  if i==4
   ylabel('Amplitudes of Approxiamtions')
   end
  if i==lev
        xlabel('time (# of data points)')
   end
  end
end

eval(['save W' f 'p detx appx dety appy detz appz'])
```

RMSWP.m

```
%
% RMS value of the details in wavelet decomposition from
%  procesed data file wm_c_.mat
%
%                   Program :  RMSwp.M
%

 m=input('Input motor file extension (wm_c_ , no p or .mat required). ','s');
 s=input('Input motor signal for processing. ','s');
 eval(['load ' m 'p'])

if s=='Ix'
 y='detx';
elseif s=='Iy'
 y='dety';
elseif s=='Iz'
 y='detz';
elseif s=='Vc'
 y='detx';
elseif s=='V1'
 y='dety';
else s=='V2'
 y='detz';
end

 y1=eval([y '(1,:)']);
 y2=eval([y '(2,:)']);
 y3=eval([y '(3,:)']);
 y4=eval([y '(4,:)']);
 y5=eval([y '(5,:)']);
 y6=eval([y '(6,:)']);
 y7=eval([y '(7,:)']);
 y8=eval([y '(8,:)']);

 sum1=0;
 sum2=0;
 sum3=0;
 sum4=0;
 sum5=0;
 sum6=0;
 sum7=0;
 sum8=0;

 N=6000;

 for k=1:N;
 sum1=sum1+(y1(k))^2;
 sum2=sum2+(y2(k))^2;
 sum3=sum3+(y3(k))^2;
 sum4=sum4+(y4(k))^2;
 sum5=sum5+(y5(k))^2;
 sum6=sum6+(y6(k))^2;
 sum7=sum7+(y7(k))^2;
 sum8=sum8+(y8(k))^2;
 end
 rms1=sqrt(sum1/N);
 rms2=sqrt(sum2/N);
 rms3=sqrt(sum3/N);
 rms4=sqrt(sum4/N);
 rms5=sqrt(sum5/N);
```

```
rms6=sqrt(sum6/N);
rms7=sqrt(sum7/N);
rms8=sqrt(sum8/N);

['Data ' m ' signal ' s ' rms for level 1 = ' num2str(rms1)]
['Data ' m ' signal ' s ' rms for level 2 = ' num2str(rms2)]
['Data ' m ' signal ' s ' rms for level 3 = ' num2str(rms3)]
['Data ' m ' signal ' s ' rms for level 4 = ' num2str(rms4)]
['Data ' m ' signal ' s ' rms for level 5 = ' num2str(rms5)]
['Data ' m ' signal ' s ' rms for level 6 = ' num2str(rms6)]
['Data ' m ' signal ' s ' rms for level 7 = ' num2str(rms7)]
['Data ' m ' signal ' s ' rms for level 8 = ' num2str(rms8)]

eval(['save r' m s ' rms1 rms2 rms3 rms4 rms5 rms6 rms7 rms8'])
```

WRMSPROS.m

```
%
% Processing Wavelet RMS values for each motor and signal
%
%  wrmspros.m
%

clear;

m=input('Input processed motor number. ');
c=input('Input number of cycles. ');
s=input('Input signal type. ','s');

rmsm=zeros(c-1,8);

for i=1:c
   eval(['load rwm' num2str(m) 'c' num2str(i-1) s]);
   rmsm(i,:)=[rms1 rms2 rms3 rms4 rms5 rms6 rms7 rms8];
end

for i=1:8
   figure(i)
   plot(rmsm(:,i))
   title(['RMS values for motor' num2str(m) ', signal ' s ', level '
num2str(i)])
   xlabel('Cycle Number (1 is intial or 0)')
   if (s=='Ix')|(s=='Iy')|(s=='Iz')
      ylabel('RMS of Current')
   else
      ylabel('RMS of g"s')
   end
end
```

WRMSFIT8.m

```
%
% Regresion Fit of Wavelet RMS values for each motor and all level; RMS %  vs
cycle
%
%  wRMSfit8.m
%

clear;

% Input Motor #, Cycles, and Signal type

m=input('Input motor number. ');
c=input('Input number of cycles. ');
s=input('Input signal type (Ix,Iy,Iz,Vc,V1,V2). ','s');

% Sets-up Matrix with levels vs cycles

eval(['wRMSm' num2str(m) s '=zeros(8,c);']);

% Inputs appropiate motor cycle and signal to load into matrix

for j=0:c-1
   eval(['load rwm' num2str(m) 'c' num2str(j) s]);
   eval(['wRMSm' num2str(m) s '(:,' num2str(j+1)
')=[rms1;rms2;rms3;rms4;rms5;rms6;rms7;rms8];']);
end

% Shows end result matrix with appropriate name

eval(['wRMSm' num2str(m) s]);

% Matrix is the set equal to generic Y for evaluation, number of cycles vector

Y=eval(['wRMSm' num2str(m) s]);
X=[0:c-1];

% Nth Degree Polynomial fit

N=1;

% Evaluation for all 8 levels

for l=1:8

clear P S Y1 D DY SDY SSDY RMSerror;

[P,S]=polyfit(X,Y(l,:),N);
[Y1]=polyval(P,X,S);

% RMSerror calcualtion

E=abs(Y(l,:)-Y1);
EY=E./(Y(l,:));
SEY=EY.^2;
SSEY=sum(SEY);
RMSerror=sqrt(SSEY/c);

% Plotting of original and fitted polynomial with RMS error

figure(1)
```

```
plot(X,Y(l,:))
hold
plot(X,Y(l,:),'ro')
aux=axis;
plot(X,Y1)
if ((s=='ix')&(l==7))|((s=='iy')&(l==7))|((s=='iz')&(l==7))
sf1=sprintf('Fractional RMS Error = %.4f',RMSerror);
text(aux(2)*3/6,aux(4)-aux(4)/60,sf1)
sf2=sprintf('Slope = %.4f',P(1));
text(aux(2)*3/6,aux(4)-aux(4)/90,sf2)
else
sf1=sprintf('Fractional RMS Error = %.4f',RMSerror);
text(aux(2)*3/6,aux(4)-aux(4)/50,sf1)
sf2=sprintf('Slope = %.4f',P(1));
text(aux(2)*3/6,aux(4)-aux(4)/10,sf2)
end
title(['M' num2str(m) ' signal ' s ' for level ' num2str(l)])
xlabel('Cycle #')
ylabel(['RMS value for level ' num2str(l)])

end
```

CCM.m

```
%
% m-file: ccm.m
%
%   Corrcoef calculation using 1s of signal for Ix,Iy,Iz
%       Vc,V2:00,V10:00
%

clear;
f=input('Input motor file (only motor # and cycle, no .dat needed). ','s');
eval(['load ' f 'L1.dat']);

Ix=eval([f 'l1(1,1:12000)']);
Iy=eval([f 'l1(2,1:12000)']);
Iz=eval([f 'l1(3,1:12000)']);
Vc=eval([f 'l1(4,1:12000)']);
V1=eval([f 'l1(8,1:12000)']);
V2=eval([f 'l1(9,1:12000)']);

eval(['clear ' f 'L1']);

Ix=Ix';Iy=Iy';Iz=Iz';Vc=Vc';V1=V1';V2=V2';

X=[Ix Iy Iz Vc V1 V2];

eval(['C' f '=corrcoef(X)']);

eval(['save CC' f ' C' f])
```

CH1.m

```
%
% Ch1.m  Coherence program
%  Will load appropraite motor data and signals for
%   Coherence calcualtion.
%

clear;

Fs=12000;
Noverlap=0;
m=input('Input motor file name (m_c_11, .dat not needed). ','s');
s1=input('Input first signal for coherence calculation. ','s');
s2=input('Input second signal for coherence calculation. ','s');
nfft=8192;
n=120000;

eval(['load ' m '.dat']);

if s1=='Ix'
   S1=eval([m '(1,:)']);
elseif s1=='Iy'
   S1=eval([m '(2,:)']);
elseif s1=='Iz'
   S1=eval([m '(3,:)']);
elseif s1=='Vc'
   S1=eval([m '(4,:)']);
elseif s1=='V1'
   S1=eval([m '(8,:)']);
else
   S1=eval([m '(9,:)']);
end

if s2=='Ix'
   S2=eval([m '(1,:)']);
elseif s2=='Iy'
   S2=eval([m '(2,:)']);
elseif s2=='Iz'
   S2=eval([m '(3,:)']);
elseif s2=='Vc'
   S2=eval([m '(4,:)']);
elseif s2=='V1'
   S2=eval([m '(8,:)']);
else
   S2=eval([m '(9,:)']);
end

eval(['clear ' m]);

[c,f]=cohere(S1,S2,nfft,Fs,hanning(nfft),Noverlap);

% Plot coherence and Set threshold values

plot(f,c)
title(['Coherence of ' m ', signals ' s1 ' vs. ' s2])
xlabel('frequency (Hz)')
ylabel('magnitude ( 1 - 0 )')

threshold=input('Input threshold value. ');
```

```
% Run peak ID routine
% Copy coherence spectrum


yt=c;
ind=(find(yt<threshold));
yt(ind)=threshold;

% finding local maxima

datasize = length(yt);

count = 0;
for i = 2 : datasize-1
   if ( (yt(i-1) < yt(i)) & (yt(i+1) < yt(i)) )
      count = count+1;
      maxima(count,:) = [ f(i) yt(i) ];
    end
end

['Peak values (frequency and Amplitude) for ' m ' signals ' s1 ' vs. ' s2 ...
   ' with threshold = ' num2str(threshold)]
maxima

[rmax,cmax]=size(maxima);

   plot(f,c)
   hold
   plot(maxima(:,1),maxima(:,2),'ro')
   aux=axis;
   if rmax<16
   for k=1:rmax
      sf=sprintf('%.2f , %.2f',maxima(k,1),maxima(k,2));
      text(aux(2)*4.5/6,aux(4)-aux(4)*k/20,sf)
   end
   end
title(['Coherence of ' m ', signals ' s1 ' vs. ' s2 ', with threshold = '
num2str(threshold)])
xlabel('frequency (Hz)')
ylabel('magnitude of coherence ( 0 to 1 )')
```

CCPLOT1.m

```
%
% m-file: ccplot1
%  Groups and Plots abs val of corrcoef for each cycle
%


clear;

m=input('Input Motor #. ');
n=input('Input # of cycles for this motor. ');

for i=0:n-1,
 eval(['load ccm',int2str(m),'c',int2str(i)]);
end

for i=1:n,

Ixy(i)=eval(['Cm',int2str(m),'c',int2str(i-1),'(1,2)']);
Ixz(i)=eval(['Cm',int2str(m),'c',int2str(i-1),'(1,3)']);
IxVc(i)=eval(['Cm',int2str(m),'c',int2str(i-1),'(1,4)']);
IxV1(i)=eval(['Cm',int2str(m),'c',int2str(i-1),'(1,5)']);
IxV2(i)=eval(['Cm',int2str(m),'c',int2str(i-1),'(1,6)']);

Iyz(i)=eval(['Cm',int2str(m),'c',int2str(i-1),'(2,3)']);
IyVc(i)=eval(['Cm',int2str(m),'c',int2str(i-1),'(2,4)']);
IyV1(i)=eval(['Cm',int2str(m),'c',int2str(i-1),'(2,5)']);
IyV2(i)=eval(['Cm',int2str(m),'c',int2str(i-1),'(2,6)']);

IzVc(i)=eval(['Cm',int2str(m),'c',int2str(i-1),'(3,4)']);
IzV1(i)=eval(['Cm',int2str(m),'c',int2str(i-1),'(3,5)']);
IzV2(i)=eval(['Cm',int2str(m),'c',int2str(i-1),'(3,6)']);

VcV1(i)=eval(['Cm',int2str(m),'c',int2str(i-1),'(4,5)']);
VcV2(i)=eval(['Cm',int2str(m),'c',int2str(i-1),'(4,6)']);

V1V2(i)=eval(['Cm',int2str(m),'c',int2str(i-1),'(5,6)']);

end

figure(1)
plot(abs(Ixy))
axis('auto')
hold
aux=axis;
for k=1:3
   I=[sum(abs(Ixy))/n sum(abs(Ixz))/n sum(abs(Iyz))/n];
   Ixyz=['sum|Ixy|/n'; 'sum|Ixz|/n'; 'sum|Iyz|/n'];
   sf=sprintf('%s = %.2f',Ixyz(k,:),I(:,k));
   text(aux(2)*4/6,aux(4)-k*(aux(4)-aux(3))/5,sf)
end
plot(abs(Iyz),'ro')
plot(abs(Iyz))
plot(abs(Ixz),'mx')
plot(abs(Ixz))
title(['For M' num2str(m) ', Ix vs. Iy (-), Ix vs. Iz (x) and Iy vs. Iz (o)'])
xlabel('Cycle #')
ylabel('|Correlation Coefficient Value|')

figure(2)
plot(abs(IxVc))
```

```
axis('auto')
hold
plot(abs(IxV1),'ro')
plot(abs(IxV1))
plot(abs(IxV2),'gx')
plot(abs(IxV2))
aux=axis;
for k=1:3
   I=[sum(abs(IxVc))/n sum(abs(IxV1))/n sum(abs(IxV2))/n];
   IxV=['sum|IxVc|/n'; 'sum|IxV1|/n'; 'sum|IxV2|/n'];
   sf=sprintf('%s = %.4f',IxV(k,:),I(:,k));
   text(aux(2)*4/6,aux(4)-k*(aux(4)-aux(3))/10,sf)
end
title(['For M' num2str(m) ', Ix Current vs. Vc (-), V10:00 (o), V2:00 (x)'])
xlabel('Cycle #')
ylabel('|Correlation Coefficient Value|')

figure(3)
plot(abs(IyVc))
axis('auto')
hold
plot(abs(IyV1),'co')
plot(abs(IyV1))
plot(abs(IyV2),'rx')
plot(abs(IyV2))
aux=axis;
for k=1:3
   I=[sum(abs(IyVc))/n sum(abs(IyV1))/n sum(abs(IyV2))/n];
   IyV=['sum|IyVc|/n'; 'sum|IyV1|/n'; 'sum|IyV2|/n'];
   sf=sprintf('%s = %.4f',IyV(k,:),I(:,k));
   text(aux(2)*4/6,aux(4)-k*(aux(4)-aux(3))/12,sf)
end
title(['For M' num2str(m) ', Iy Current vs. Vc (-), V10:00 (o), V2:00 (x)'])
xlabel('Cycle #')
ylabel('|Correlation Coefficient Value|')

figure(4)
plot(abs(IzVc))
axis('auto')
hold
aux=axis;
for k=1:3
   I=[sum(abs(IzVc))/n sum(abs(IzV1))/n sum(abs(IzV2))/n];
   IzV=['sum|IzVc|/n'; 'sum|IzV1|/n'; 'sum|IzV2|/n'];
   sf=sprintf('%s = %.4f',IzV(k,:),I(:,k));
   text(aux(2)*4/6,aux(4)-k*(aux(4)-aux(3))/10,sf)
end
plot(abs(IzV1),'mo')
plot(abs(IzV1))
plot(abs(IzV2),'cx')
plot(abs(IzV2))
title(['For M' num2str(m) ', Iz Current vs. Vc (-), V10:00 (o), V2:00 (x)'])
xlabel('Cycle #')
ylabel('|Correlation Coefficient Value|')

figure(5)
plot(abs(VcV1))
axis('auto')
hold
aux=axis;
for k=1:3
   I=[sum(abs(VcV1))/n sum(abs(V1V2))/n sum(abs(VcV2))/n];
```

```
   Vc12=['sum|VcV1|/n'; 'sum|V1V2|/n'; 'sum|VcV2|/n'];
   sf=sprintf('%s = %.4f',Vc12(k,:),I(:,k));
   text(aux(2)*4/6,aux(4)-k*(aux(4)-aux(3))/10,sf)
end
plot(abs(V1V2))
plot(abs(V1V2),'ro')
plot(abs(VcV2))
plot(abs(VcV2),'mx')
title(['For M' num2str(m) ', Vc vs. V10:00 (-), Vc vs. V2:00 (x) and V10:00 vs
V2:00 (o)'])
xlabel('Cycle #')
ylabel('|Correlation Coefficient Value|')
```

Appendix B Motor Current Frequencies Caused by Bearing Vibrations

Table B.1. Motor current spectra frequencies caused by bearing vibrations (bearing SKF 6505)

	$f_{mc} = f_e + m^* f_v$				$f_{mc} = f_e - m^* f_v$			
Harmonic	**Cage Train**	**Ball**	**Outer Race**	**Inner Race**	**Cage Train**	**Ball**	**Outer Race**	**Inner Race**
1	72	197	164	217	48	77	44	97
2	83	334	268	374	37	214	148	254
3	95	470	372	531	25	350	252	411
4	106	607	476	688	14	487	356	568
5	118	744	580	845	2	624	460	725
6	129	880	684	1002	9	760	564	882
7	141	1017	788	1159	21	897	668	1039
8	152	1154	892	1316	32	1034	772	1196
9	164	1291	996	1473	44	1171	876	1353
10	176	1427	1100	1630	56	1307	980	1510
11	187	1564	1204	1787	67	1444	1084	1667
12	199	1701	1308	1944	79	1581	1188	1824
13	210	1838	1412	2102	90	1718	1292	1982
14	222	1974	1516	2259	102	1854	1396	2139
15	233	2111	1620	2416	113	1991	1500	2296
16	245	2248	1723	2573	125	2128	1603	2453
17	256	2384	1827	2730	136	2264	1707	2610
18	268	2521	1931	2887	148	2401	1811	2767
19	279	2658	2035	3044	159	2538	1915	2924
20	291	2795	2139	3201	171	2675	2019	3081

Table B.2. Motor current spectra frequencies caused by bearing vibrations (bearing SKF 6506, European)

	$f_{mc} = f_e + m^* f_v$				$f_{mc} = f_e - m^* f_v$			
Harmonic	**Cage Train**	**Ball**	**Outer Race**	**Inner Race**	**Cage Train**	**Ball**	**Outer Race**	**Inner Race**
1	71	194	164	218	49	74	44	98
2	83	328	267	375	37	208	147	255
3	94	462	370	533	26	342	250	413
4	106	596	474	690	14	476	354	570
5	117	730	577	848	2	610	457	728
6	129	864	681	1005	9	744	561	885
7	140	998	784	1163	20	878	664	1043
8	152	1132	888	1320	32	1012	768	1200
9	163	1266	991	1478	43	1146	871	1358
10	175	1401	1095	1635	55	1281	975	1515
11	186	1535	1198	1793	66	1415	1078	1673
12	198	1669	1302	1950	78	1549	1182	1830
13	209	1803	1405	2108	89	1683	1285	1988
14	221	1937	1509	2265	101	1817	1389	2145
15	232	2071	1612	2423	112	1951	1492	2303
16	244	2205	1716	2580	124	2085	1596	2460
17	255	2339	1819	2738	135	2219	1699	2618
18	267	2473	1923	2895	147	2353	1803	2775
19	278	2607	2026	3053	158	2487	1906	2933
20	290	2741	2130	3210	170	2621	2010	3090

Appendix C Coherence Functions for Specified Signal Pairs

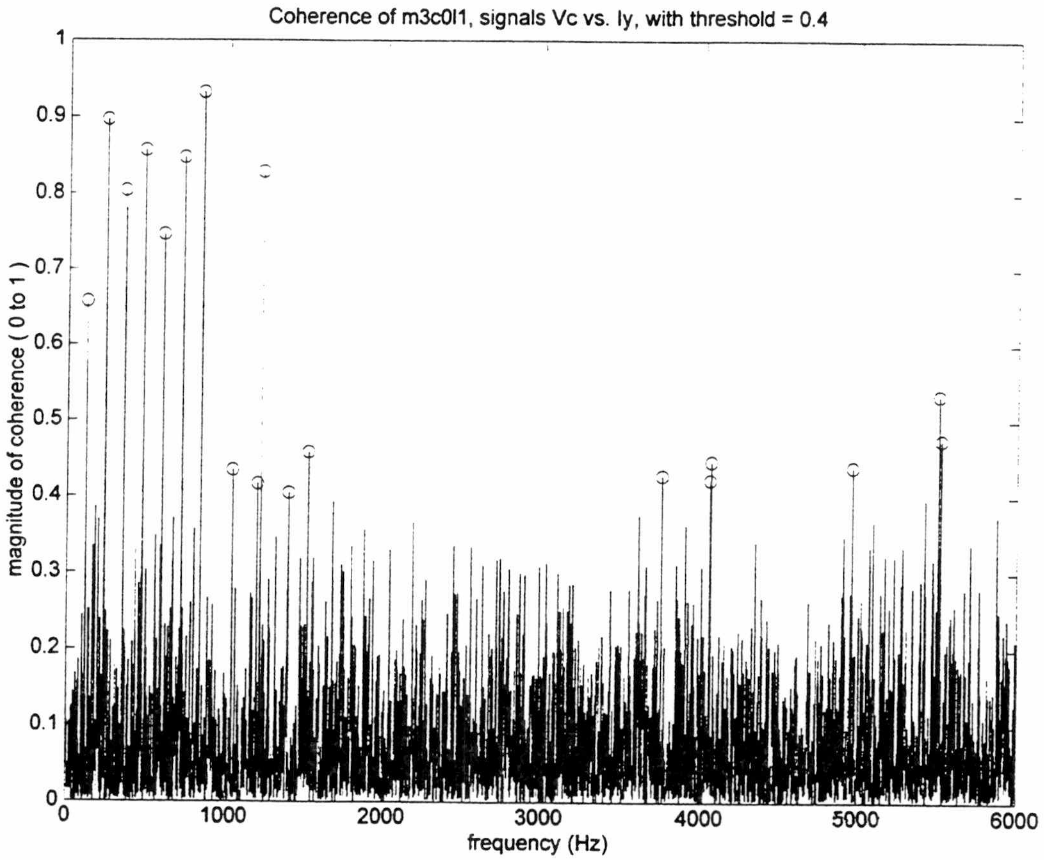

Figure C.1. Initial coherence function for motor #3 using signals Vc and Iy.

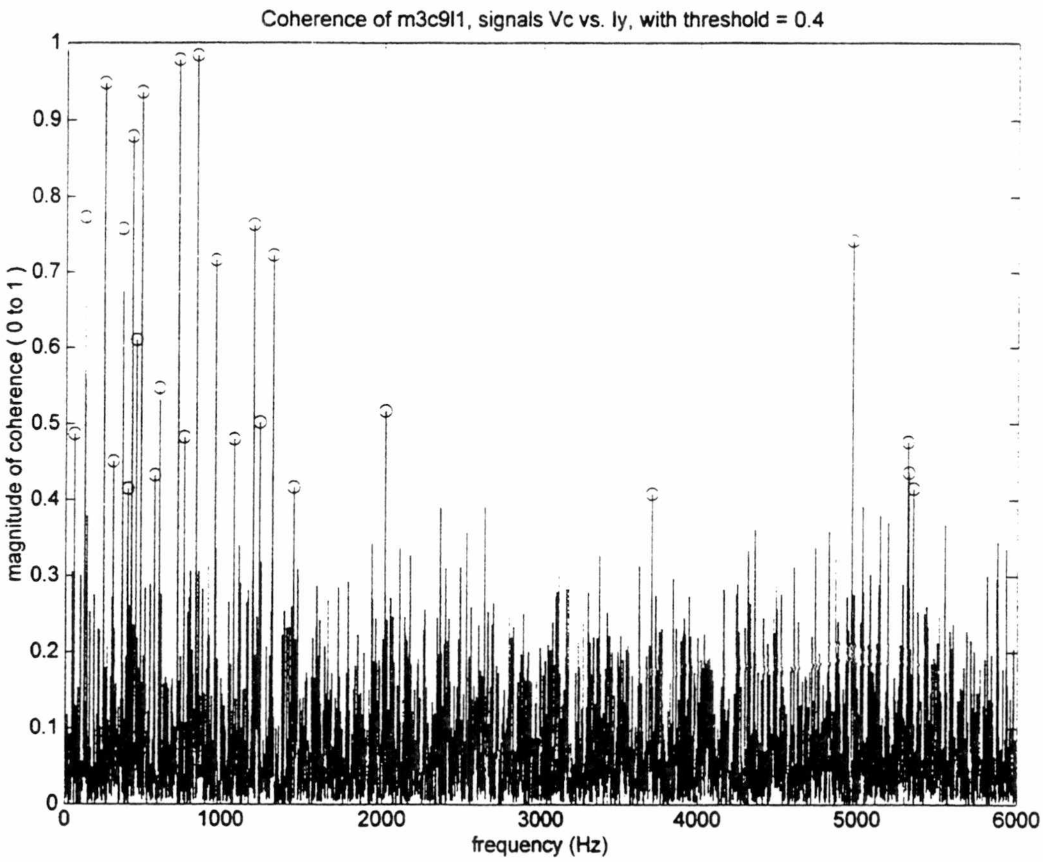

Figure C.2. Final coherence function for motor #3 using signals Vc and Iy.

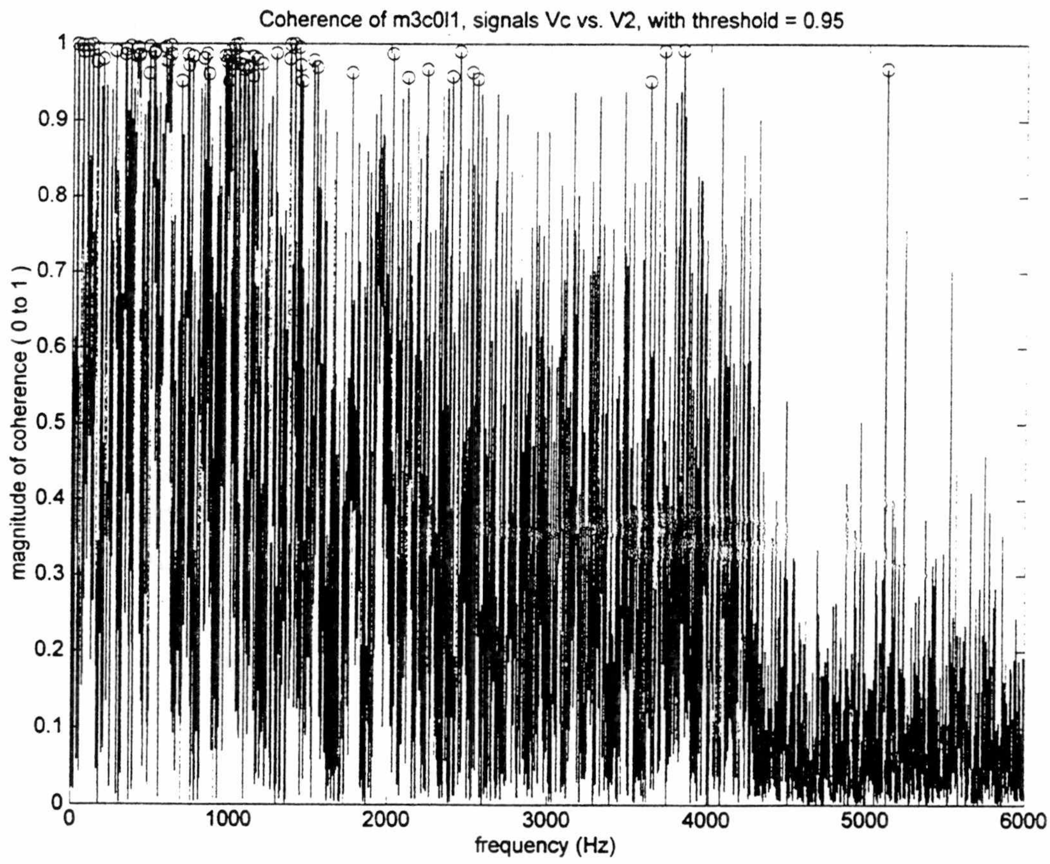

Figure C.3. Initial coherence function for motor #3 using signals Vc and V2.

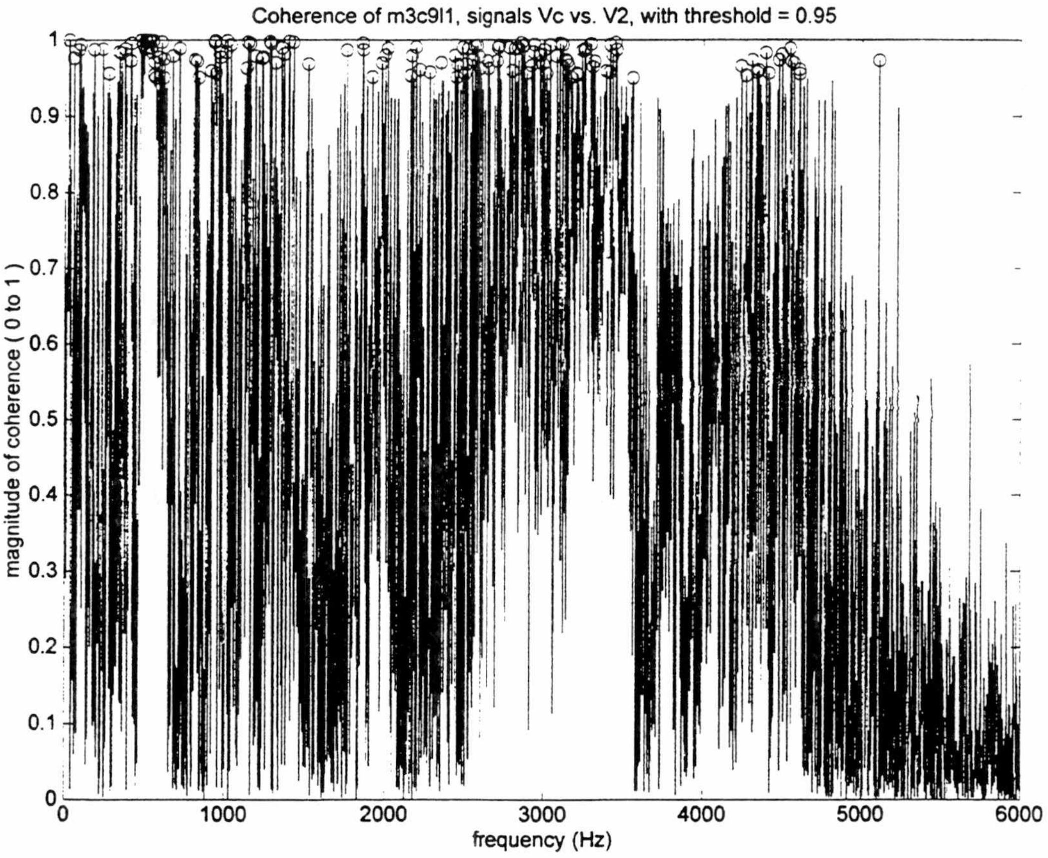

Figure C.4. Final coherence function for motor #3 using signals Vc and V2.

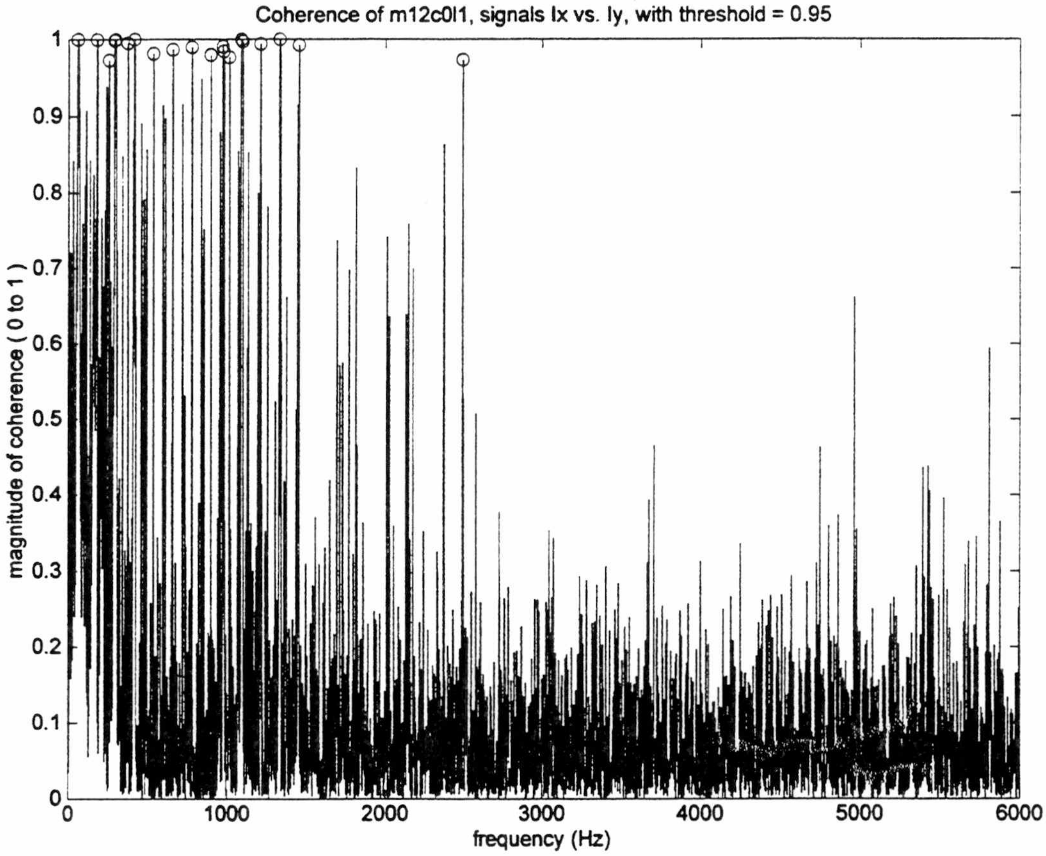

Figure C.5. Initial coherence function for motor #12 using signals Ix and Iy.

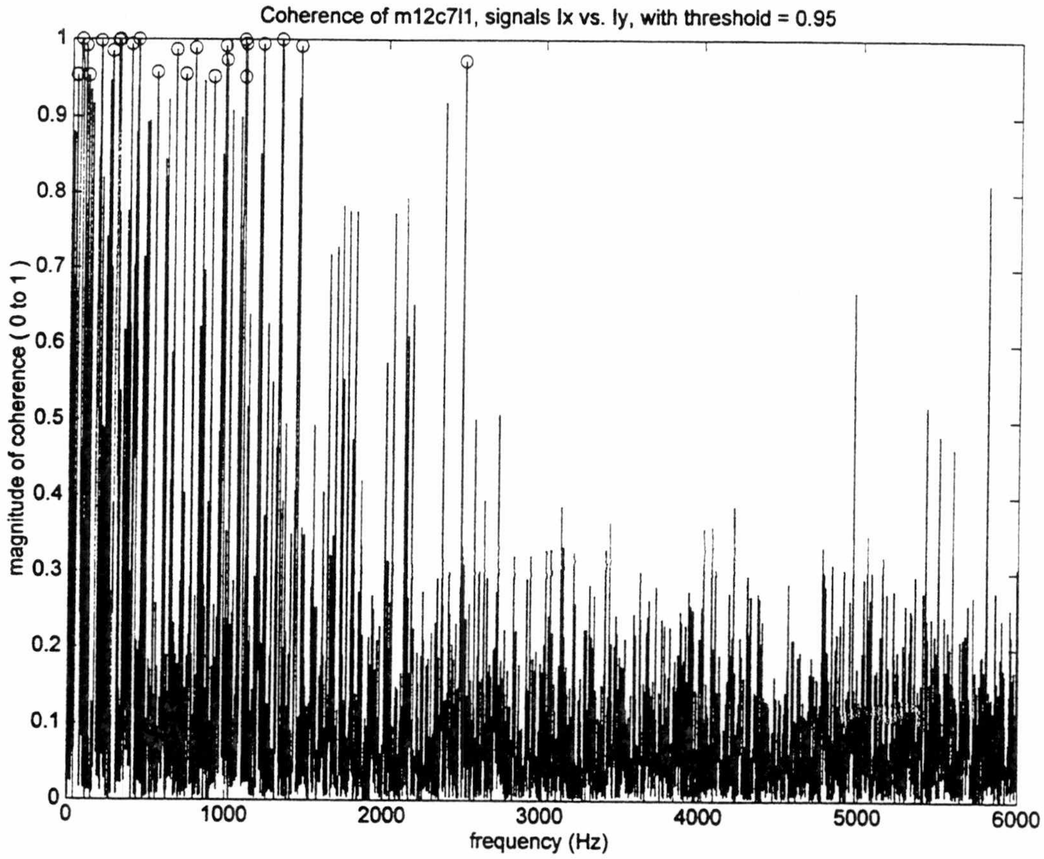

Figure C.6. Final coherence function for motor #12 using signals Ix and Iy.

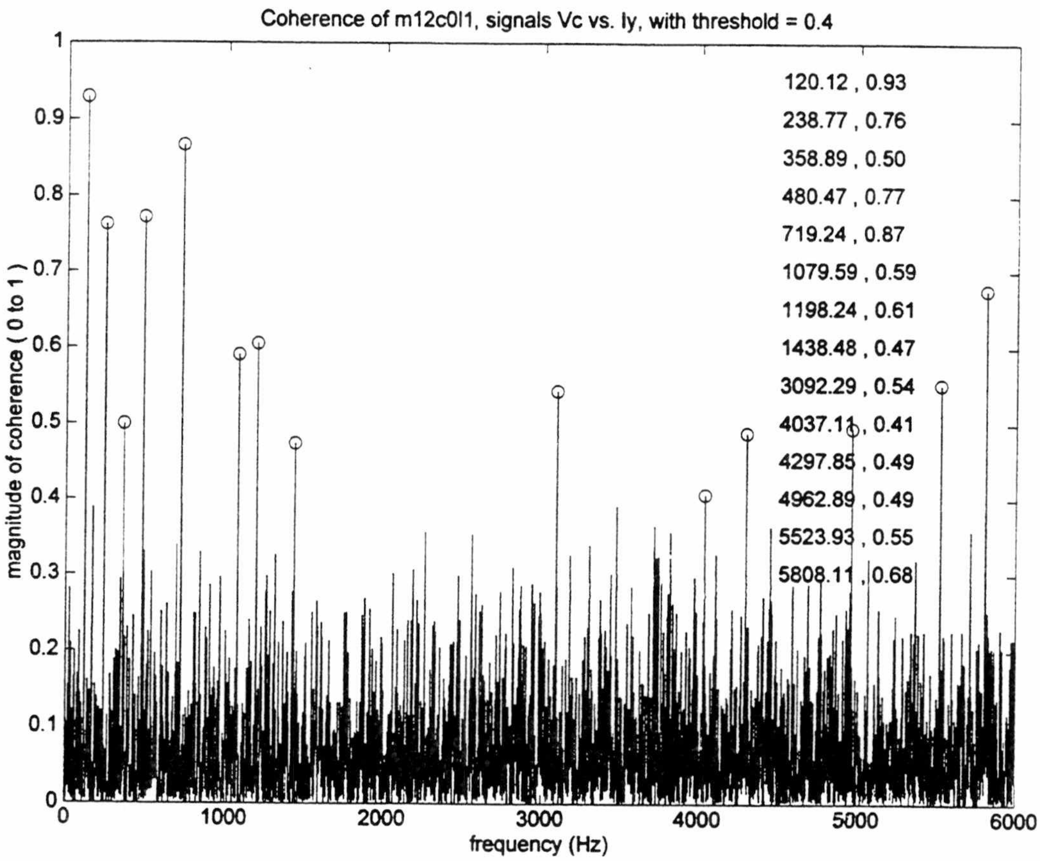

Figure C.7. Initial coherence function for motor #12 using signals Vc and Iy.

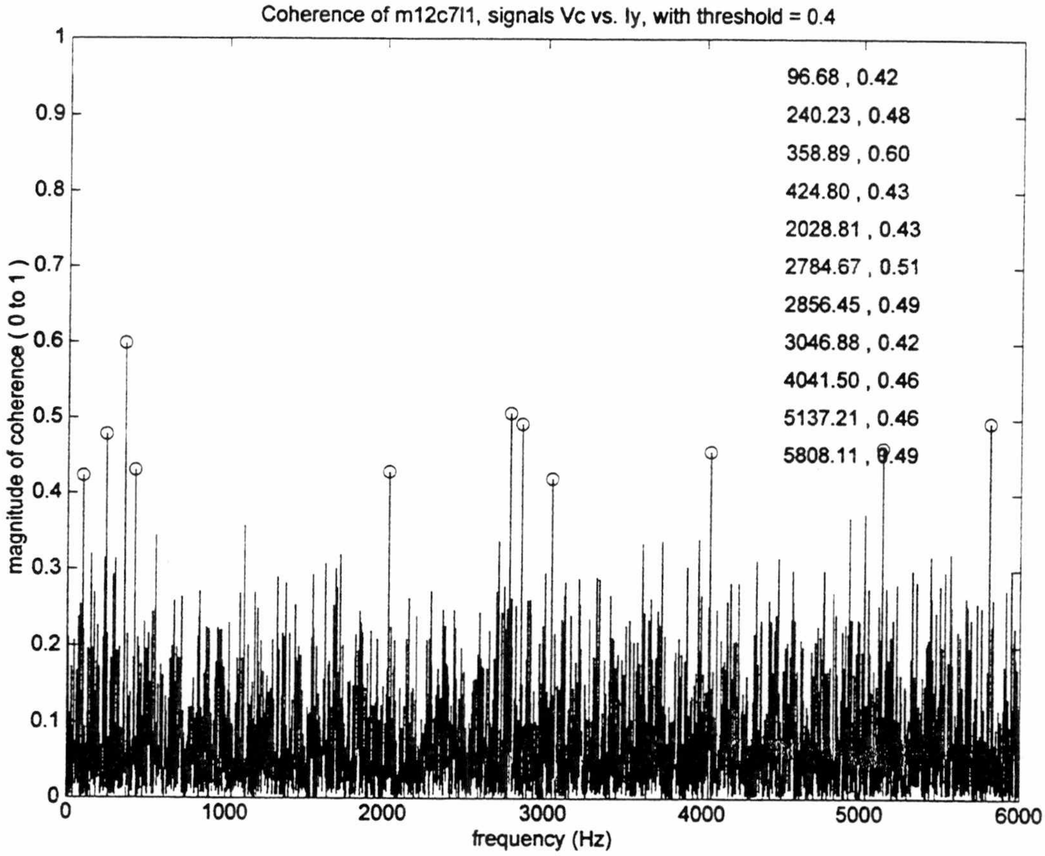

Figure C.8. Final coherence function for motor #12 using signals Vc and Iy.

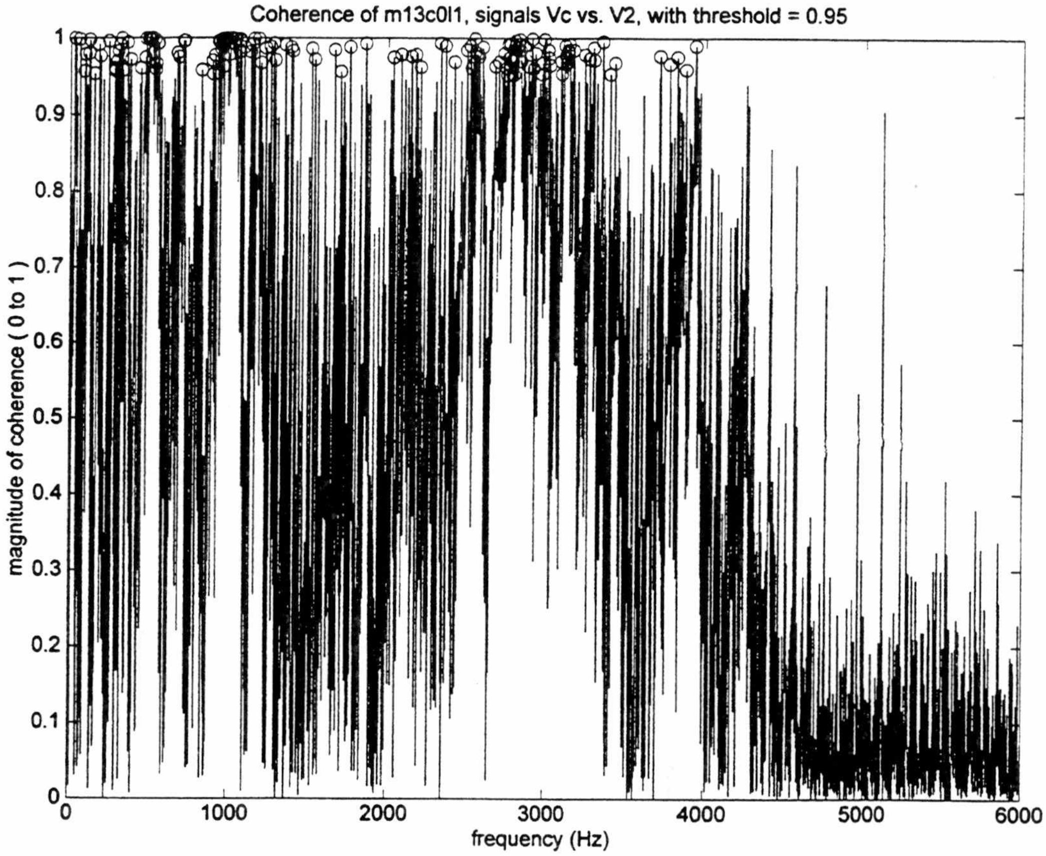

Figure C.9. Initial coherence function for motor #13 using signals Vc and V2.

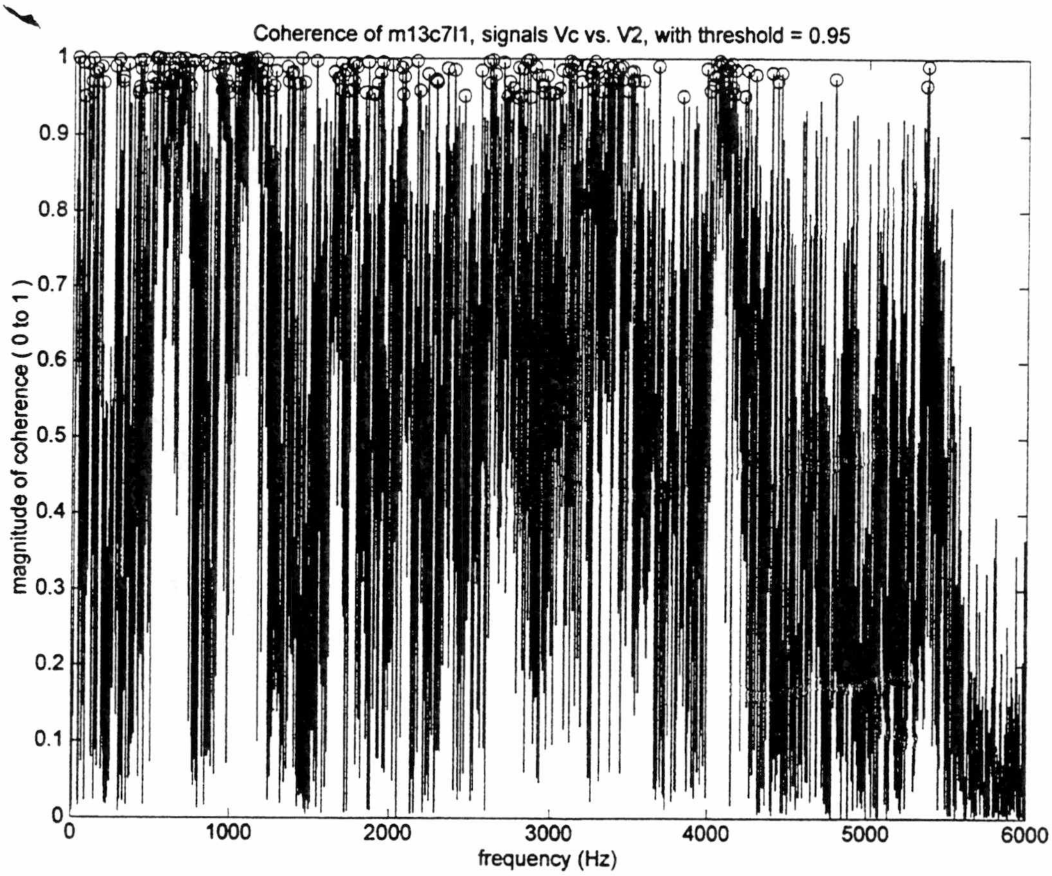

Figure C.10. Final coherence function for motor #13 using signals Vc and V2.

VITA

James Patrick McClanahan was born in Richlands, Virginia on January 30, 1964. He attended elementary school (grades K through 7th) and junior high (8th and 9th grades) in the public system for Buchanan County, Virginia. He then transferred to the public system of Washington County, Virginia where he graduated from Abingdon High School in 1982. He entered The University of Tennessee in the fall of 1982 majoring in Nuclear Engineering. He then transferred in the spring of 1986 to Emory and Henry College located in Emory, Virginia. He graduated from Emory and Henry College in May 1988 receiving Bachelor of Science degrees in Physics and Applied Mathematics. He then began working at Nuclear Fuel Services, Inc. in July of 1989. While working at Nuclear Fuel Services, he obtained a Master's of Business Administration in March 1992 from Bristol University, Bristol, Tennessee. Then, in August of 1994, he left Nuclear Fuel Services to re-enter The University of Tennessee's Nuclear Engineering Department. He obtained his Bachelor of Science degree in Nuclear Engineering form The University of Tennessee in the spring of 1996. He immediately began pursuit of his Master's of Science degree in Nuclear Engineering, again, at The University of Tennessee. The Master's of Science in Nuclear Engineering was finished in December 1998.

He is presently working toward his PhD. in Nuclear Engineering at The University of Tennessee.